CHAPTER 3

ANALYSIS, MODELING AND SIMULATION OF CONTINUOUS EXTRUSION PROCESS

3.1 INTRODUCTION

In this chapter analysis, modeling and simulation of continuous extrusion process for non-ferrous metals and alloys is presented including connecting CAE processes and FEM. A simulation package (DEFORM 3D) is used to analyze the Continuous Extrusion forming of Pure Aluminum feedstock (AA 1100) and Pure Copper(C 101) feedstock. Simulation results are used to suggest design modifications in the geometry and tooling required for the Continuous Extrusion setup to get an optimum result. The Simulation results are compared with the analytical results to generate knowledge as well as validating result. Analysis of the continuous extrusion process for Aluminum and copper feedstock's of different diameter at different extrusion wheel speed and for different die arrangement in abutment die chamber using upper bound method has been done. The analysis of forces required starting from entry of feedstock in the groove of extrusion wheel up to its final extrusion through the die orifice has been done. Therefore complete estimation of element of total extrusion power has been made in this chapter using upper bound technology.

In section 3.2 continuous extrusion process has been defined. A brief propose of computer aided engineering is introduced in section 3.3. Role of Finite Element formulation has been presented in section 3.3.The process of simulation procedure and steps to be followed is presented in section 3.5. A sample Simulation of Continuous Extrusion process for circular rod of various metals and alloys has been performed in section 3.6. Parametric studies on process parameters of Continuous Extrusion process is presented in 3.14. In section 3.16 a brief discussion about the contact pressure, primary grip zone and secondary grip zone has been done. Section 3.17 deals with the estimation of all power terms in continuous extrusion process. Few examples are taken in section 3.18 to illustrate the analysis of continuous extrusion process completely.

3.2 FEM PROCEDURE

The finite element method is a numerical method for solving differential and integral equations. In this method, the unknown variables to be determined are approximated by piecewise continuous functions. The coefficients of the functions are adjusted in such a manner that the error in the solution is minimized. Usually, the coefficients of the functions of a particular element are the values at certain points in the element called nodes. During the solution process, the differential equations get converted to algebraic equations or ordinary differential equations that can be solved by finite difference equations. The finite element method consists of following steps:

1. Pre - processing
2. Developing elemental equations
3. Assembling equations
4. Applying boundary conditions
5. Solving the system of equations
6. Post – processing

The two basic formulations used in finite element technique are Eulerian and Langrangian.

In Eulerian formulation, the domain is fixed region in space (called control volume). However, in a Langrangian formulation the domain consists of a set of material particles that changes its shape continuously with the deformation. The updated Langrangian formulation is an incremental method in which the domain is updated incrementally. Further, the measure of deformation used in Eulerian formulation is the rate of deformation tensor and the constitutive equation is expressed in terms of the stress and rate of deformation tensors. On the other hand, in Updated Lanrangian formulation, the measure of deformation is an incremental stress and incremental strain tensors. Like that of Eulerian formulation, the governing equations of the updated Langrangian formulation also are non- linear and need an iterative scheme to obtain a solution.

The updated Langrangian formulation has been used in this thesis and the details of its governing equations has been presented in Appendix C.

3.3 FINITE ELEMENT FORMULATION

This study applies commercial finite element code DEFORM-3D [Yang Tung-Sheng et al. (2009)] to simulate the plastic deformation behavior during the helical gear forging process.

The basic equations of the rigid-plastic finite element are as follows:

Equilibrium equation:

$$\sigma_{ij,j} = 0 \tag{3.1}$$

Compatibility and incompressibility equations

$$\dot{\varepsilon}_{ij} = \frac{1}{2}(u_{ij} + u_{ji})$$

$$\dot{\varepsilon}_v = u_{ij} = 0 \tag{3.2}$$

Constitutive equations:

$$\sigma'_{ij} = \frac{2\bar{\sigma}}{2\dot{\bar{\varepsilon}}}\dot{\varepsilon}_{ij},\ \bar{\sigma} = \sqrt{\frac{3}{2}\acute{\sigma}_{ij}\acute{\sigma}_{ij}},\ \dot{\bar{\varepsilon}} = \sqrt{\frac{3}{2}(\dot{\varepsilon}_{ij}\dot{\varepsilon}_{ij})} \tag{3.3}$$

Boundary conditions:

$$\sigma_{ij}n_i = F_j \text{ on } S_F,\ u_i = U_i \text{ on } S_U \tag{3.4}$$

Where σ_{ij} and $\dot{\varepsilon}_{ij}$ are the stress and the strain rate, respectively, $\bar{\sigma}$ and $\dot{\bar{\varepsilon}}$ are the effective stress and the effective strain rate, respectively, F_j is the force on the boundary surface of S_F, and U_i is the deformation velocity on the boundary surface of S_U. The weak form of rigid- plastic FEM can be determined by applying the variation method to Eqs. (3.1) – (3.4), i.e.

$$\int_V \bar{\sigma}\delta\bar{\varepsilon}dv + K\int \varepsilon_V\,\delta\varepsilon_V dV - \int_{S_F} F_i\,\delta u_i dS = 0 \tag{3.5}$$

Where V and S are the volume and the surface area of the material, respectively, and K is the penalty constant. The most important and crucial part of simulation in software is the selection of appropriate material model. DEFORM-3D contains various material models (for elastic-plastic, rigid-plastic and porous material), and each model has different suitability, so selection of correct material model as per the requirement is the prime necessity to get the accurate results.

Most of the material models require detailed material properties such as young's modulus of elasticity, strain hardening exponent, and strength coefficient, etc., as input to

preprocessor before running the solver. In addition to material properties, preprocessor also require input of detailed process parameters such as friction coefficient, extrusion wheel velocity, heat transfer coefficients etc. Yielding criteria which is used for solving of problem is Von Mises (in the Deform3D). Eqs. (3.6) and (3.7) show effective strain and effective stress respectively.

$$\bar{\varepsilon} = \frac{\sqrt{2}}{3}\sqrt{(\varepsilon_{1-}\varepsilon_2)^2 + (\varepsilon_{2-}\varepsilon_3)^2 + (\varepsilon_{3-}\varepsilon_1)^2} \quad (3.6)$$

$$\bar{\sigma} = \frac{1}{\sqrt{2}}\sqrt{(\sigma_{1-}\sigma_2)^2 + (\sigma_{2-}\sigma_3)^2 + (\sigma_{3-}\sigma_1)^2} \quad (3.7)$$

Where $\varepsilon_i$and σ_i are principle strain and principle stress in direction i respectively.

3.4 COMPUTER AIDED ENGINEERING (CAE) SIMULATION PROCEDURE

Figure 3.1 shows the general procedure of proposed CAE process. To conduct CAE simulation, it is first to be represented in detail i.e. in geometry content, and therefore, a CAD model in a suitable format is made for the metal forming simulation systems. The CAE engineers need to create the simulation test models for a given deformation system. The physical model idealizes the real engineering problems and abstracts to comply with certain physical theory with assumptions.

The mathematical model specifies the mathematical equations such as the differential equations on FEM analysis along with detailed boundary and initial conditions and their constraints. The numerical model describes the element type, mesh density and solution parameters. Usually, most CAE packages have part of built in content of these models, but users still need to prepare and input most of the model information into a CAE system.

The CAE simulation process consists of four main steps (1) pre-processing (2) simulation engine (3) post processing and (4) result analysis and evaluation. After the simulation, the calculated results need to be analyzed and evaluated. If the results and solutions are satisfactory the suggested changes and modifications for the metal forming system (part design, tooling design, process configuration and material selection) can be made for next round of simulation. The process is therefore, iterative in nature [Fu et al. (2006)].

The integrated numerical simulation of continuous extrusion process, including metal forming process and tooling deformation provides a systematic approach for

simultaneously modeling of mechanical deformation behaviors, metallurgical phenomena and thermal phenomenon of the metal forming processes. Besides, the interaction and interplay of these physical behaviors and phenomena, their interaction to each other are also taken into consideration. On the other hand, the simulation and analysis of tooling deformation and stress strain distribution during the process can be conducted simultaneously along with the simulation. From the perspective of Continuous Extrusion process, the physical phenomena and mechanical flow behaviors of the body affect the die deformation and stress strain distribution [Fu et al. (2006), Kumar et al. (2010)].

The integrated simulation and analysis frame work for continuous extrusion process shows the forming process simulation including die structure and stress analysis etc. In the continuous extrusion process simulation there are three main issues to be addressed, viz., metallurgical phenomena modeling, mechanical behavior modeling and the thermal phenomena modeling.

[DEFORM 3D, 2009)] DEFORM is a Finite Element Method (FEM) based process simulation system designed to analyze various forming and heat treatment processes used by metal forming and related industries. By simulating manufacturing processes on a computer, this advanced tool allows designers and engineers to:

1. Reduce the need for costly shop floor trials and tooling and processes.
2. Improve tool and die design to reduce production and material costs.
3. Shorten lead time in bringing a new product to market.

Among the vast range of capabilities some capabilities of the DEFORM tool are as follows:

1. Coupled modeling of deformation and heat transfer for simulation of Cold, Warm and hot forming processes.
2. Extensive material database for many common alloys
3. Contour plots of temperature, strain, stress, damage etc.
4. Self-contact boundary condition with robust remeshing allows a simulation to continue to completion even after a lap or fold is formed.

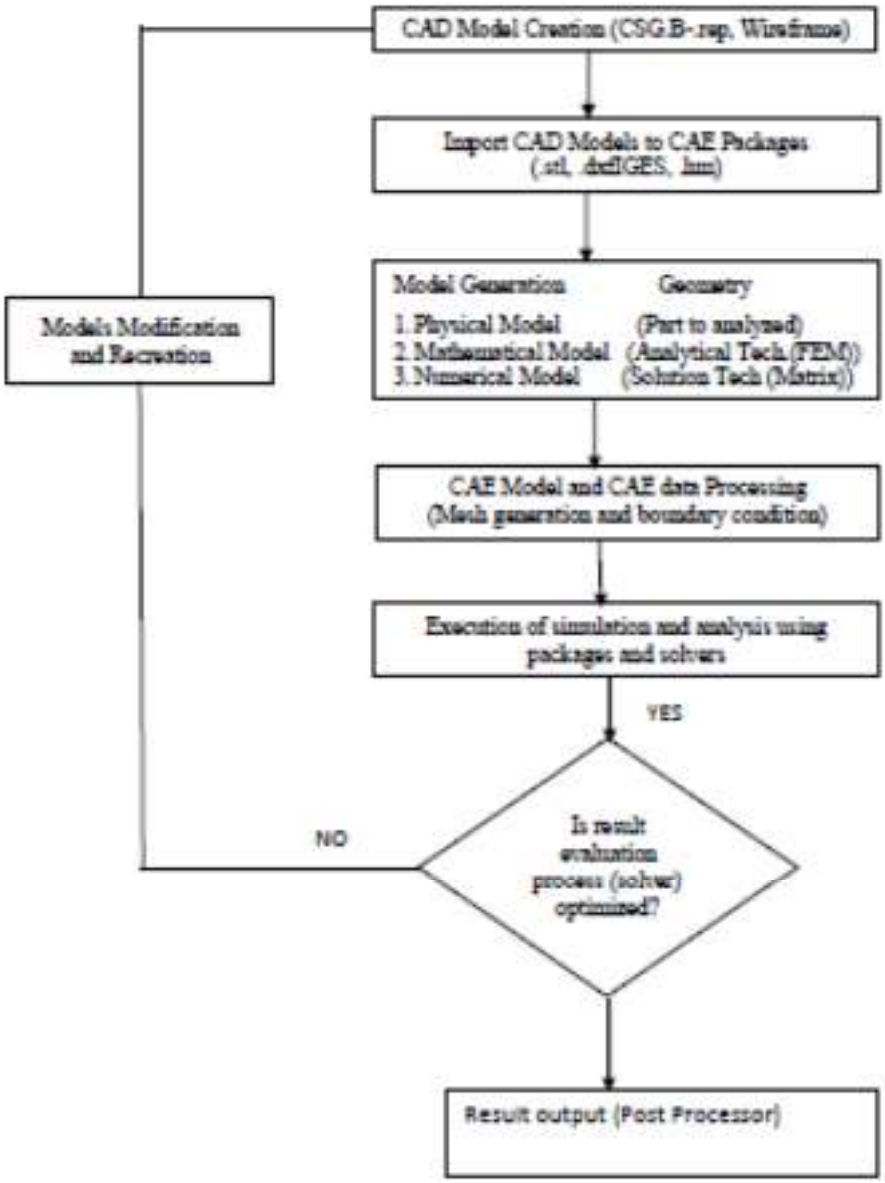

Figure 3.1: Implementation of CAE process, [Fu et al. (2006)]

The metallurgical phenomena modeling is focused on microstructure prediction and structure change analysis of the deforming body in the forming process. The mechanical modeling reveals the plastic flow behavior of the work piece. The optimization process optimizes the process conditions of interests. The interaction and dependency and behaviors are also shown in the frame work. The plastic work generated in the forming

process can be converted into thermal energy which could result in the thermal phenomena change in the deforming body.

3.5 DETAILS OF SIMULATION STEPS

The FEM package DEFORM-3D is used to simulate continuous extrusion process of pure aluminum rod at cold and warm conditions. The finite element result is used to investigate the effective stress distribution and maximum forming load under various process parameters conditions.

The simulation process consists of following five steps:

1. Initial geometry- In this step CAD model of the work piece, extrusion wheel, coining wheel, extrusion shoe, abutment and die as .stl file is imported into the pre-processor of the simulation package (DEFORM-3D).
2. Material data and Meshing- In this step, already existing file material and their material properties are assigned to previously imported products. Also there is a provision for defining new raw materials. The material properties available from the literature can be imported easily in this step. Meshing can be done with the use of tetrahedral elements.
3. Defining the boundary conditions-Different types of boundary conditions such as velocity of extrusion and coining wheel. Coefficient of friction between extrusion wheel and coining wheel and temperature of the work piece are applied. Several possible combinations of these boundary conditions are tested to get the best possible results. Finally a data base file (.db) is generated. This file is run in the simulation engine.
4. Simulation engine-Performs the numerical analysis and writes the information in the data base file.
5. Post-processing-this is used to extract the information from data base file. In this step different types of defects, load requirement and torque required for extrusion are studied. Effective stress, effective strain, velocity distribution and damage distribution are also found. This step gives the modifications required in geometry or boundary conditions to obtain the optimum result.

3.6 Simulation of Continuous Extrusion process

3.6.1 Finite element preprocessing

For carrying out a continuous extrusion process simulations, first it needs to represent the metal forming system to be simulated in its detailed geometry content, i.e., to create the computer models of the deformation system and the metal forming process. The solid models of the continuous extrusion process elements such as Extrusion wheel, coining wheel, extrusion shoe, abutment, die and work piece (rod) are shown in figures below.

The work piece has been meshed with tetrahedral mesh elements in the continuous extrusion process simulations. Sparse FE solver and Newton-Raphson iteration method has been used to the elastic- plastic material as a work piece. Deformation and thermal boundary condition has been added in the simulation.

Sparse solver package, in conjunction with several finite element strategies, has been used for the numerical simulation like deformation of Rigid Visco-Plastic materials. Some of the features of the solver are: It is able to deal with large systems of equations arising from finite element problems, takes into account the structural symmetry of the finite element matrices, It is able to reproduce fractional –step schemes blue at the solver level, the computational cost increases close to linearly with the number of unknowns, the parallelization of the code is under development.

Assumptions made during simulations of Continuous Extrusion process are as follows:

a. Work piece material is assumed to be Rigid Visco-Plastic materials
b. Due to the nature of work piece to be Rigid Visco-Plastic materials coulomb friction coefficient has been used.
c. No sticking friction condition is assumed.

Pre –Processor includes simulation control which can control the numerical behavior of the simulation. Main controls deals with specifying the simulation title, unit system, geometry type, etc.

Stopping and step controls are used to specify the time step, the total number of steps and criteria used to terminate the simulation. Processing conditions like the environment temperature, convection coefficient can be specified under processing conditions.

The DEFORM system uses time dependent non-linear problems by generating a series of FEM solutions at discrete time increments (in step control section).At each time increment, the velocities, temperatures, and other key variables of each node in the finite element mesh are determined based on boundary conditions, thermo mechanical properties of the work piece materials and possibly solutions at previous steps.

The iteration controls specify criteria for the FEM solver which uses to find a solution at each step of the problem simulation. For most of the problems, the default values should be acceptable.

The sparse solver is a direct solution that makes use of the sparseness of FEM formulation to improve the solution speed. The conjugate-gradient solver tries to solve the FEM problem by iteratively by approximating to the solution .For certain problems, this solver offers tremendous advantages over the sparse solver.

An iteration method is the manner in which the simulation solution is updated (or iterated upon) to try to approach the converged step solution.

The Newton–Raphson method is recommended for most problems because it generally converges in less iteration than the other available methods. However, solutions are more likely to fail to converge with this method than with other methods.

The Direct method is more likely to converge than Newton-Raphson, but will generally require more iteration to do so. In the case of porous materials, the direct method is the only method currently available.

Recommended solver for general forming with Rigid Visco-Plastic materials objects is Sparse FE solver.

The sparse solver is a direct solution that makes use of the sparseness of FEM formulation to solve for the temperature and heat transfer problems. Currently, this is the only solver available for solving thermal problems.

Material properties of Pure Aluminum rod and its chemical composition has been given below in the Table 3.1and 3.2 respectively.

Table 3.1: Material data for Pure Aluminum Rod for continuous extrusion simulations

S. No.	Parameters	Details
Geometry data		
1	Wheel diameter, *D* mm	350
2	Die diameter, *d* mm	6,7,8
3	Flash-gap size, *G* mm	1
4	Die length, *L* mm	10
Simulation data		
1	Wheel velocity, *N*RPM	4,6,8
2	Feedstock Initial temperature ^{0}C	20
3	Environment temperature ^{0}C	20
4	Time steps seconds	5
5	Die temperature ^{0}C	450
Material data (Feedstock)		
1	Yield stress N/mm^2	31.9
2	Strain rate sensitivity	0.22
3	Heat capacity N/mm^2 ^{0}C	2.3
4	Conductivity N/s^{0}C	238
5	Convection coefficient N/s^{0}C mm	0.02
6	Emissivity	0.3
7	Boltzmann constant N/s^{0}C mm^4	5.669X10^{-11}
8	Interface heat transfer coefficient N/s^{0}Cmm	30
9	Friction coefficient (Interface)	0.8(Feedstock and Wheel groove), 0.9(Shoe and Feedstock),0.95(Abutment and Feedstock) 0.1(Die and Feedstock)

Table 3.2: Chemical composition of Pure Aluminum Rod for continuous extrusion simulations

Elements	Si	Fe	Cu	Mn	Mg	Cr	Others total	Aluminum balance
%	0.5	0.45	0.1	0.05	0	0.1	1%	99%

Pure Aluminum rods are manufactured by up casting process in highly controlled atmosphere so that its purity is not affected by foreign elements.

Yield and ultimate tensile strength in the table have been given for strain rate 0.001/sand they can be changed for other strain rates. Mechanical properties such as tensile strength and hardness for Pure Aluminum rod have been performed and it will be reported in chapter5.Results are very similar to the references and literatures.

3.7 Simulation of 8 mm Aluminum feedstock

The finite element simulation of Aluminum feedstock for 8 mm diameter has been done for different wheel velocities, different friction conditions, different extrusion ratios and the table below shows the input parameters used in the simulations.

The Finite Element Simulation model and CAD model for 8 mm diameter Aluminum feedstock is shown below in Figure 3.2(a) and (b) respectively.

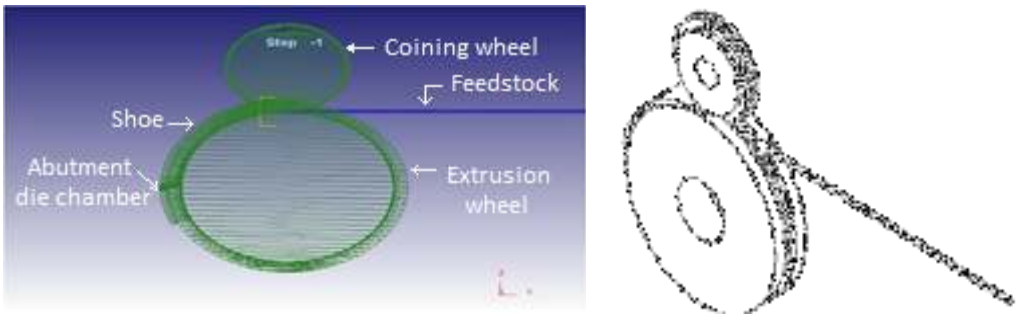

(a) (b)

Figure 3.2: (a) and (b) shows FEA Simulation mesh model and CAD model respectively for 8mm diameter Aluminum feedstock

3.8 Simulation results for 8 mm Aluminum feedstock

The following parameters have been studied after successful run of the finite element simulations for 8mm diameter Aluminum feedstock:

a. The total load required for deformation of the feedstock.
b. The torque required for deformation of the feedstock.
c. The effective stress distribution.
d. The effective strain distribution
e. Damage distribution
f. Temperature distribution
g. Velocity distribution

The details of tetrahedron mesh elements for simulation of 8 mm diameter Aluminum feedstock material has been shown below in Table 3.3.

Table 3.3 Details of tetrahedron mesh elements for 8 mm diameter feedstock

S. No.	Objects	Mesh-Elements
1	Work piece	72580
2	Extrusion Wheel	157019
3	Extrusion shoe	26757
4	Coining Wheel	75902
5	Abutment	75380
6	Die	46132

Figures 3.3 to 3.11 shown below depict the detailed distributions of load, torque, effective stresses, effective strains, temperature and damage value respectively.

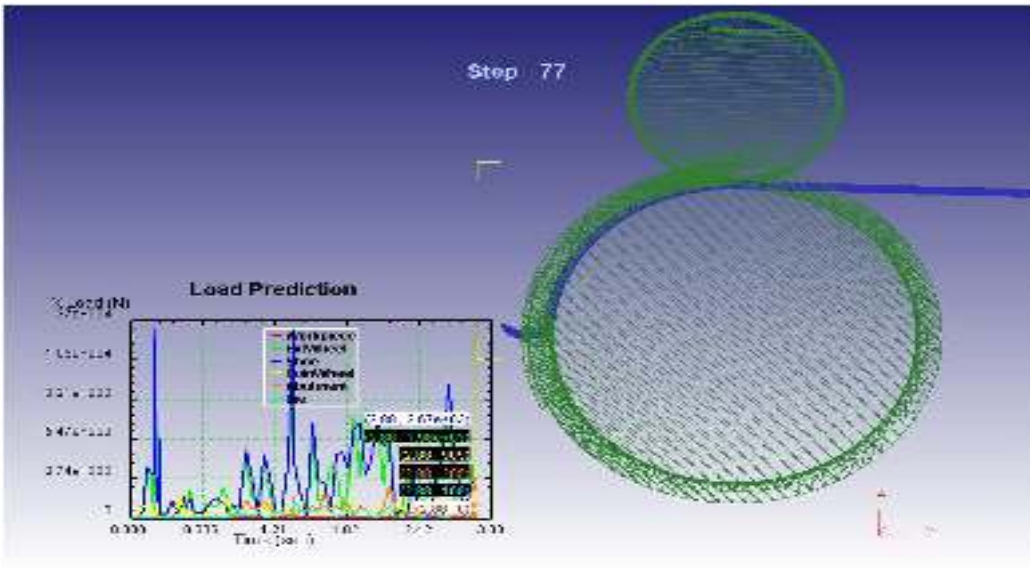

Figure 3.3: X-load distribution for 8 mm Aluminum feedstock material

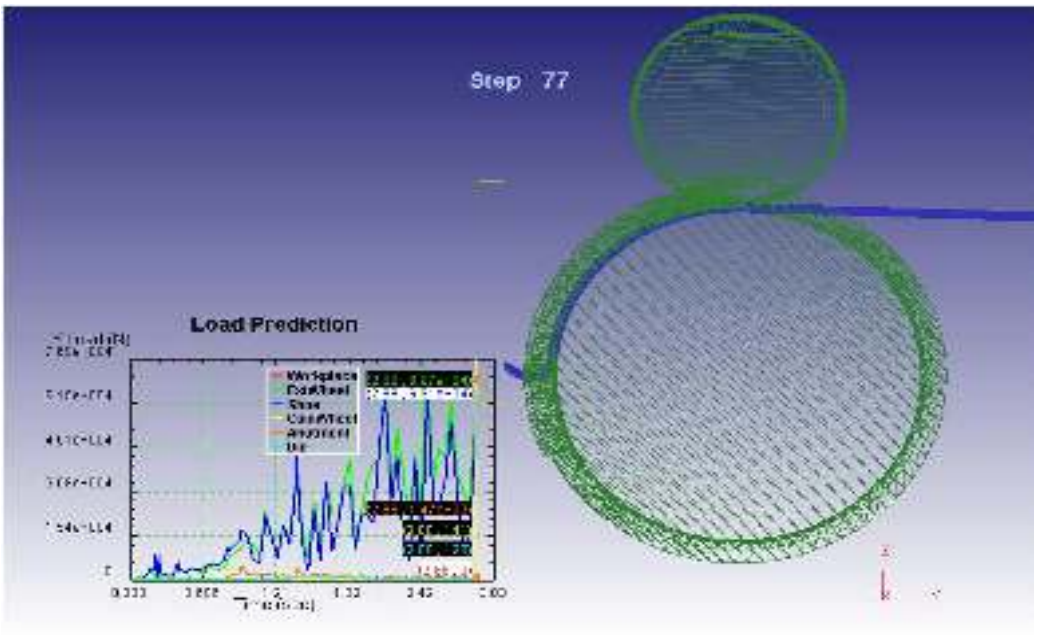

Figure 3.4: Y-load distribution for 8 mm Aluminum feedstock material

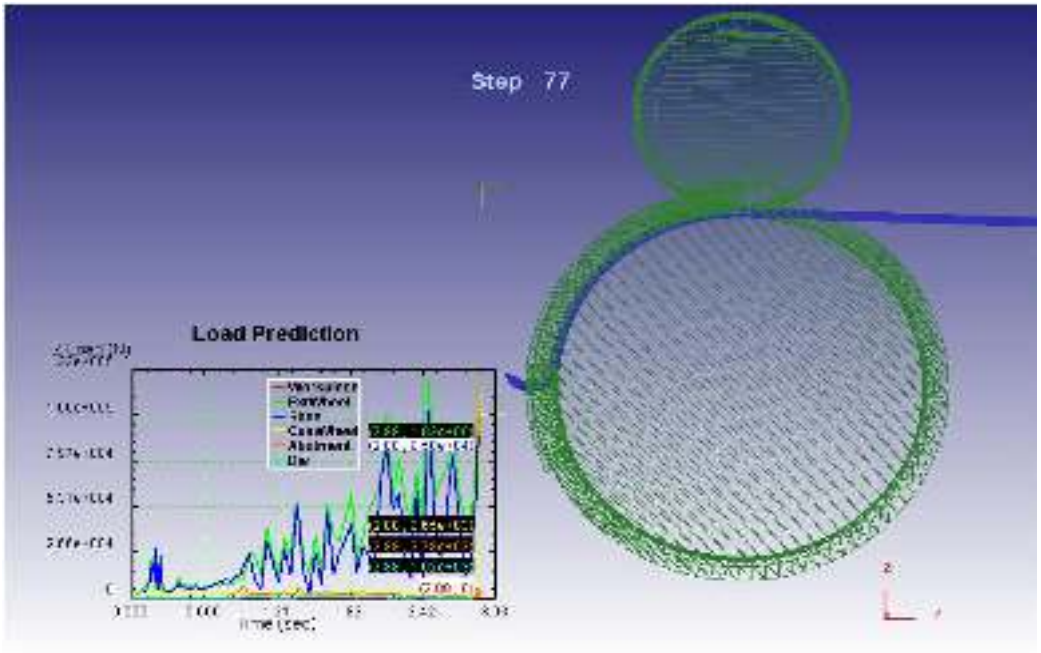

Figure 3.5: Z load distribution for 8 mm Aluminum feedstock material

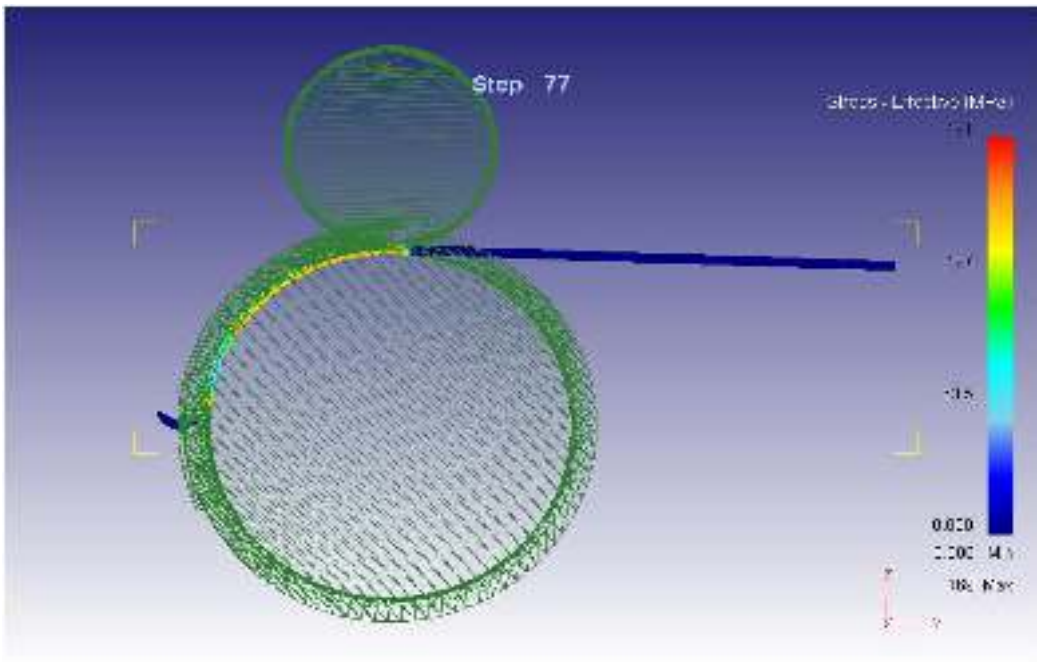

Figure 3.6: Effective stress distribution for 8 mm Aluminum feedstock material

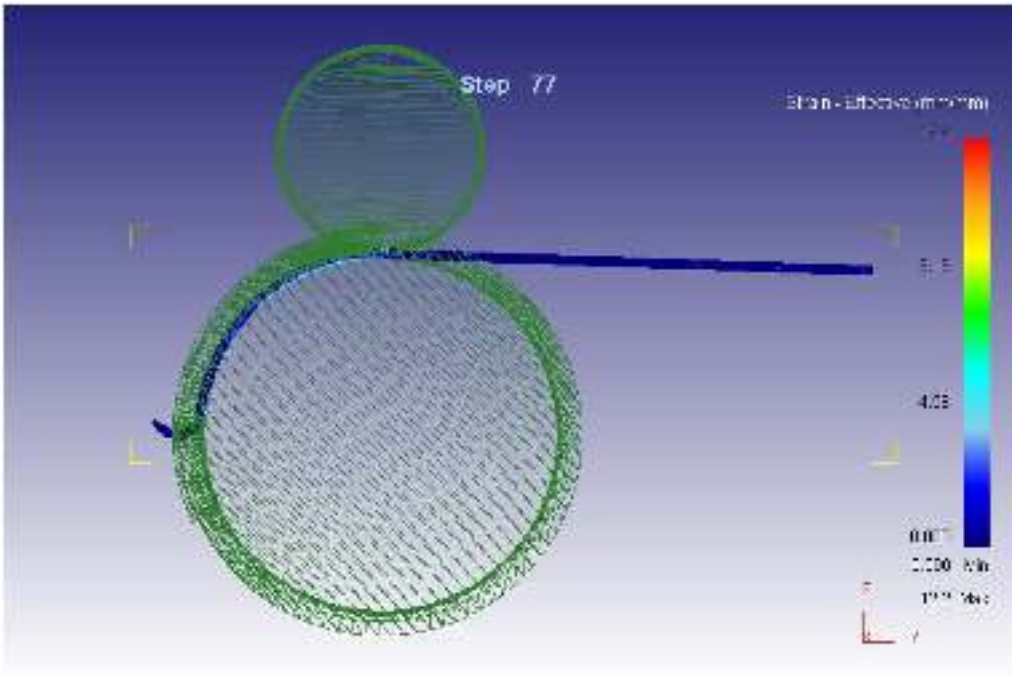

Figure 3.7: Effective strain distribution for 8 mm Aluminum feedstock material

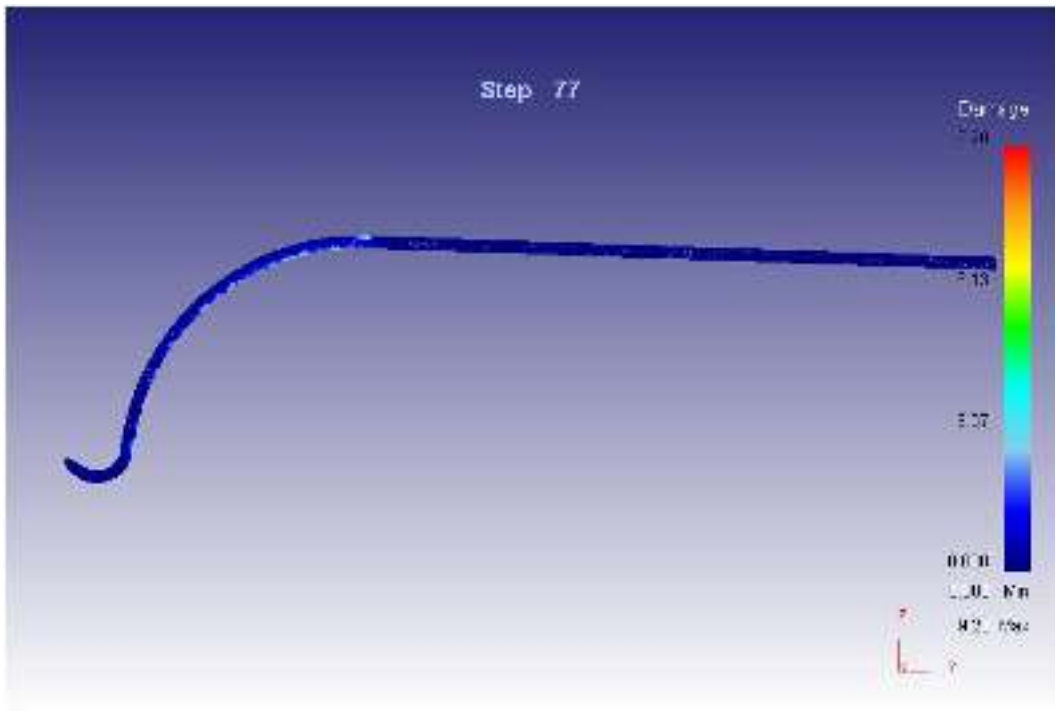

Figure 3.8: Damage distribution for 8 mm Aluminum feedstock material

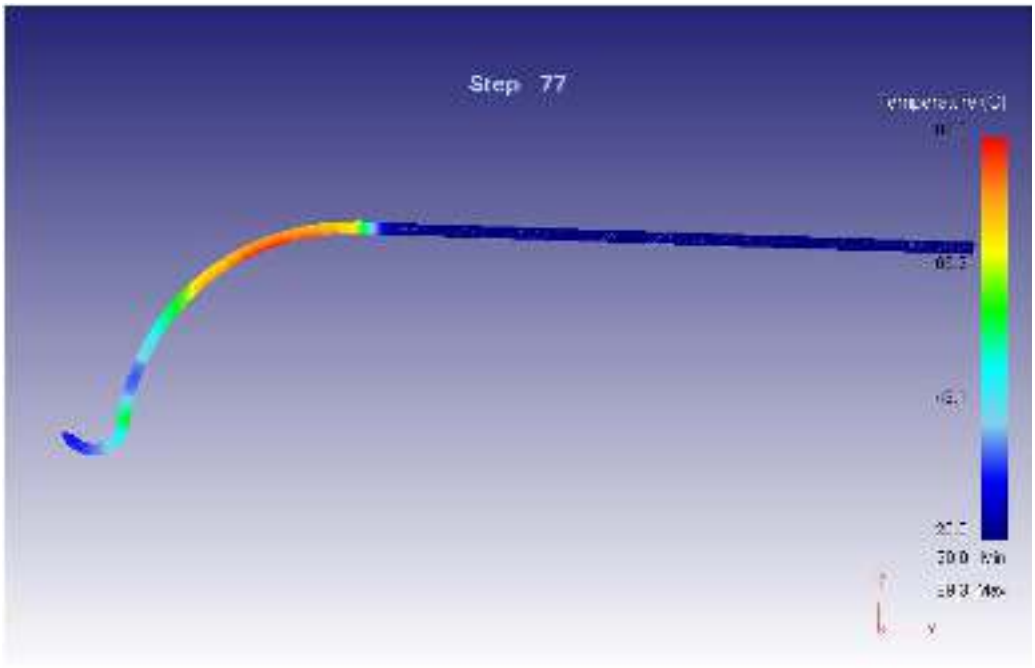

Figure 3.9: Temperature distribution for 8 mm Aluminum feedstock material

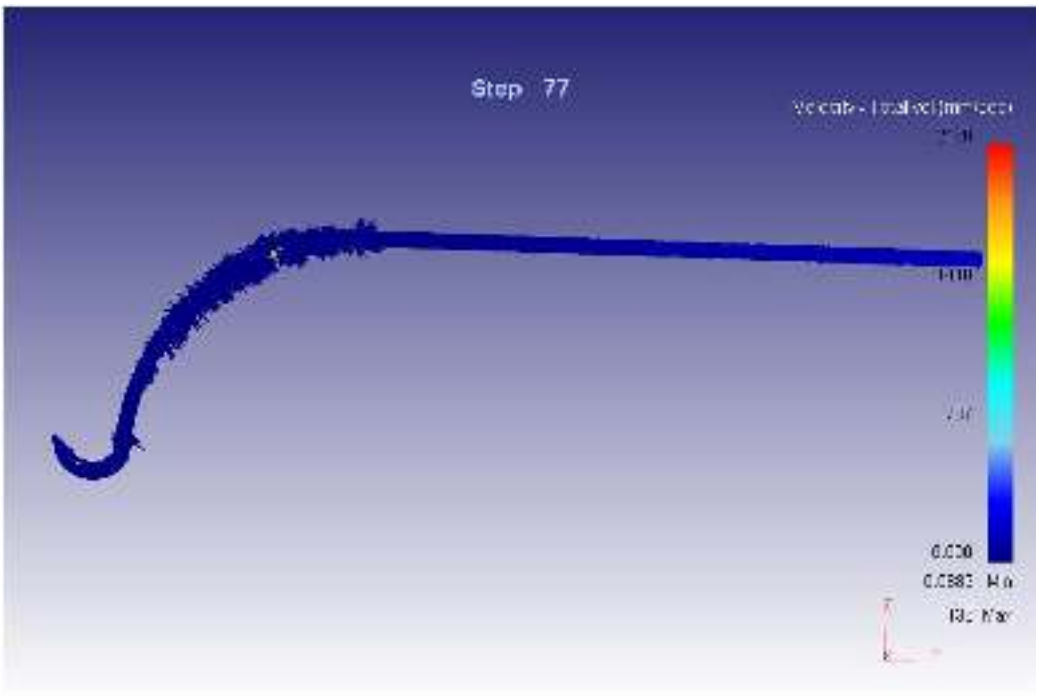

Figure 3.10: Velocity distribution for 8 mm Aluminum feedstock material

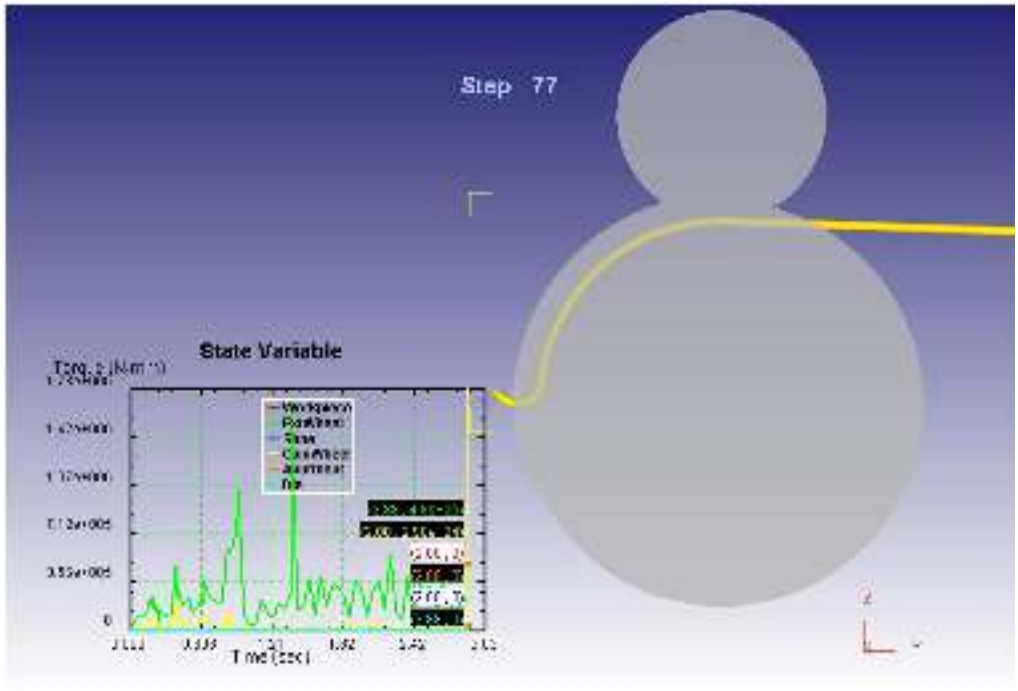

Figure 3.11: Torque distribution for 8 mm Aluminum feedstock material

Table 3.4: The results of simulation for 8 mm diameter Aluminum feedstock.

S. No.	Parameters	Obtained value
1	Total Load	223 kN
2	Total torque	1.78kN-m
3	Effective stress	191MPa
4	Effective strain	12.2
5	Damage value	3.07
6	Maximum temperature	89.3

3.9 Results and Discussions for Simulation of 8 mm diameter Aluminum alloy feedstock

The simulation results for 8 mm diameter Aluminum feedstock material has been tabulated in Table 3.4. The distribution of load in X, Y and Z directions are shown in Figure 3.3-3.5.The distribution of the effective stress, effective strains, temperature and damage are shown in Fig 3.6-3.9. For the analysis of numerical simulation results, the plastic deformation of the feedstock material in whole continuous extrusion process is divided into two basic stages. In the first stage of plastic deformation, deformation of the feedstock material takes place from the entry of feedstock material in the grooved portion of extrusion wheel until it hits the abutment. The second stage of plastic deformation consists of deformation of feedstock material after striking the abutment till the extrusion of feedstock material through the die orifice.

The effective stress distribution curve as shown in Figure 3.6 depicts that stresses increase rapidly at the initial stage during the first stage of forming and then decrease gradually till the feedstock material strikes the abutment. When the feedstock material is extruded through the die orifice, the stresses rises rapidly and then drops sharply thereafter. This type of sudden changes in the value of stress occurs because of the flow characteristics of the feedstock material which depends on the temperature, strain and strain rate. The flow stress characteristics of feedstock material reveals that the flow stress values of AA 1100 increases with increase of strain and strain rate but decreases with increase in temperature. Therefore, when the mechanical energy is converted into heat energy, there is reduction in the value of effective stresses. Since the flow stress of

AA 1100 decreases in a rapid manner with increase in the value of temperature, it is tough to achieve the control of temperature and stresses in continuous extrusion process. If the pressure generated is insufficient for the extrusion to take place, the relative slip between the extrusion wheel and feedstock material will increase thereby increasing the temperature and causing the flow stress to be reduced thereby resulting in faster extrusion. This is the reason for fluctuation of frictional drag in continuous extrusion process. However, the fluctuation of frictional drag is preferred to maintain as small as possible to ensure a well-controlled continuous extrusion process.

The temperature in the close vicinity of the extrusion shoe is higher than other regions in continuous extrusion process. This is because when the feedstock material enters in the primary gripping zone, the friction is very high and heat generated due to plastic deformation between the feedstock material and extrusion shoe is also very high as the extrusion shoe is stationary. However, as far as effective stresses are concerned, the values of effective stresses are higher and maximum in the close vicinity of extrusion wheel than in any other regions. This is because the driving force for the continuous extrusion process comes from the wheel torque and the location closer to the extrusion wheel is subjected to higher compressive forces. The upsetting of the feedstock material with 0.05 effective strains as shown in strain distribution from entry of feedstock material till it hits the abutment in the first stage of forming. In the first stage of forming, increase in the value of rate of strain is very low because of small amount of plastic deformation during this stage. But the heating of feedstock material takes place in this stage because of friction and plastic deformation involved with the feedstock material in this stage. The temperature increases gradually from 20ºC to 42ºC when the feedstock material strikes the abutment in the first stage of forming.

When the extrusion of feedstock material takes place through the abutment die chamber in the second stage of forming, the value of effective strain increases sharply as shown in Fig 3.7 and strain rate also changes rapidly because of huge amount of plastic deformation and high speed of extrusion in this stage. As a result temperature rises which can be clearly seen Fig 3.9. The increase in the value of temperature occurs because of friction and plastic deformation involved in the process. During the first stage of plastic deformation, the increase in the value of temperature occurs due to upsetting of the

feedstock material and the friction involved between the grooves of extrusion wheel and feedstock material. In the second stage of forming, the temperature rise takes place due to large amount of plastic deformation when the feedstock material reaches the die orifice. Figure 3.8 depicts the damage distribution. Damage, generally relates to the chances of fracture of a part. In general, designing with a damage value from 0 to 1 is considered to be safe from fracture. Damage value decreases with the increase of the extrusion wheel angular velocities.

Figure 3.10 shows the velocity distribution of Aluminum feedstock material during continuous extrusion process. The change in the flow velocity is higher in the close vicinity of flash gap than that of die. With increase in extrusion wheel angular velocity, the metal flow velocity increase in the die orifice gradually.

Figure 3.11 shows the time evolution of the calculated torque between the feedstock and the wheel. With the increase of the contact area between the wheel and the feedstock, torque increases linearly until the feedstock hits the abutment. At this point, a large extrusion pressure is generated at the front of the die. Since the extrusion speed is controlled by the frictional drag between the feedstock and the groove, it is essential that the relative slip between the two is as low as possible to ensure a stable extrusion speed. The simulation shows that the calculated torque fluctuates with time within a small range that minimizes the slip. The time fluctuations of the frictional drag are reflected in fluctuations of extrusion speed, which can at worst mechanically damage the product and at least cause unacceptable variation in the size of the product.

Because of the large ratio of cross-sectional reduction in the continuous extrusion process, it is necessary to allow for re-meshing of the computational domain during the simulation. Such re-meshing can be carried out automatically using the DEFORM system. The meshes of the feedstock are very uniform at the beginning of the simulation and after that it becomes geometry dependent meshes at steady state. The automatic mesh generation provides a very powerful tool by means of which extrusion process can be modeled. Since the large plastic deformation in the work piece causes severe mesh distortion, necessitating very frequent re-meshing of the computational domain.

3.10 Simulation of 9.5 mm diameter Aluminum rod

The details of parameters and mesh elements for simulation of 9.5 mm Aluminum feedstock material have been tabulated in Table 3.5 and Table 3.6 respectively.

Table 3.5: Simulation parameters for 9.5 mm Aluminum feedstock

S. No.	Parameters	Details
	Geometry data	
1	Wheel diameter, *D* mm	350
2	Die diameter, *d* mm	6,7,8
3	Flash-gap size, *G* mm	1
4	Die length, *L* mm	10
	Simulation data	
1	Wheel velocity, *N* RPM	4,6,8,10
2	Initial temperature ^{0}C	20
3	Environment temperature ^{0}C	20
4	Die temperature ^{0}C	450
	Feedstock Material data	
	Material	Al 1100
1	Yield stress N/mm^2	31.9
2	Strain rate sensitivity	0.22
3	Heat capacity N/mm^2 ^{0}C	2.3
4	Conductivity N/s^{0}C	238
5	Convection coefficient N/s^{0}C mm	0.02
6	Emissivity	0.3
7	Boltzmann constant N/s^{0}C mm^4	5.669X10^{-11}
8	Interface heat transfer coefficient N/s^{0}Cmm	30
9	Interface Friction coefficient	0.95(Feedstock and Wheel groove), 0.95(Shoe and Feedstock),0.95(Abutment and Feedstock) 0.05(Die and Feedstock)

Table 3.6: Details tetrahedron of mesh elements for 9.5mm diameter Aluminum feedstock

S. No.	Objects	Mesh-Elements
1	Work piece	72580
2	Extrusion Wheel	157019
3	Extrusion shoe	26757
4	Coining Wheel	75902
5	Abutment	75380
6	Die	46132

Figures 3.12 to 3.22 shown below depicts the detailed distributions of load, torque, effective stresses, effective strains, damage, temperature and damage for 9.5 mm Aluminum feedstock.

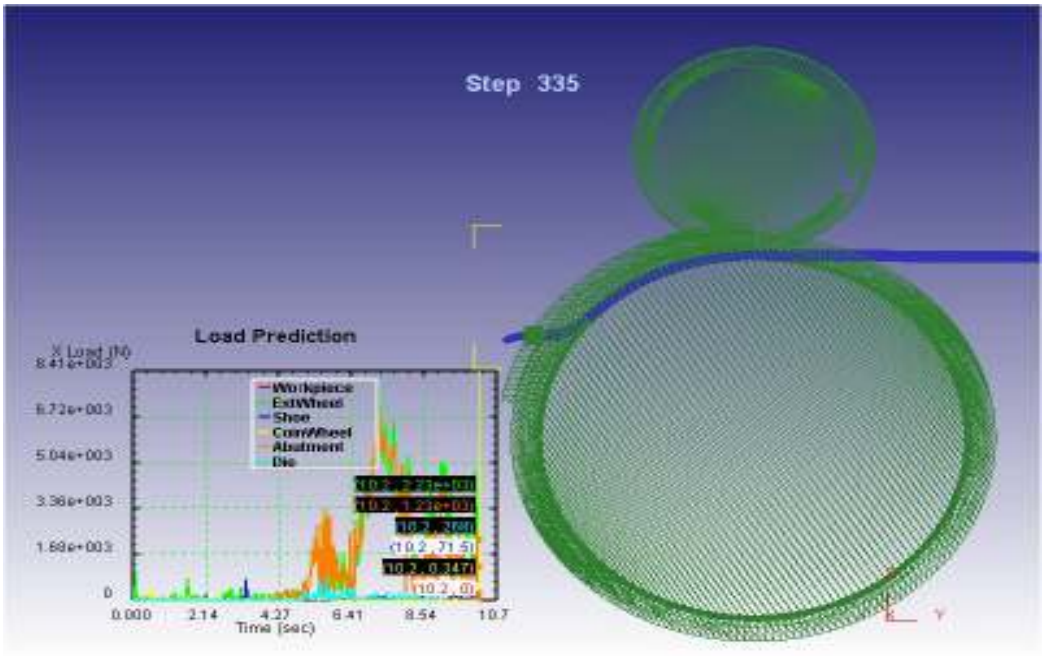

Figure 3.12: X load distribution for 9.5 mm Aluminum feedstock material

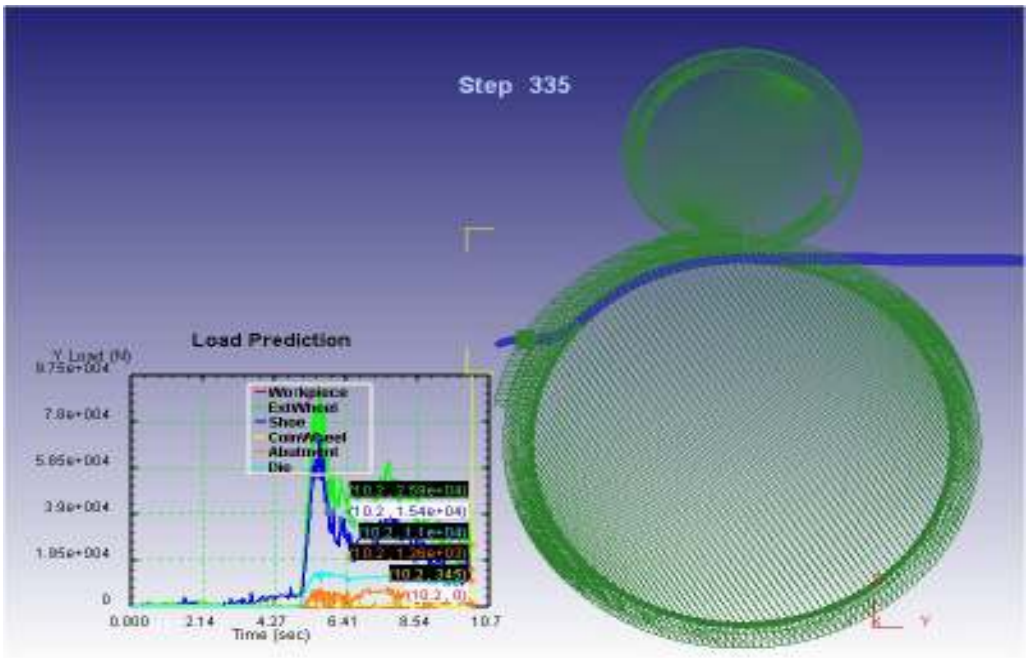

Figure 3.13: Y load distribution for 9.5 mm Aluminum feedstock material

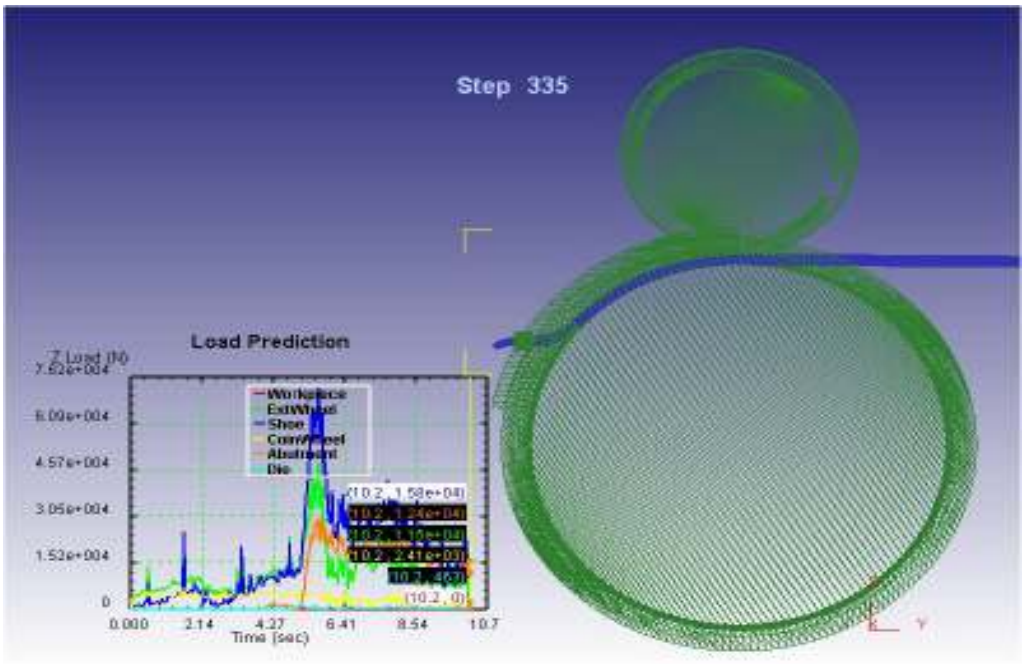

Figure 3.14: Z load distribution for 9.5 mm Aluminum feedstock material

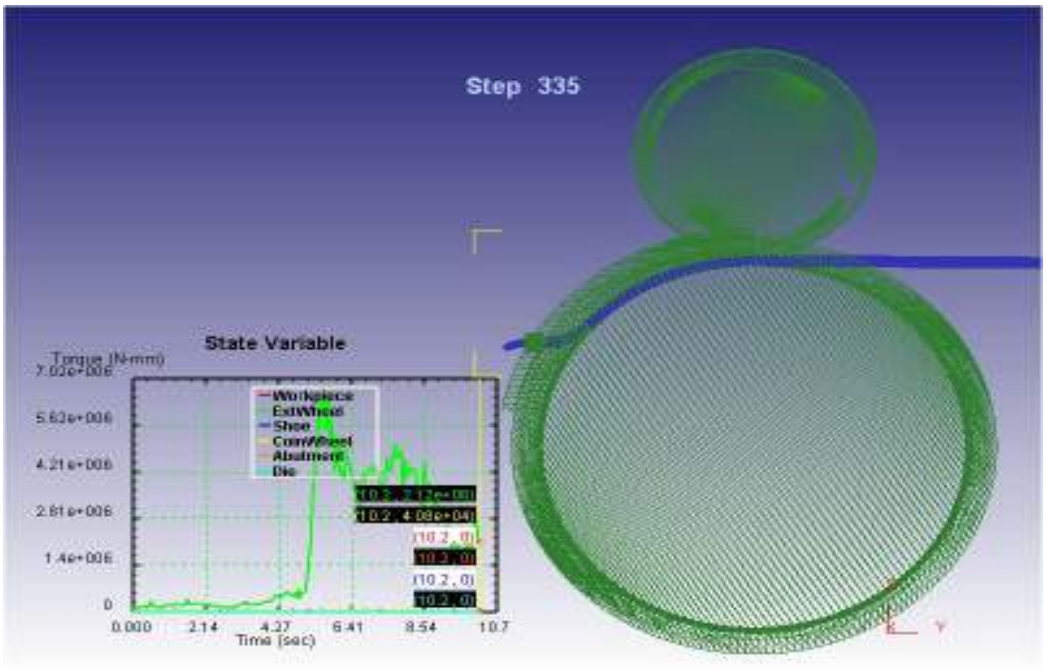

Figure 3.15: Torque distribution for 9.5 mm Aluminum feedstock material

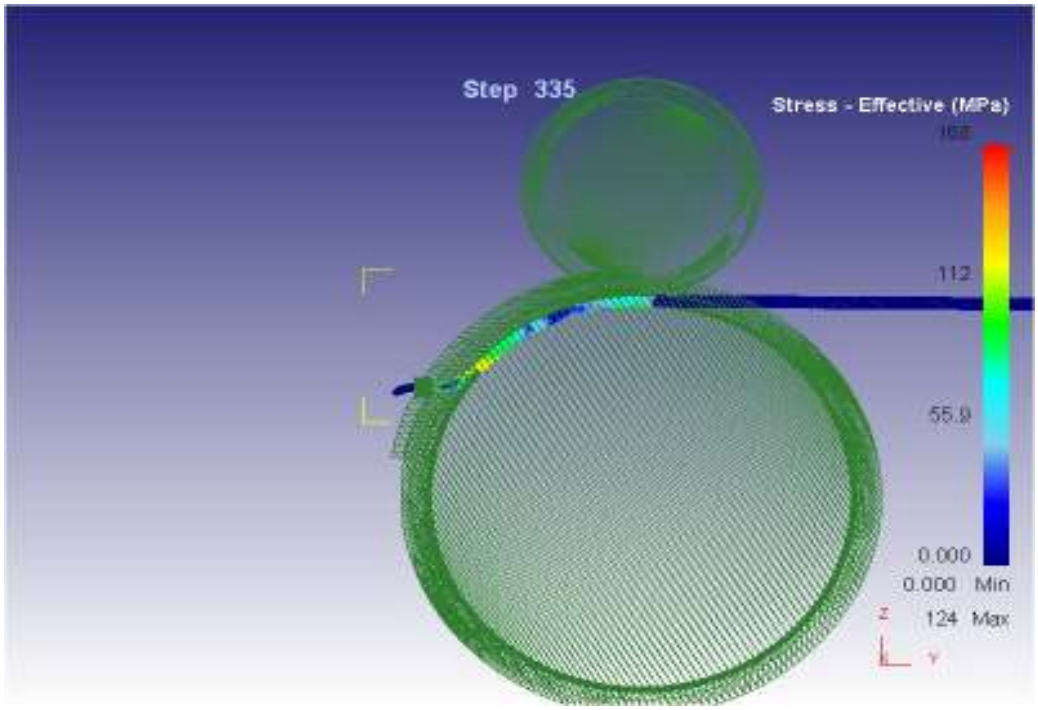

Figure 3.16: Effective stress distribution for 9.5 mm Aluminum feedstock material

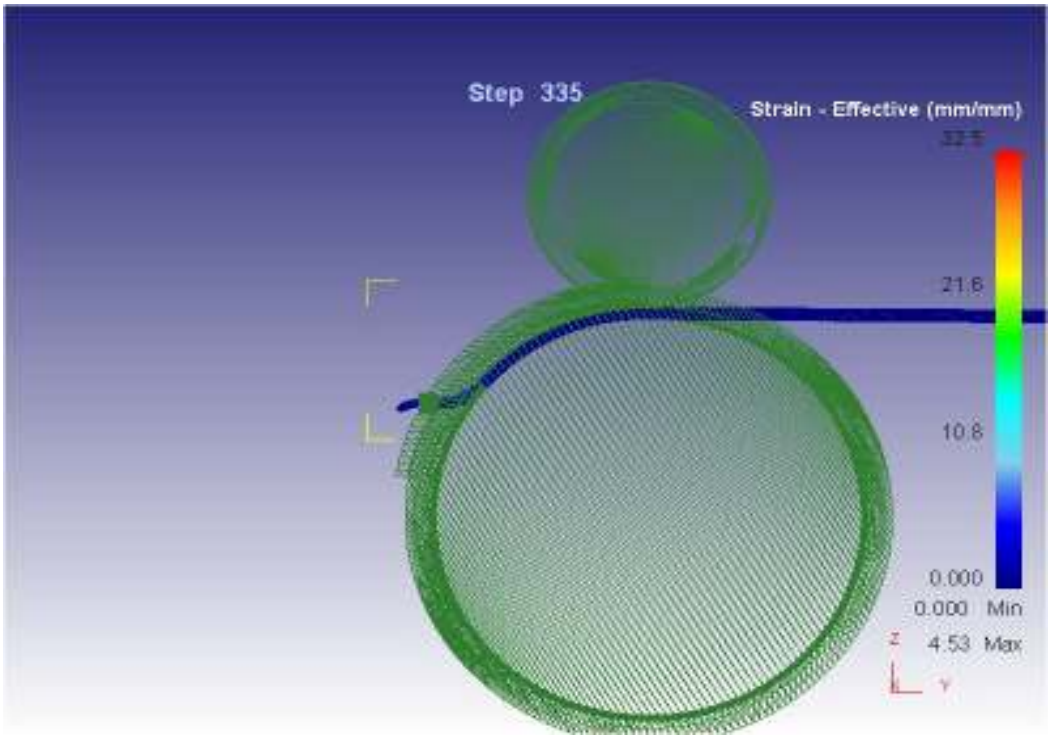

Figure 3.17: Effective strain distribution for 9.5 mm Aluminum feedstock material

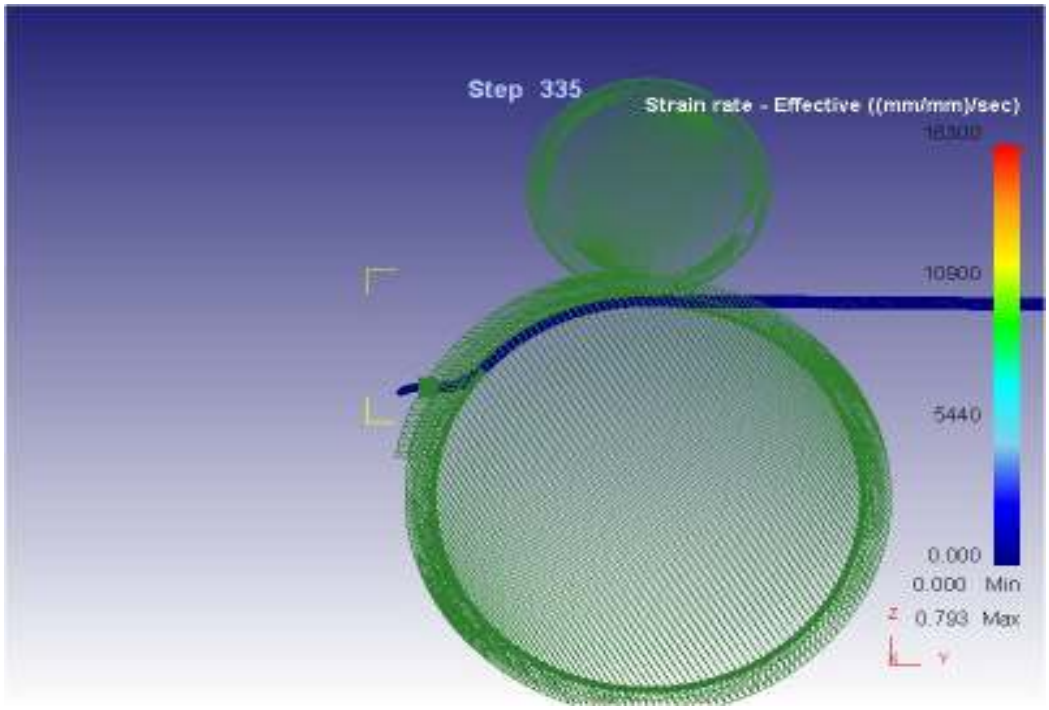

Figure 3.18: Effective strain rate distribution for 9.5 mm Aluminum feedstock material

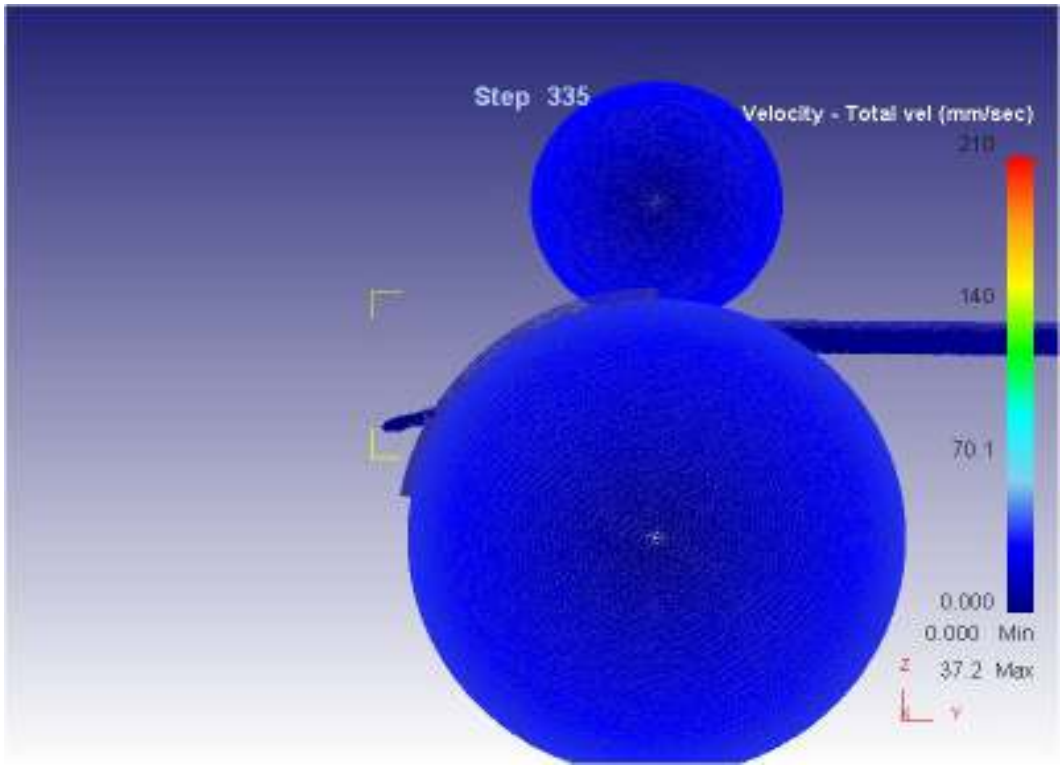

Figure 3.19: Velocity distribution for 9.5 mm Aluminum feedstock material

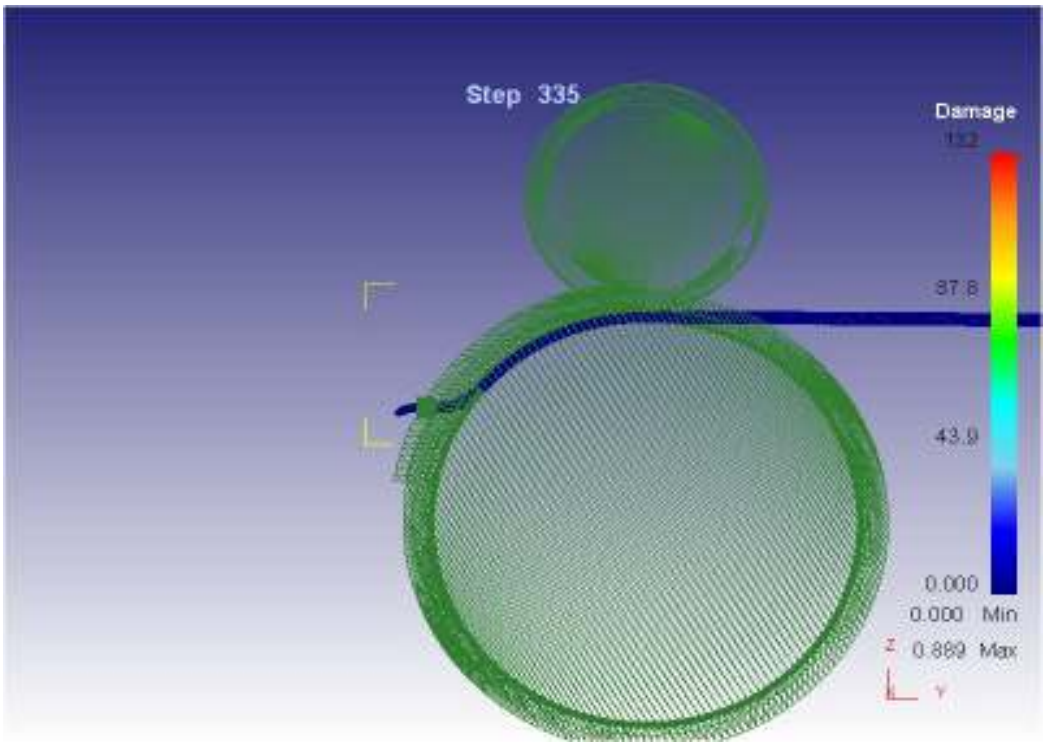

Figure 3.20: Damage distribution for 9.5 mm Aluminum feedstock material

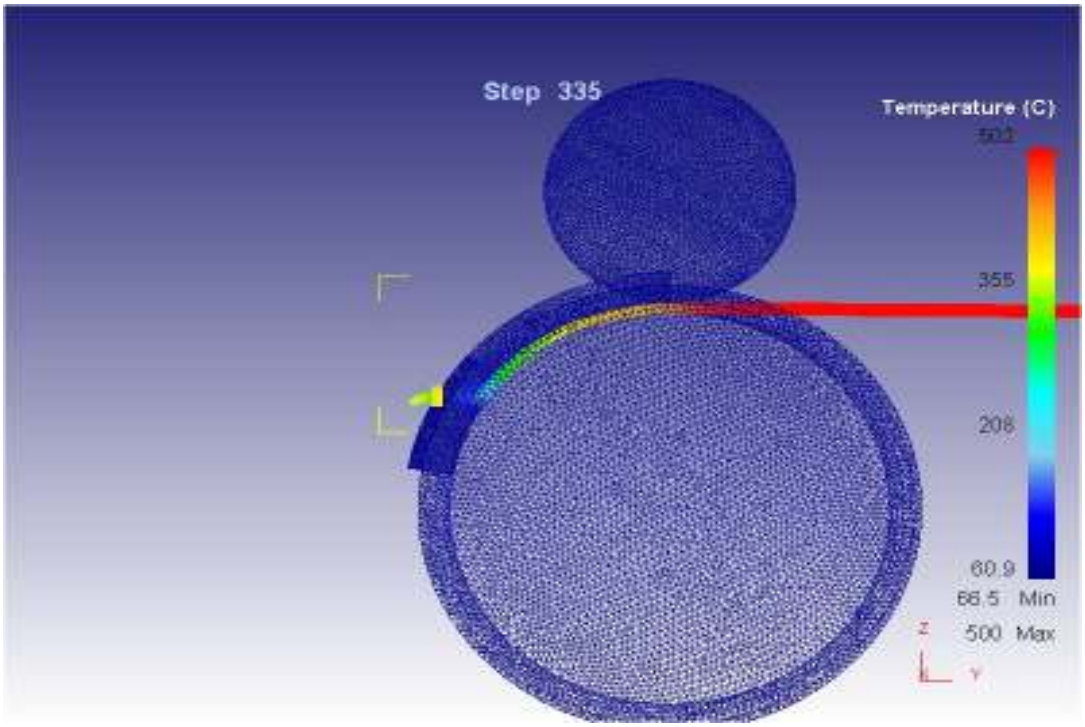

Figure 3.21: Temperature distribution for 9.5 mm Aluminum feedstock material

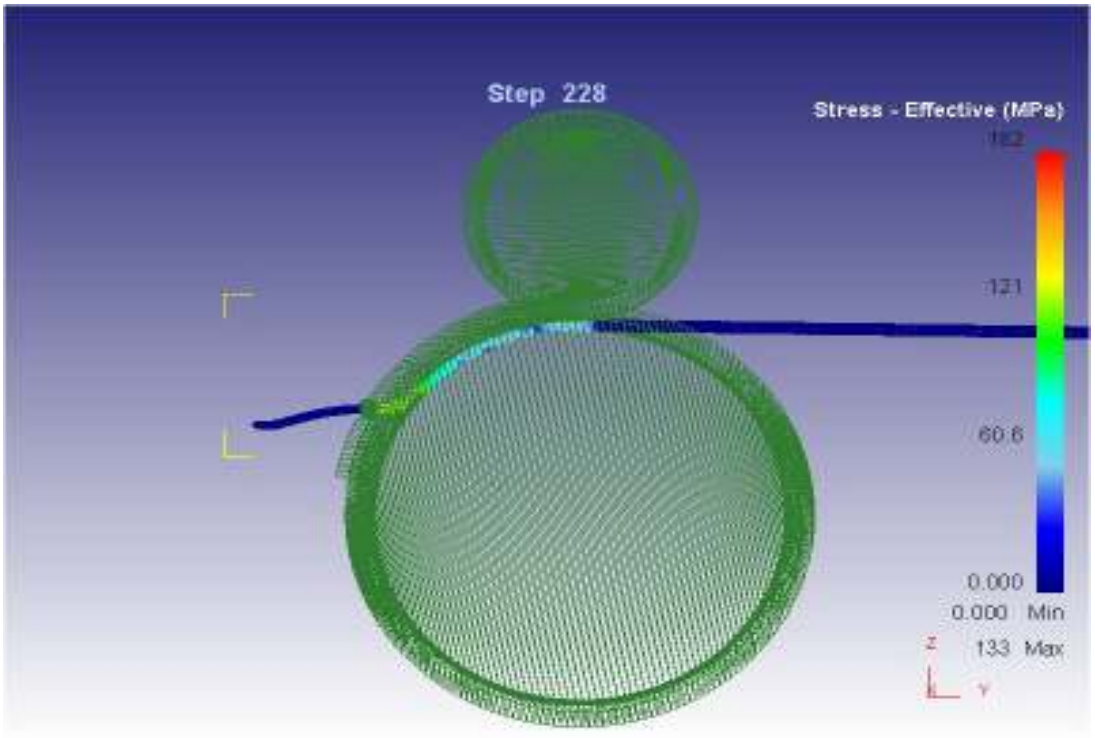

Figure 3.22: Effective stress distribution at 100 º C for 9.5 mm Aluminum feedstock materials

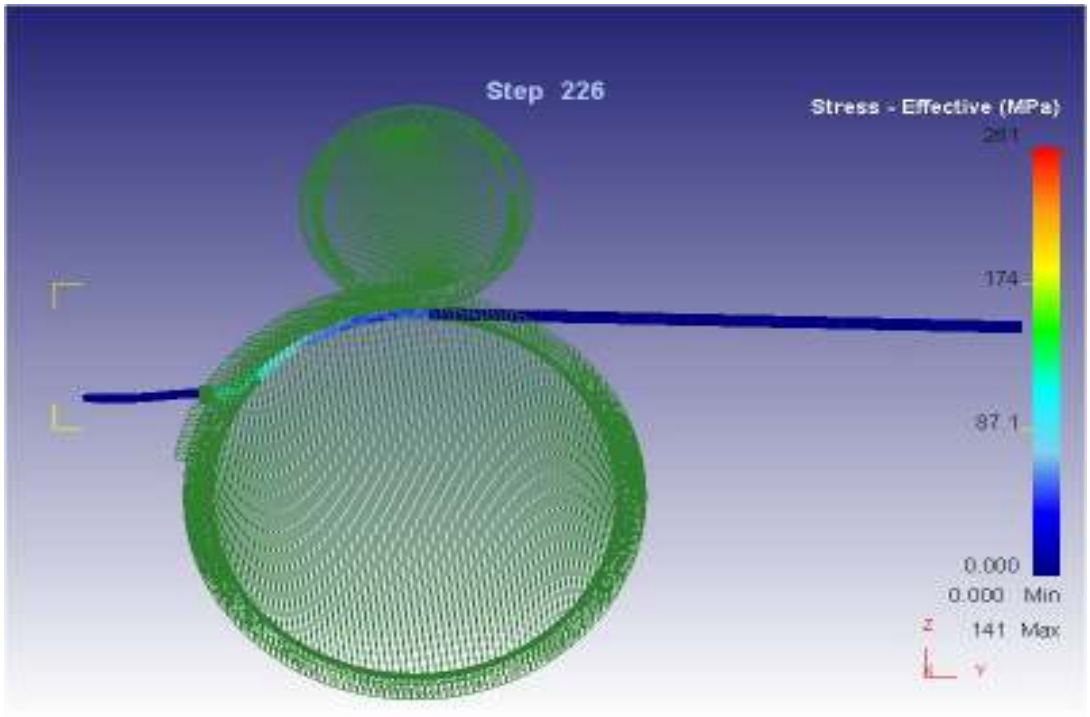

Figure 3.23: Effective stress distribution at 300 ºC for 9.5 mm Aluminum feedstock material

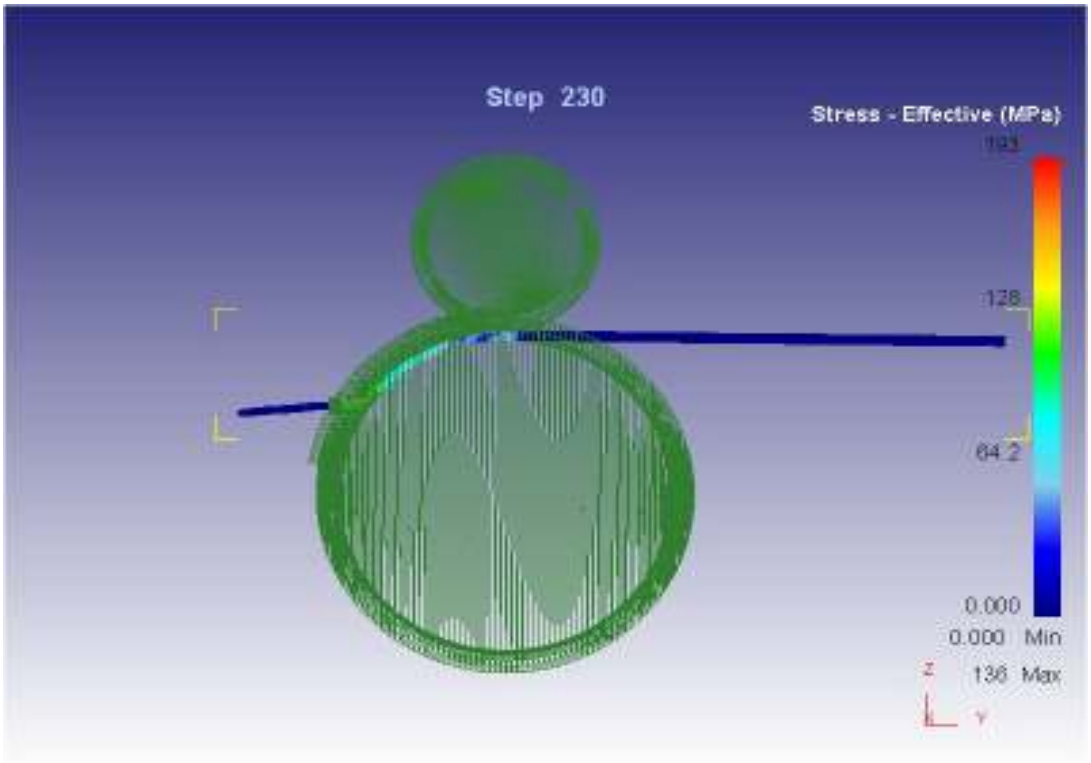

Figure 3.24: Effective stress distribution at 700 ºC for 9.5 mm Aluminum feedstock material

Distribution of effective stress

Figures3.22-3.24 shows the distribution of effective stress field under different feedstock temperature. The effective stresses near the die orifice increases considerably with increasing the temperature of feedstock. The concentrations of effective stresses are very high in the adjacent regions of the flash gap. The concentration of effective stresses varies considerably with the variation of feedstock temperatures. Since, the effective stresses are very high near the die orifice; the material of the abutment should have high strength to withstand the effective stresses.

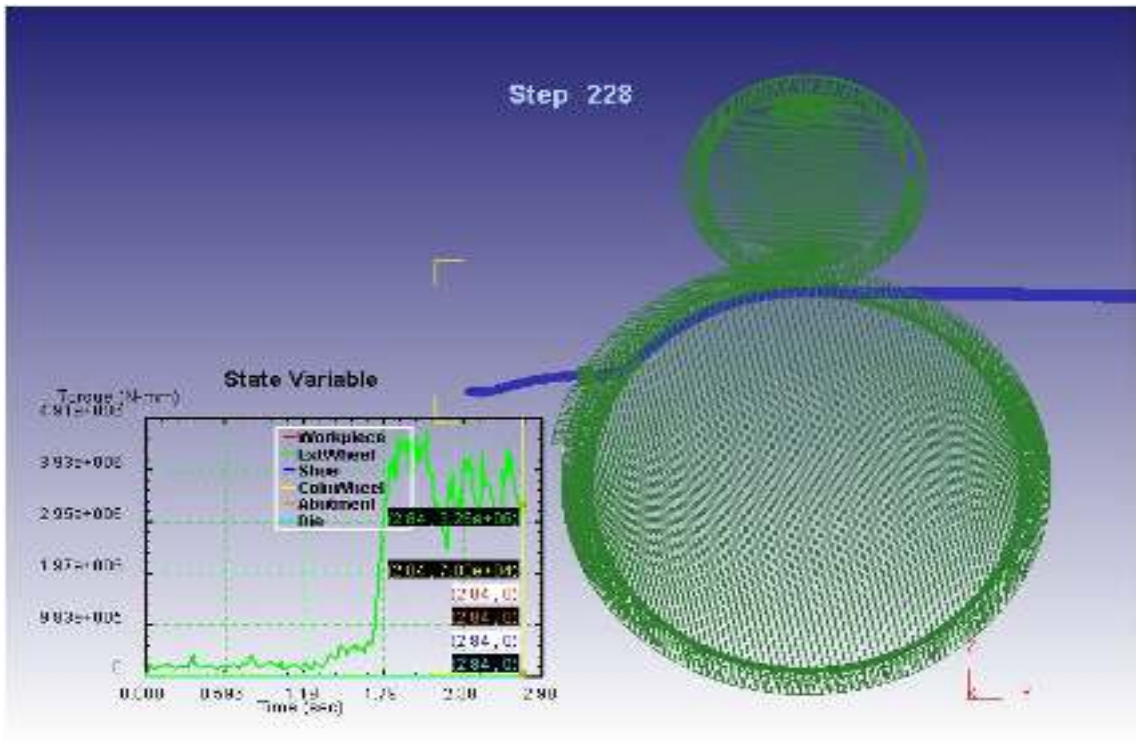

Figure 3.25: Torque distribution at 100 º C for 9.5 mm Aluminum feedstock materials

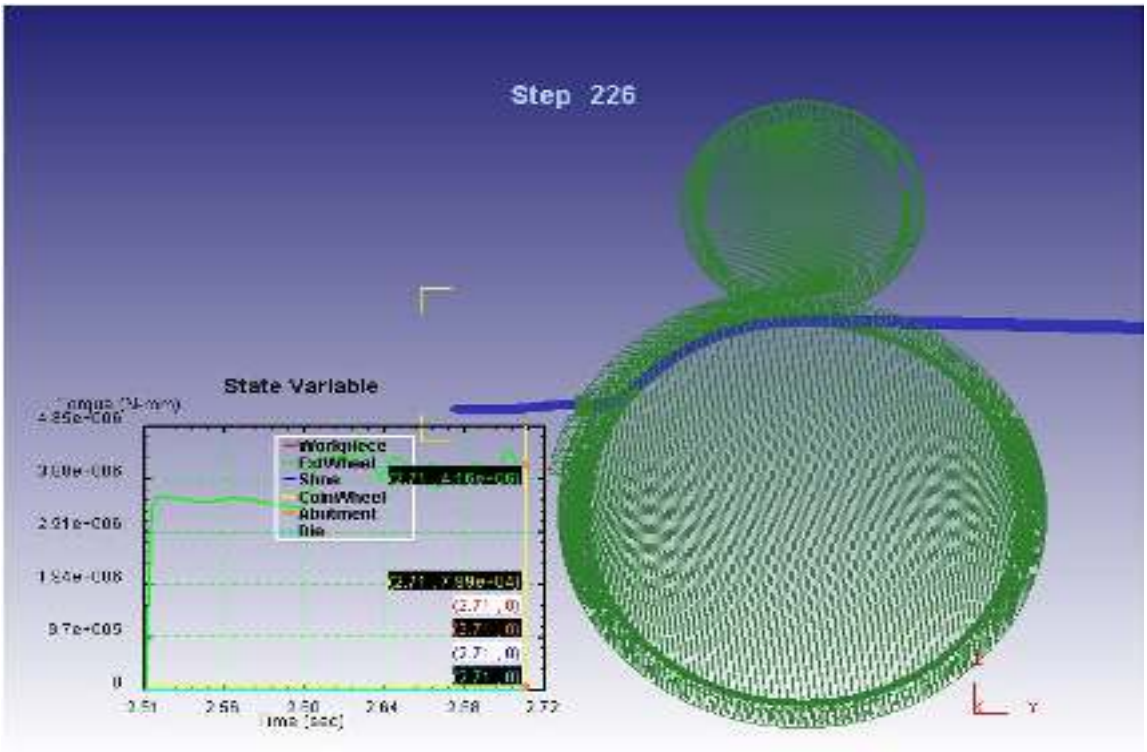

Figure 3.26: Torque distribution at 300 ºC for 9.5 mm Aluminum feedstock material

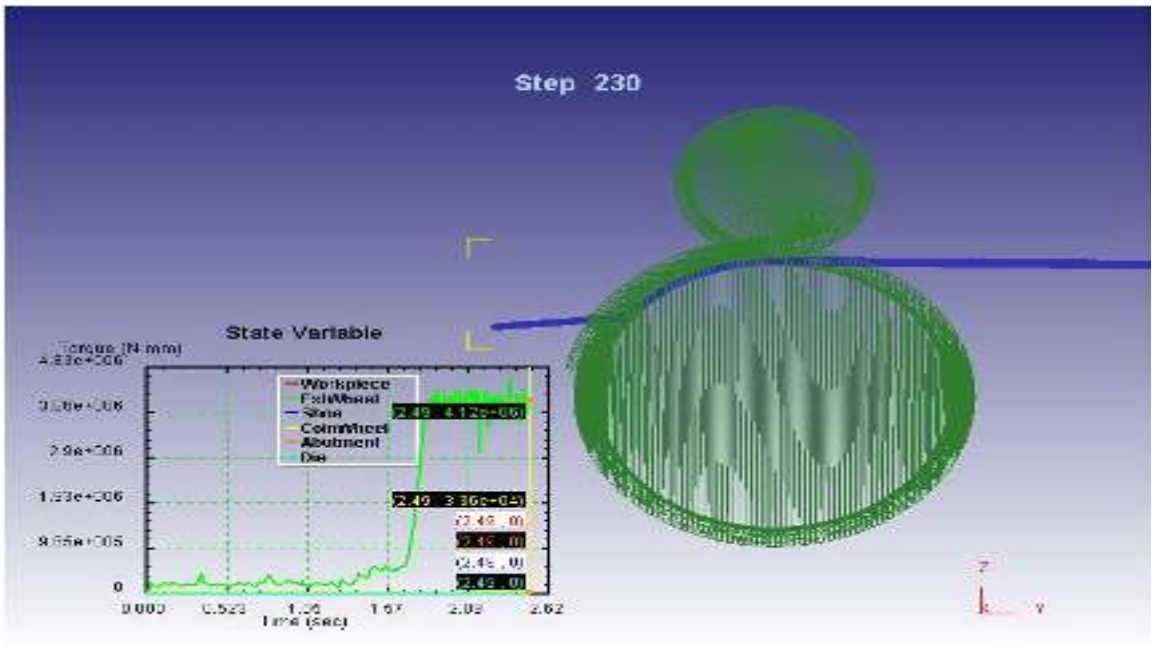

Figure 3.27: Torque distribution at 700 º C for 9.5 mm Aluminum feedstock materials

Distribution of Torque required

Figures 3.25-3.27 shows the distribution of torque under the different feedstock temperatures. The total torque required for the deformation of feedstock material is considerably reduced with the increase of feedstock temperature. Table 3.7 below shows the effect of temperature of feedstock in continuous extrusion process of Aluminum alloy on different process parameters for a specific value of extrusion wheel velocity, frictional condition, die size and die temperature.

Table 3.7: Simulation results in tabular form representing effect of feedstock temperature in Continuous Extrusion of Aluminum feedstock

Feedstock Temperature ^{0}C	Total Load kN	Torque kN-m	Effective Stresses MPa	Effective Strains mm/mm	Damage	Product Temperature ^{0}C	Strain rate mm/mm/s
100	110.96	4.91	133	8.55	0.872	239	120
300	102.79	4.85	141	8.40	0.97	359	398
700	111.95	4.83	136	8.89	0.861	701	169

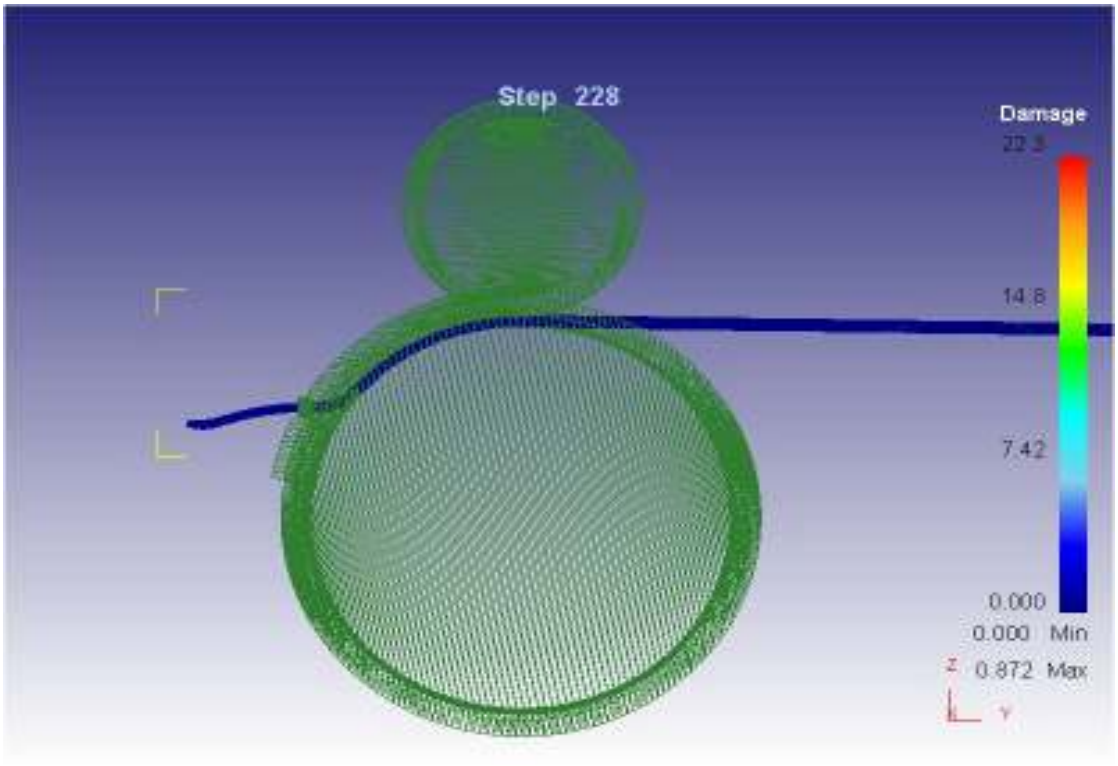

Figure 3.28: Damage distribution at 100 ºC for 9.5 mm Aluminum feedstock material

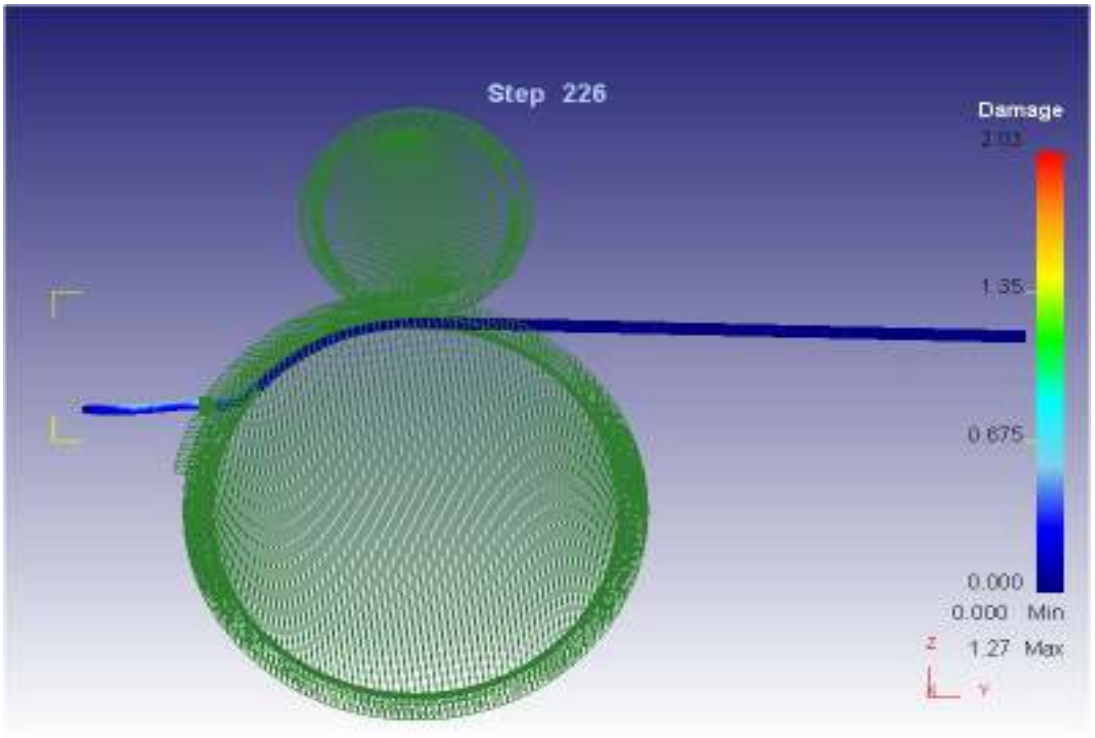

Figure 3.29: Damage distribution at 300 ºC for 9.5 mm Aluminum feedstock material

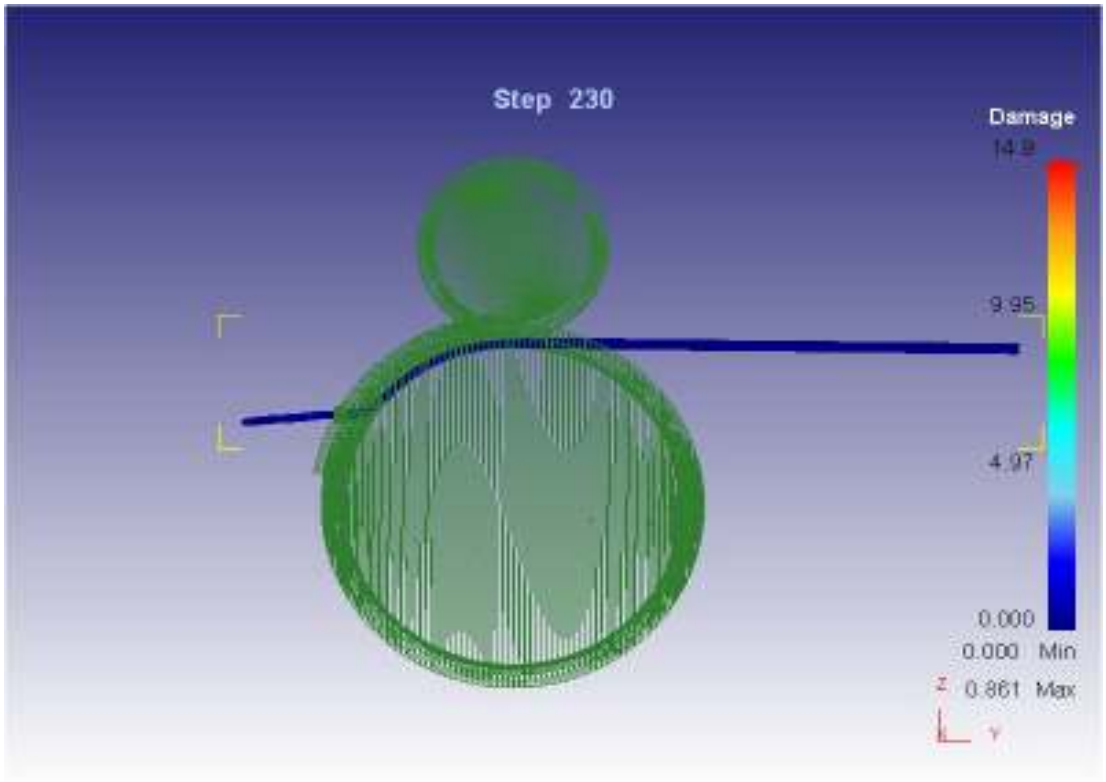

Figure 3.30: Damage distribution at 700 ºC for 9.5 mm Aluminum feedstock material

Distribution of damage field

The study of damage distribution is generally related to the quality of product obtained through the die orifice and also the quality of feedstock material at the intermediate stages of the process when it passes through the primary and secondary zone through contact spaces of extrusion wheel and shoe. In general, damage value less than 1 is considered to be safe from fracture .Figure 3.28-3.30 shows the detailed distribution of damage field under different feedstock temperatures. It can be seen from the figure that damage values lies in the safer zone under these feedstock temperatures. Damage value generally increases with the increase of feedstock temperature.

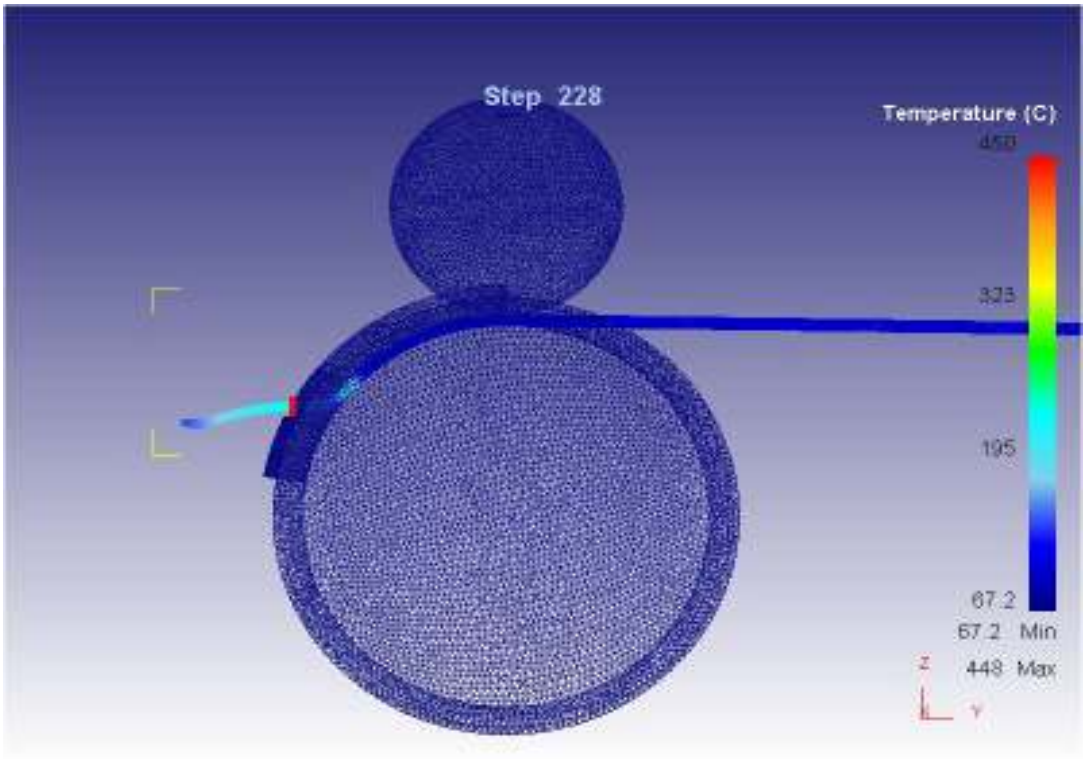

Figure 3.31: Temperature distribution at 100 ºC for 9.5 mm Aluminum feedstock material

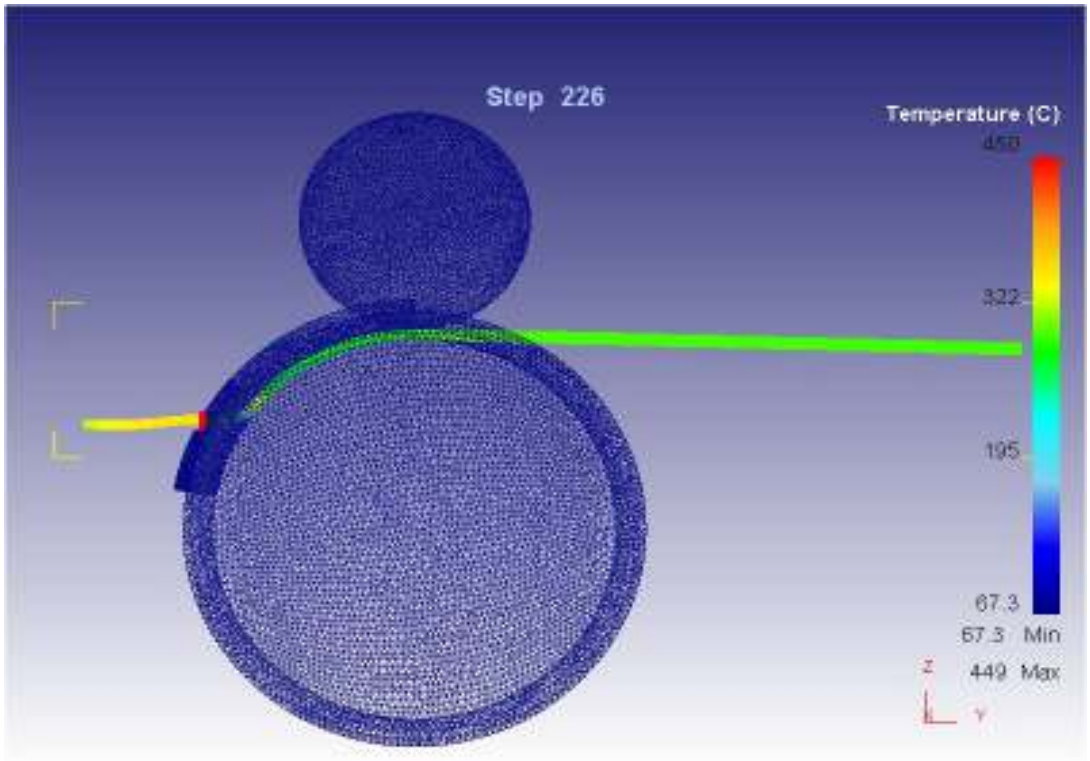

Figure 3.32: Temperature distribution at 300 ºC for 9.5 mm Aluminum feedstock material

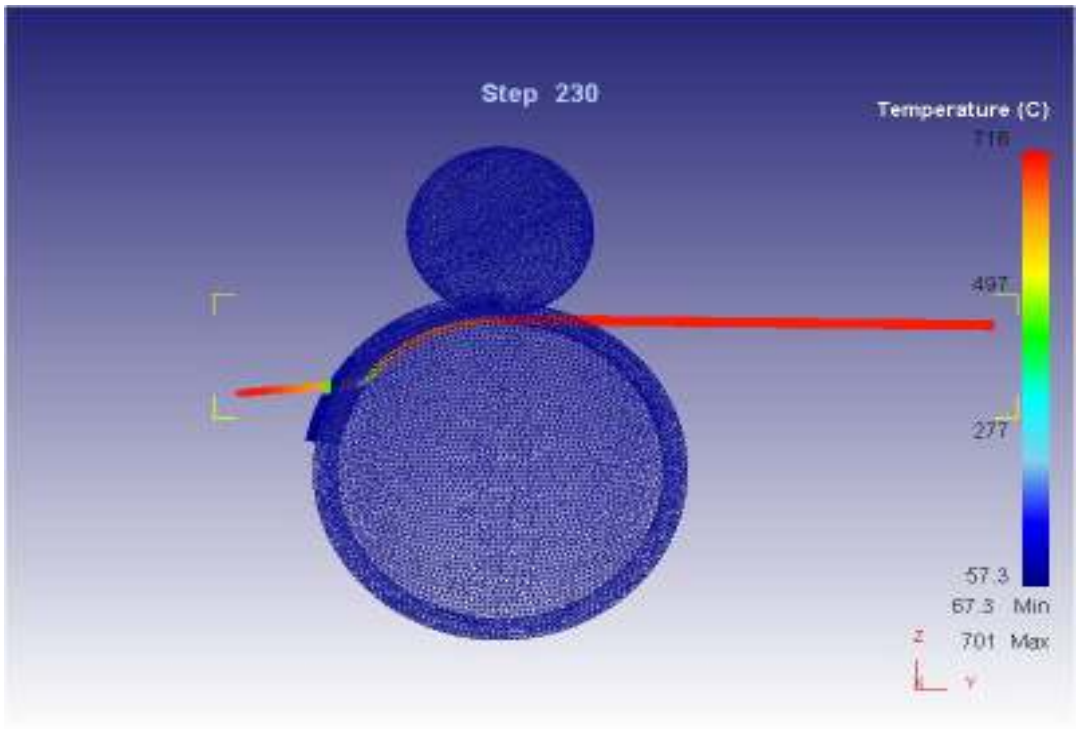

Figure 3.33: Temperature distribution at 700 ºC for 9.5 mm Aluminum feedstock material

Distribution of temperature field

Figure 3.31-3.33 shows the distribution of temperature under the different feedstock temperatures. During the deformation process, the deformation body temperature increases considerably due to friction and shear deformation. The deformation body temperature reaches to 701 ^{0}C if the feedstock temperature is very high. The toolings in continuous extrusion process cannot work for a long if the temperature exceeds to a limiting value. So, the cooling's become necessary. With increasing the temperature of feedstock, the deformation body temperature increases gradually.

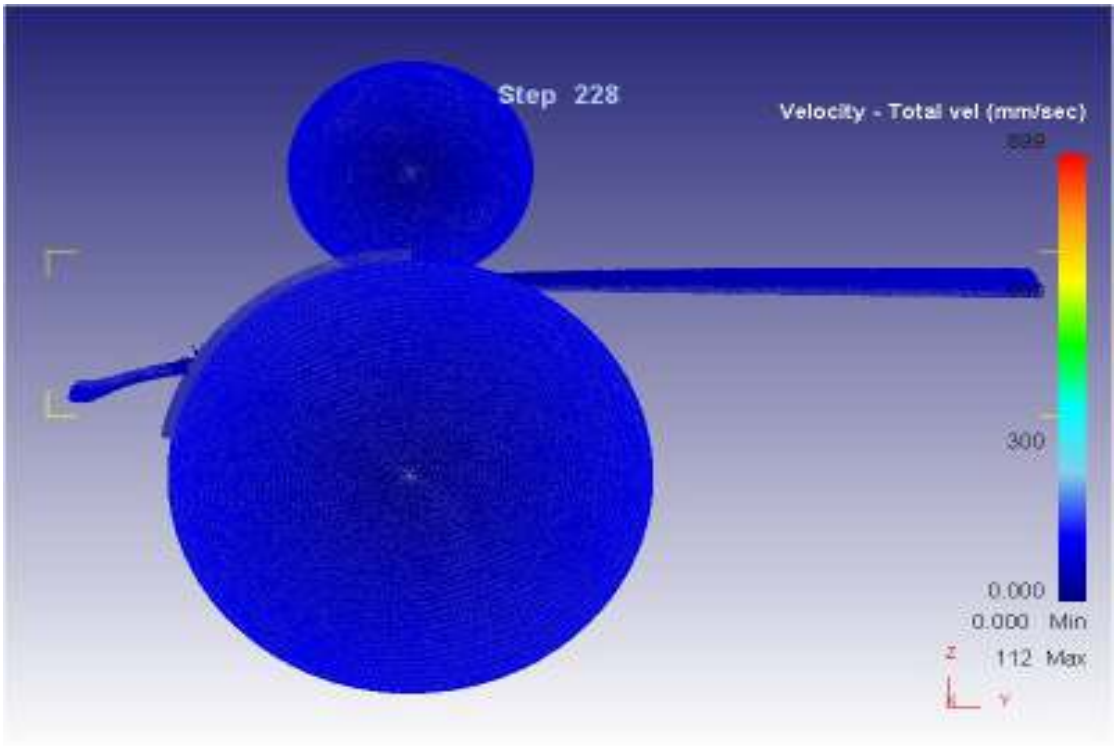

Figure 3.34: Velocity distribution at 100 ºC for 9.5 mm Aluminum feedstock material

Distribution of Velocity field

Figure 3.34-3.36 shows the distribution of deformation body velocity field under different feedstock temperatures. It is clear from the figure that material flow velocity increases with the increase of feedstock temperatures. The velocity gradient is higher in the flash gap region than that of die orifice region.

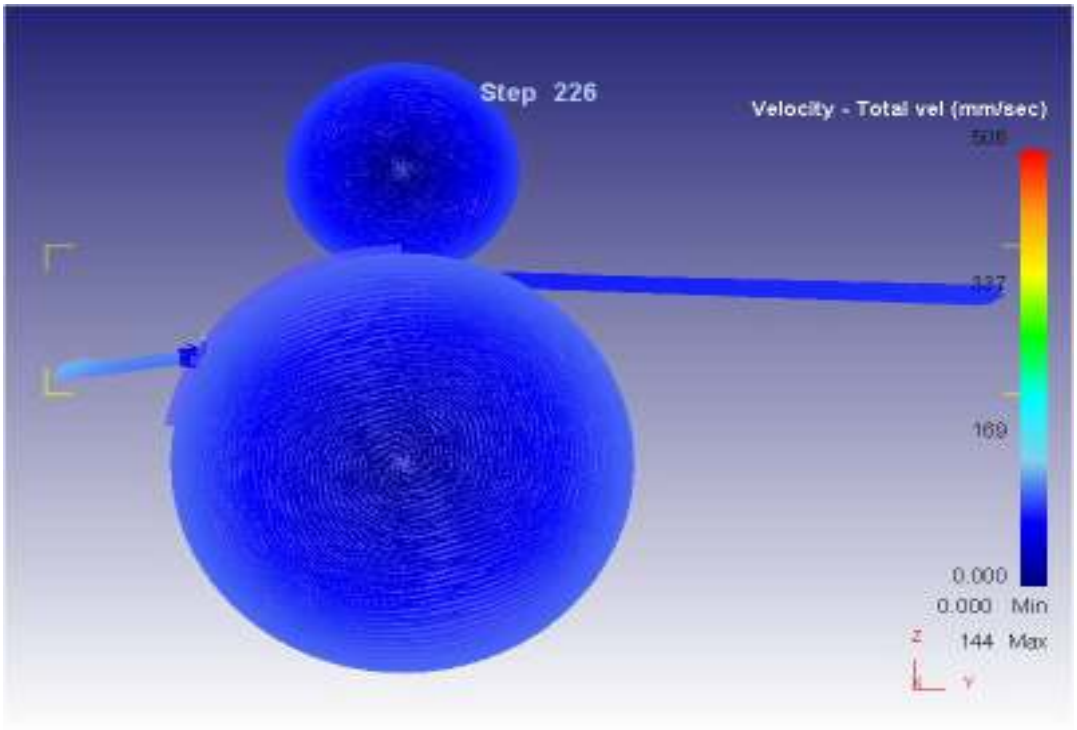

Figure 3.35: Velocity distribution at 300 ºC for 9.5 mm Aluminum feedstock material

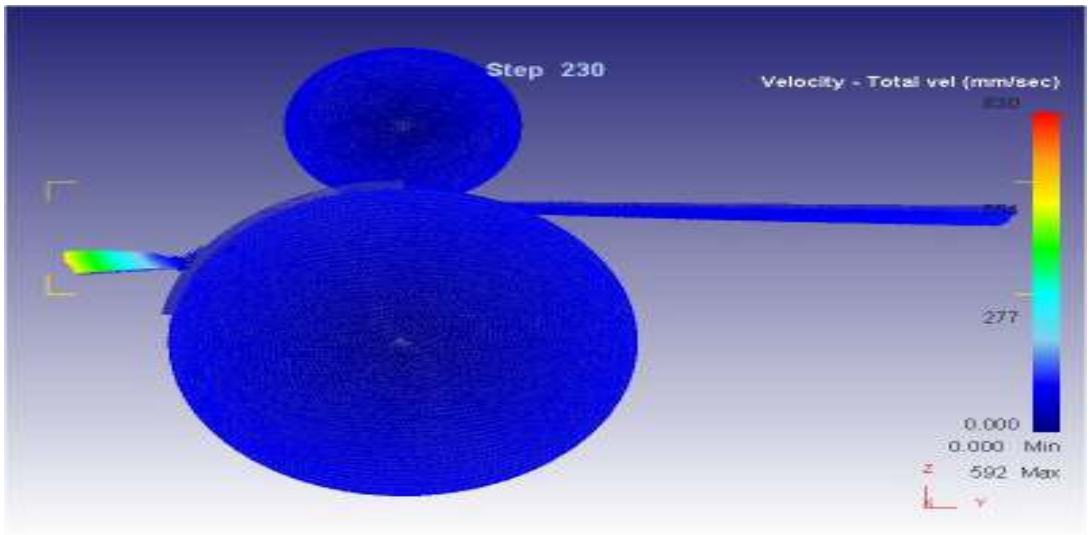

Figure 3.36: Velocity distribution at 700 ºC for 9.5 mm Aluminum feedstock material

The simulation results for simulation of 9.5 mm diameter for Aluminum feedstock material has been tabulated in Table 3.8.

Table 3.8: Results in tabular form for Simulation of 9.5 mm Aluminum feedstock

S. No.	Feedstock Diameter (mm)	Product diameter (mm)	Wheel Velocity (RPM)	Total Load (kN)	Effective Stresses (MPa)	Damage value	Product Temperature (°C)
1	9.5	6	4	222.2	160	0.7	416
			6	180	165	0.3	440
			8	119.8	168	0.5	450
			10	119	183	0.9	451
2	9.5	7	4	115.44	158	0.1	440
			6	116.63	149	0.54	448
			8	99.37	152	0.5	448
			10	95.5	170	0.7	449

3.10 Simulation of 12.5 mm diameter feedstock for Copper rod

Data for the numerical simulation and details of mesh elements for 12.5 mm Copper feedstock material has been tabulated in Table 3.9 and Table 3.10 respectively.

Table 3.9: Data for the numerical simulation of 12.5 mm Copper feedstock

S. No.	**Parameters**	Details
	Geometry data	
1	Wheel diameter, D mm	350
2	Die diameter, d mm	6,7,8
3	Flash-gap size, G mm	1
4	Die length, L mm	10
	Simulation data	
1	Wheel velocity, N RPM	4,6,8,10
2	Initial temperature ^{0}C	20
3	Environment temperature ^{0}C	20
5	Die temperature ^{0}C	450
	Feedstock Material data	
1	Yield stress N/mm^2	69
2	Strain rate sensitivity	0.3
3	Heat capacity N/mm^2 ^{0}C	390
4	Conductivity N/s^{0}C	350

5	Convection coefficient N/s^{0}C mm	0.1
6	Emissivity	0.4
7	Boltzmann constant N/s^{0}C mm^4	5.669X10^{-11}
8	Interface heat transfer coefficient N/s^{0}Cmm	30
9	Friction coefficient	0.95(Feedstock and Wheel groove), 0.95(Shoe and Feedstock),0.95(Abutment and Feedstock) 0.0.05(Die and Feedstock)

Table 3.10: Tetrahedron Mesh elements details for 12.5 mm diameter of Copper feedstock

S. No.	Objects	Mesh-Elements
1	Work piece	79561
2	Extrusion Wheel	155858
3	Extrusion shoe	27004
4	Coining Wheel	45604
5	Abutment	75964
6	Die	44434

Figures 3.37 to 3.46 shown below depict the detailed distributions of load, torque, effective stresses, effective strains, temperature and damage value.

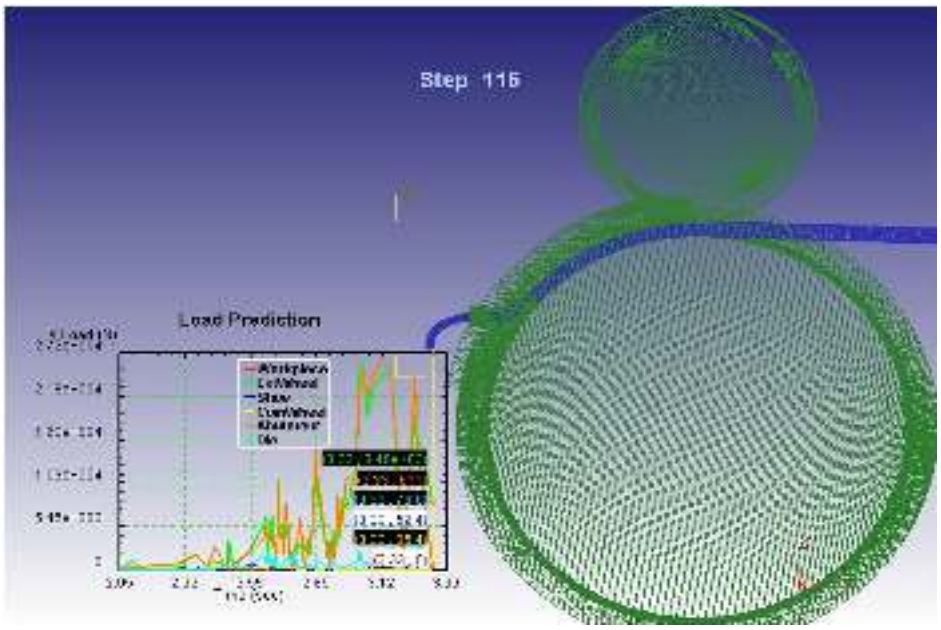

Figure 3.37: X-load distribution for 12.5 mm Copper feedstock material

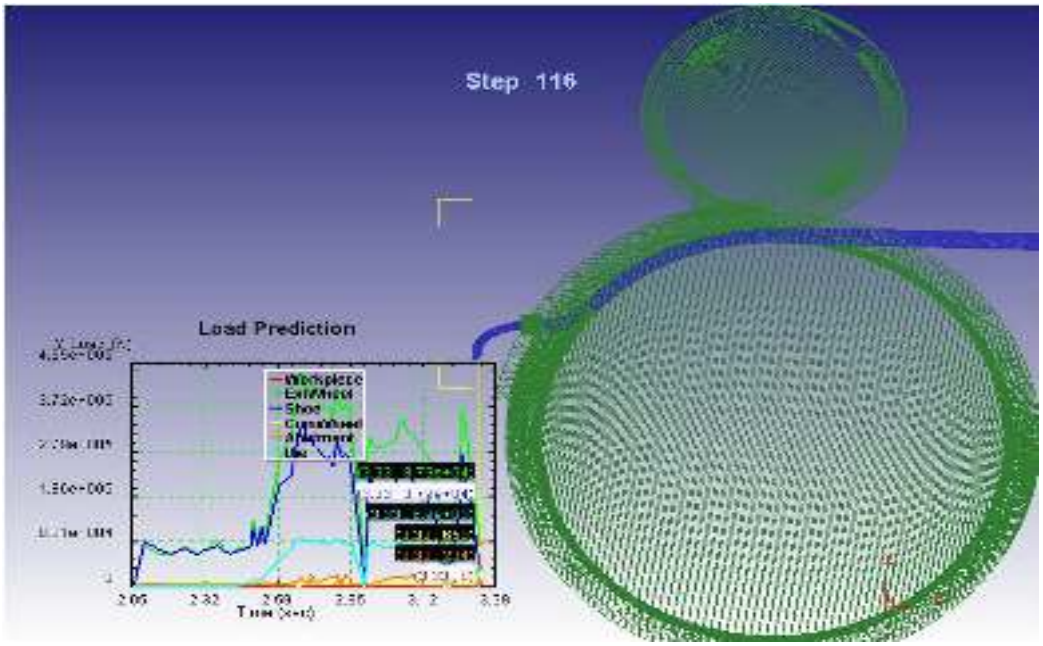

Figure 3.38: Y-load distribution for 12.5 mm Copper feedstock material

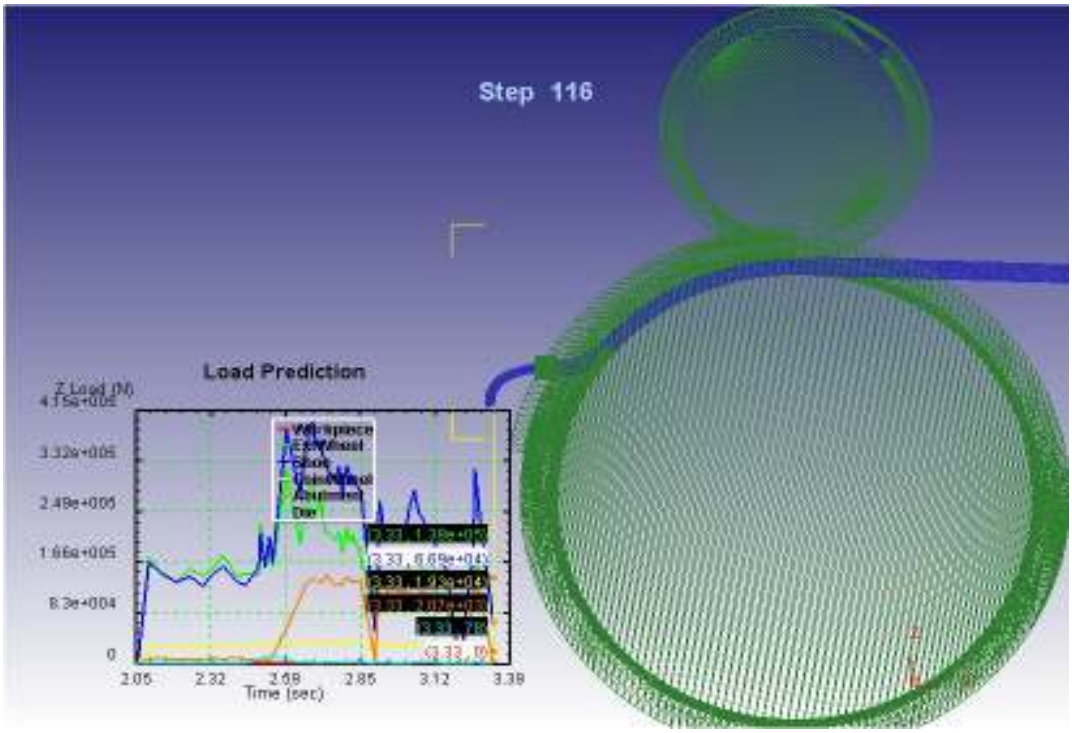

Figure 3.39: Z-load distribution for 12.5 mm Copper feedstock material

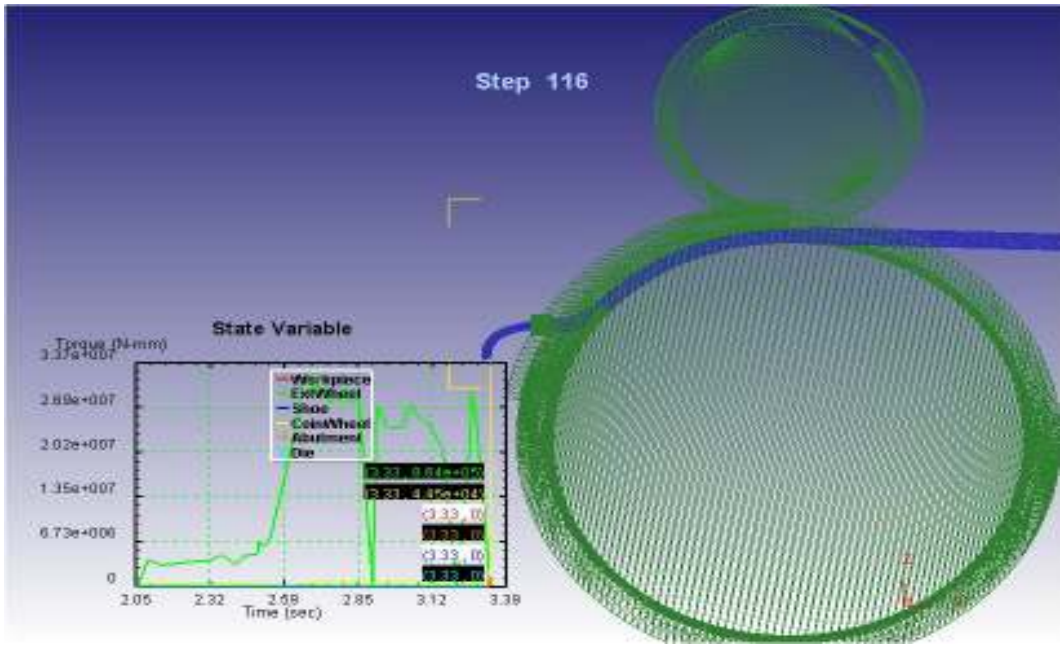

Figure 3.40: Torque distribution for 12.5 mm Copper feedstock material

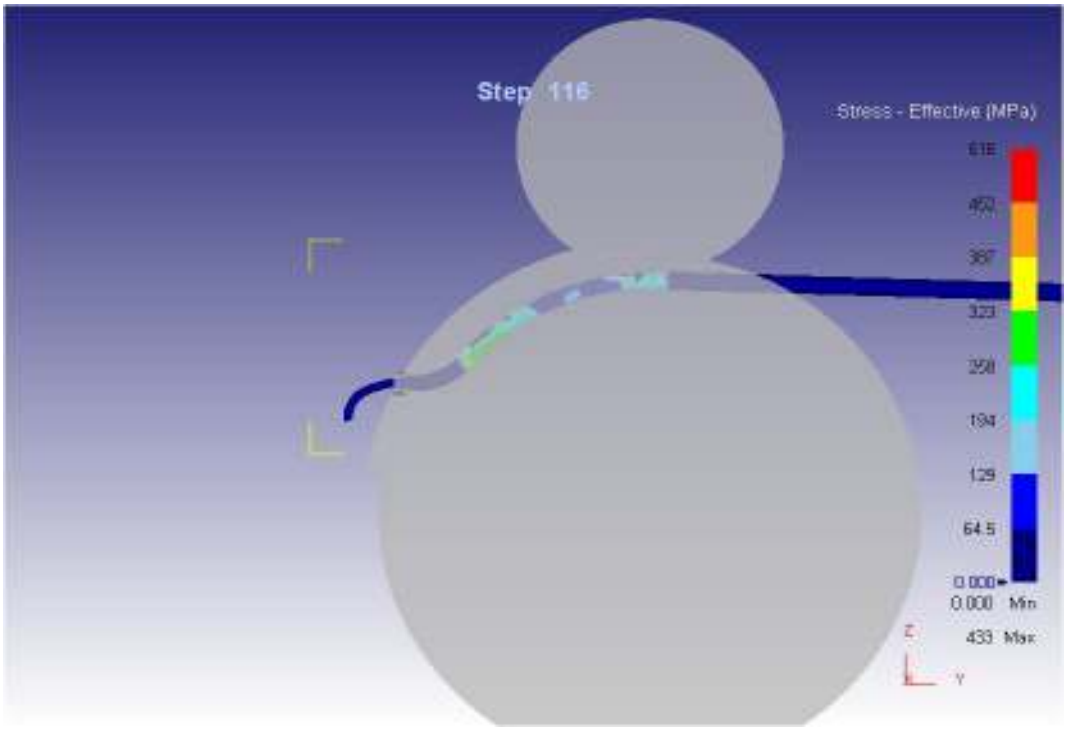

Figure 3.41: Effective stress distribution for 12.5 mm Copper feedstock material

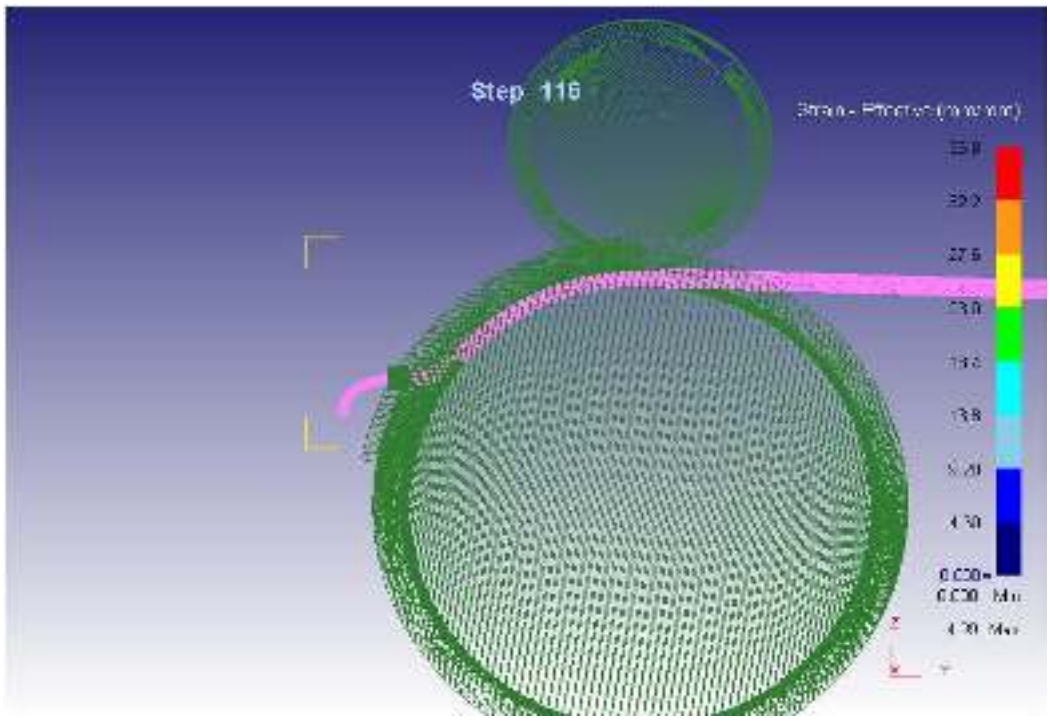

Figure 3.42: Effective strain distribution for 12.5 mm Copper feedstock material

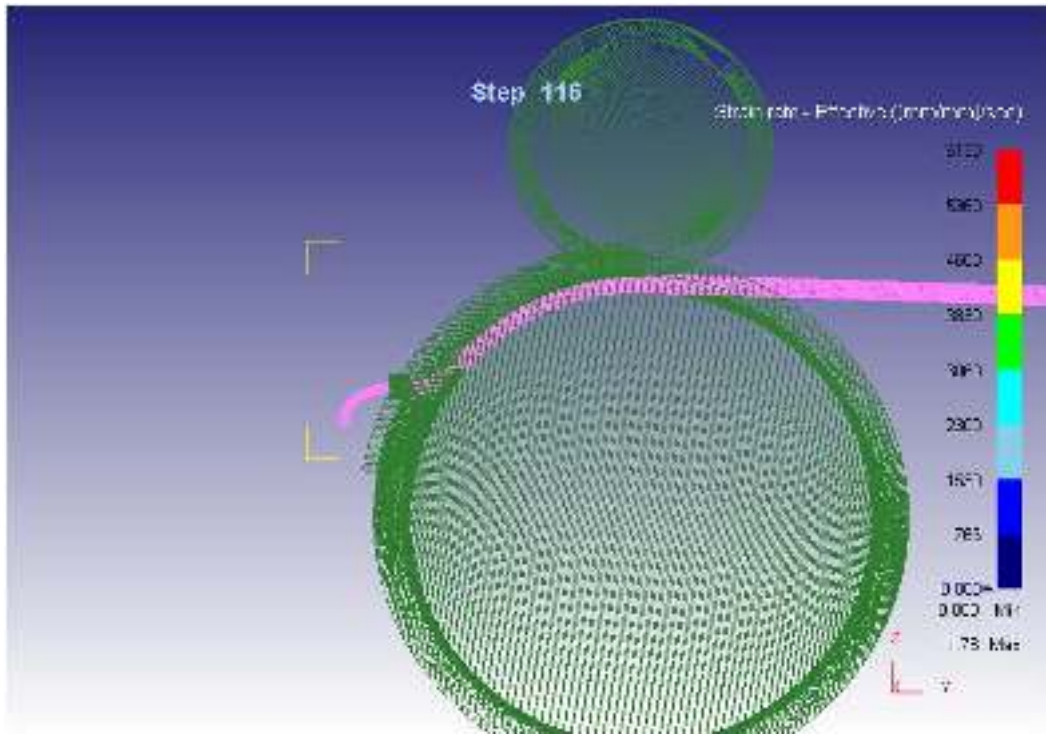

Figure 3.43: Effective strain rate distribution for 12.5 mm Copper feedstock material

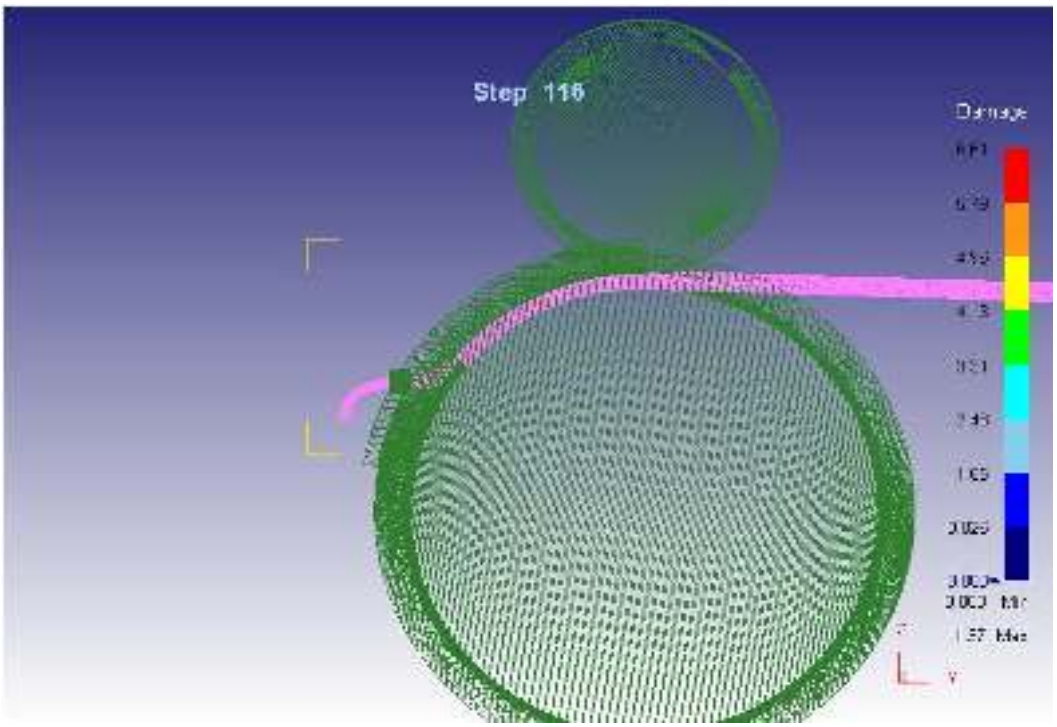

Figure 3.44: Damage distribution for 12.5 mm Copper feedstock material

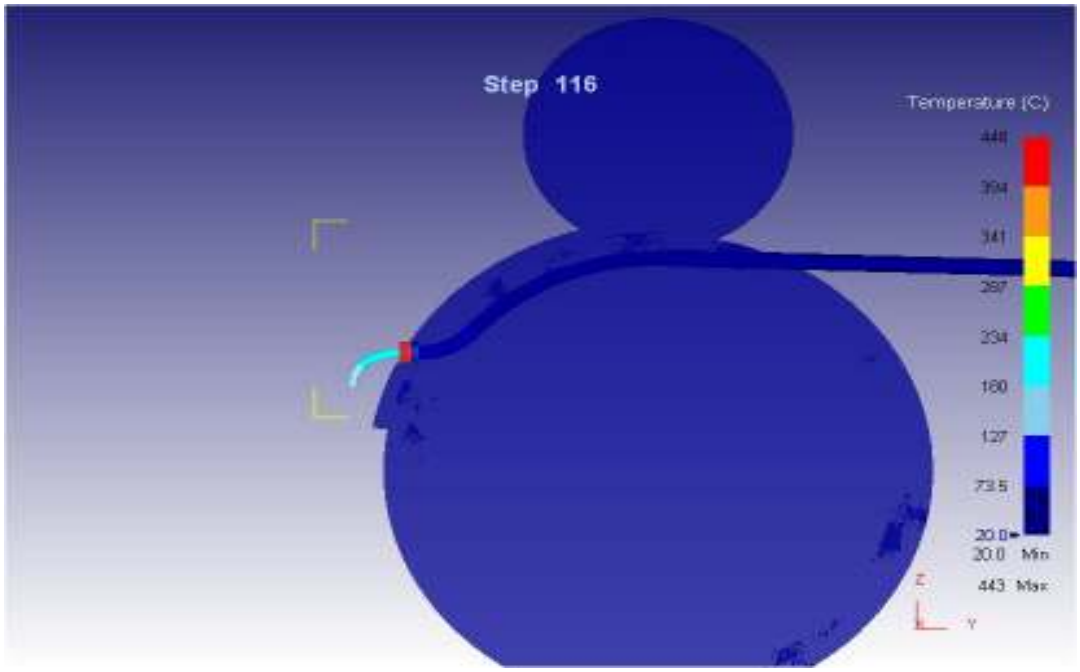

Figure 3.45: Temperature distribution for 12.5 mm Copper feedstock material

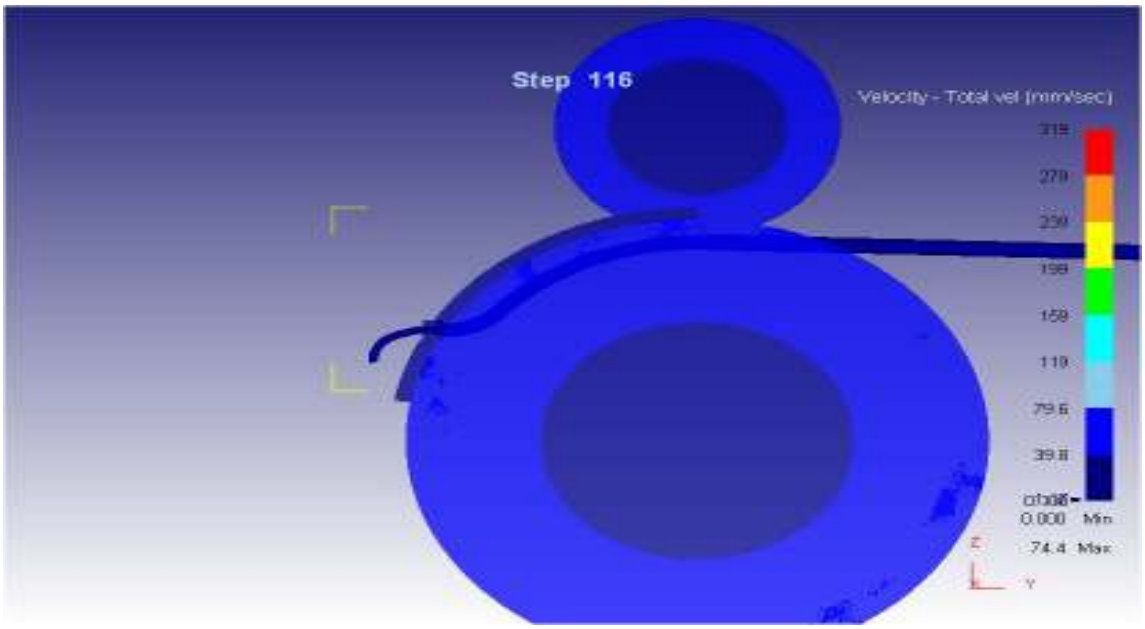

Figure 3.46: Velocity distribution for 12.5 mm Copper feedstock material

Table 3.11 below shows the results in tabular form for simulation of 12.5 mm copper feedstock material.

Table 3.11: Results in tabular form for Simulation of 12.5 mm Copper feedstock

S. No.	Feedstock Diameter (mm)	Product diameter (mm)	Wheel Velocity (RPM)	Total Load (kN)
1	12.5	6	4	794.44
			6	525.92
			8	397.91
			10	322.22
2	12.5	7	4	796.3
			6	504.62
			8	381.94
			10	312.68

3.12 Parametric study (Aluminum alloy)

Based on the results of simulation for Aluminum feedstock material of 9.5 mm diameter, parametric studies has been carried out.

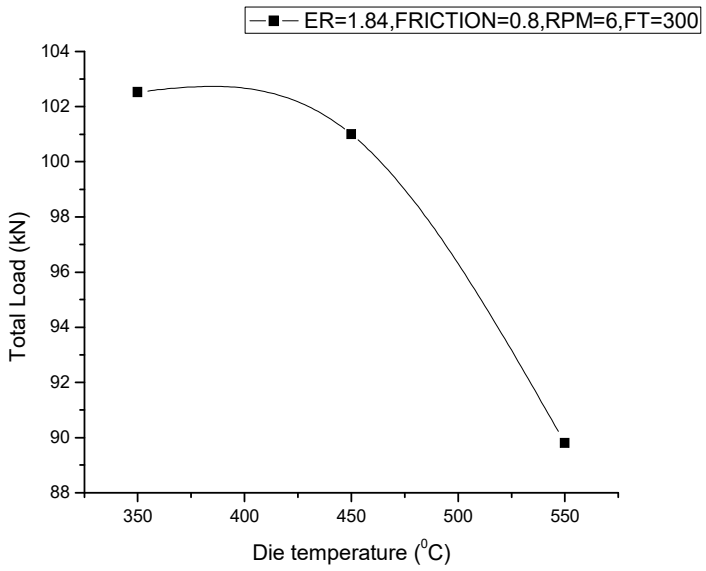

Figure 3.47: Effect of die temperature on total load

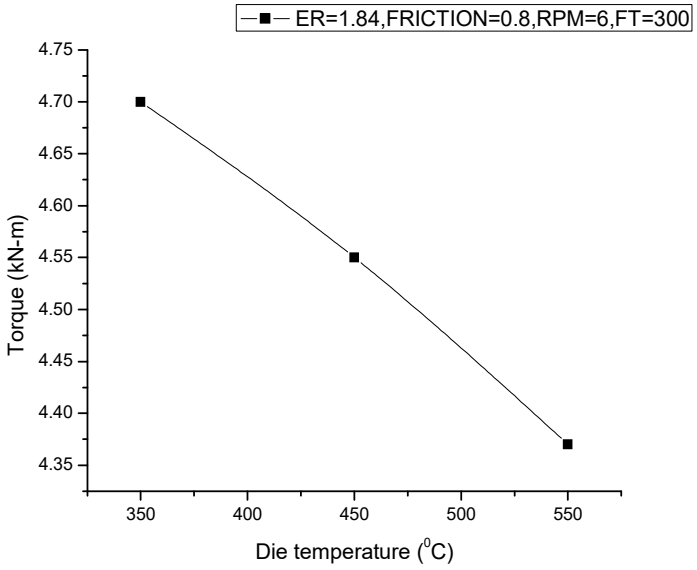

Figure 3.48: Effect of die temperature on torque required

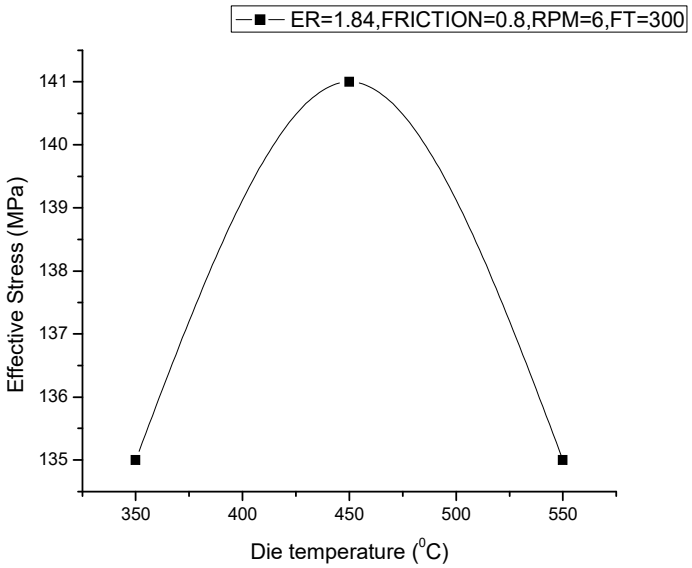

Figure 3.49: Effect of die temperature on Effective stress

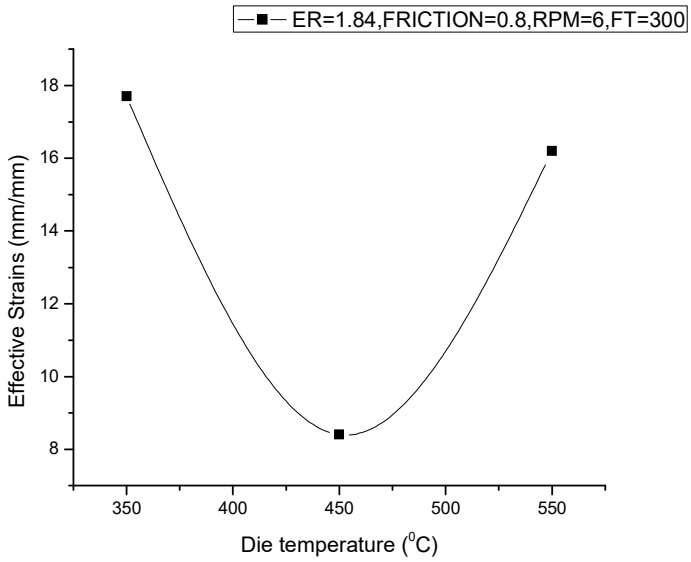

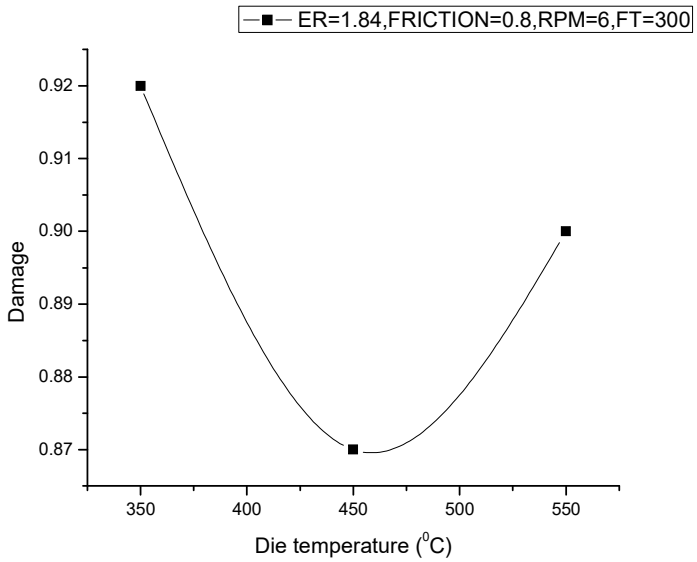

Figure 3.51: Effect of die temperature on damage value

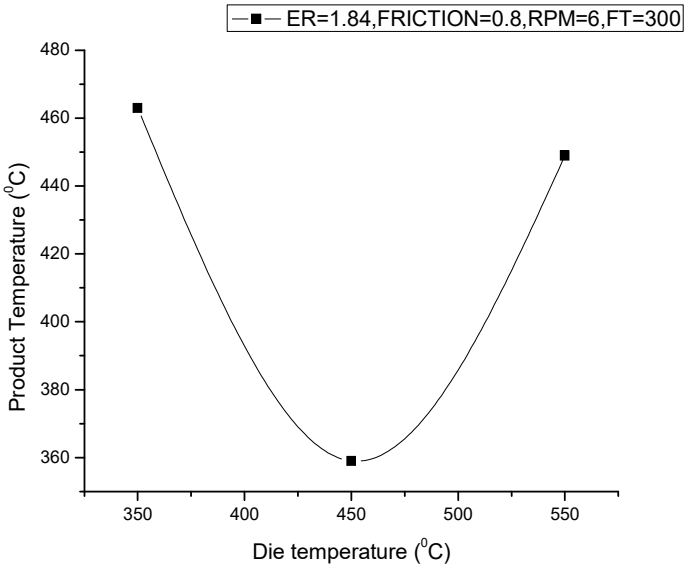

Figure 3.52: Effect of die temperature on product temperature

Figures 3.47-3.53 shows the effect of variation of die temperature versus several output process parameters such as total load required for extrusion, torque required, effective stresses, effective strains, effective strain rate, damage value and product temperature.

As die temperature increases, the total load and torque required to extrude the feedstock material decreases continuously due to reduction in flow stress of the material as increase of die temperature as shown in Figure 3.47 and 3.48 respectively.

As die temperature increases, the effective stresses increases initially due to flow characteristics of the feedstock material which depends on temperature, strain and strain rate and becomes maximum at a particular value of die temperature and then decreases with further increase in the value of die temperature when the mechanical energy is converted into heat energy as shown in Figure 3.49.

With the increase of die temperature, the effective strains decreases initially and becomes minimum at a particular value and then increases with further increase in the value of die temperature. This happens due to welding stage of the feedstock material and then further with onset of plastic deformation and increase of extrusion speed on later stage inside the die as shown in Figure 3.50.

Damage value as shown in Figure 3.51 refers to the quality of product obtained at die exit. If the value of damage lies between 0 to 1 then likelihood of fracture of extruded product is negligible. As die temperature increases the damage value decreases initially and then becomes minimum at a particular value of die temperature due to less strain and strain rate and as die temperature further increases the damage value increases as the strain, strain rate and temperature becomes prominent.

Product temperature as shown in Figure 3.52 refers to the temperature of product obtained at die exit. As die temperature increases the product temperature decreases initially and then becomes minimum at a particular value of die temperature due to less strain and strain rate and as die temperature further increases the damage value increases as the strain, strain rate and temperature becomes prominent.

As die temperature increases, strain rate increases initially due to flow characteristics of the feedstock material and becomes maximum at a particular value of die temperature and then decreases with further increase in the value of die temperature when the mechanical energy is converted into heat energy as shown in Figure 3.53.

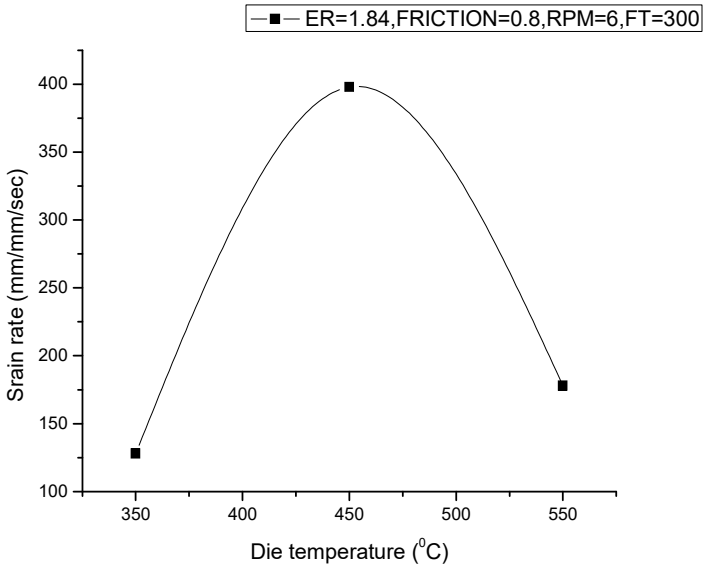

Figure 3.53: Effect of die temperature on strain rate

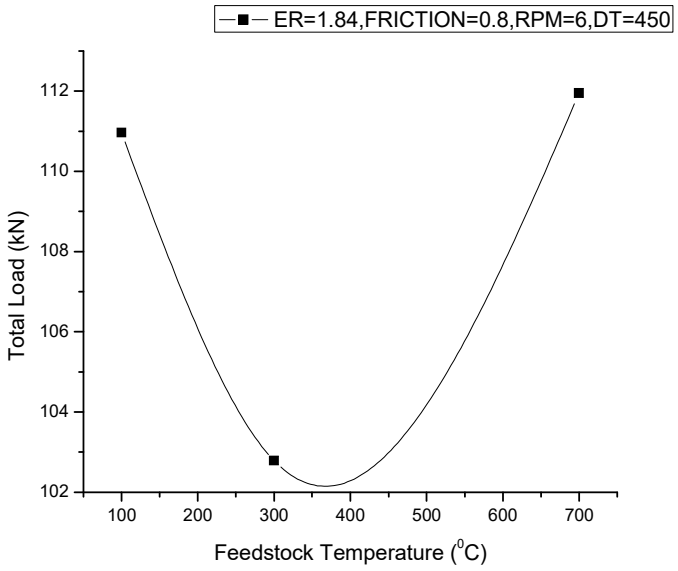

Figure 3.54: Effect of feedstock temperature on total load

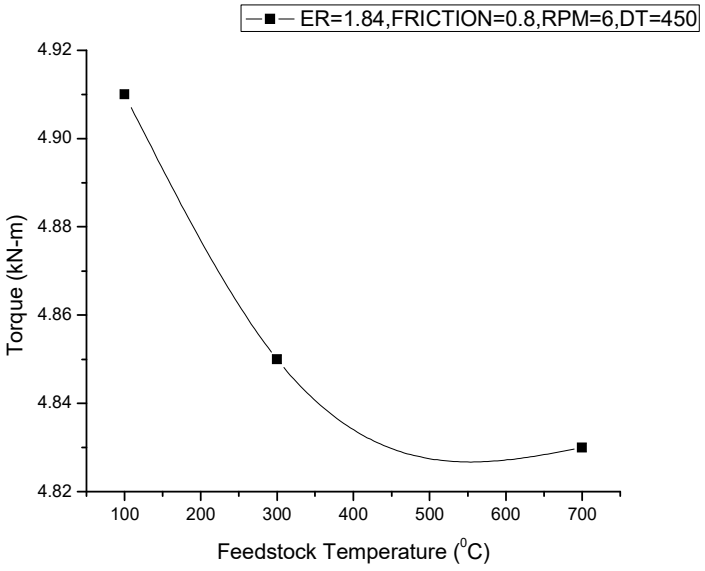

Figure 3.55: Effect of feedstock temperature on torque required

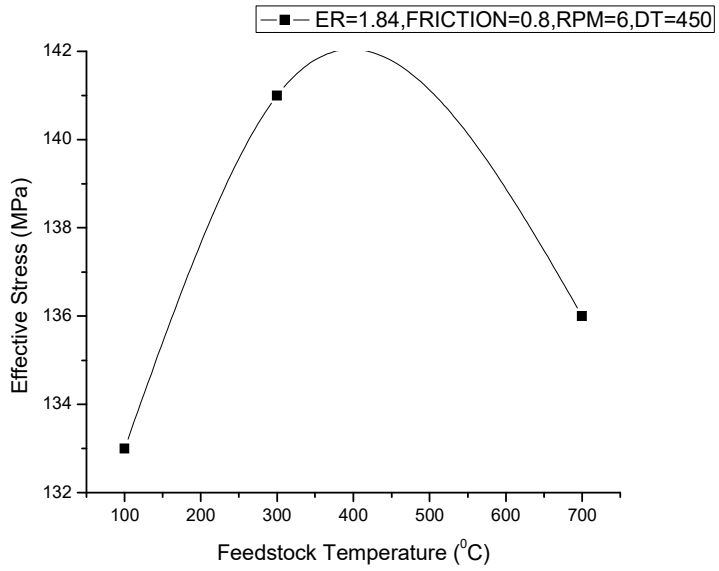

Figure 3.56: Effect of feedstock temperature on effective stresses

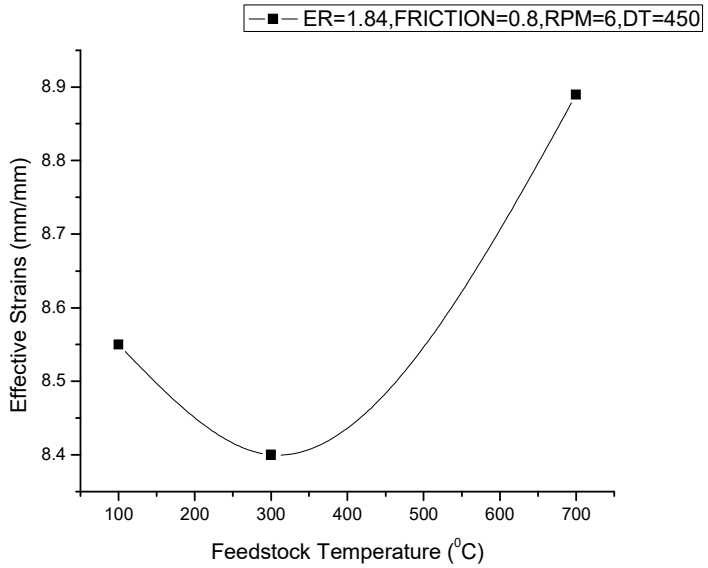

Figure 3.57: Effect of feedstock temperature on effective strains

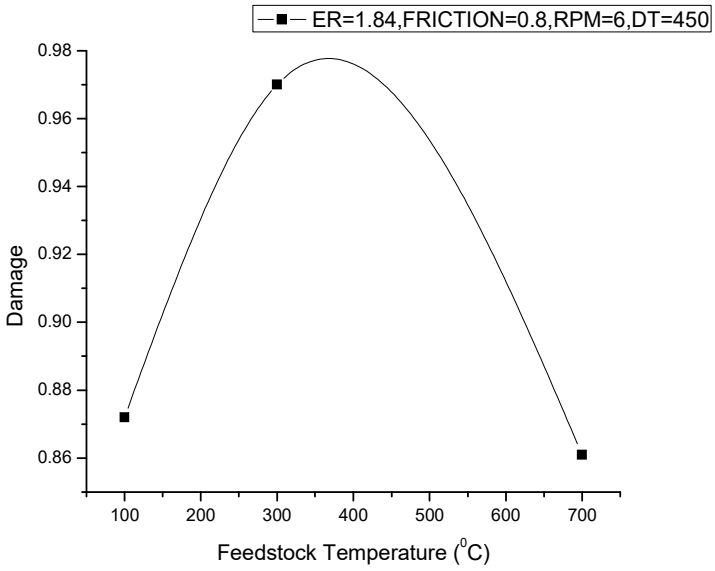

Figure 3.58: Effect of feedstock temperature on damage value

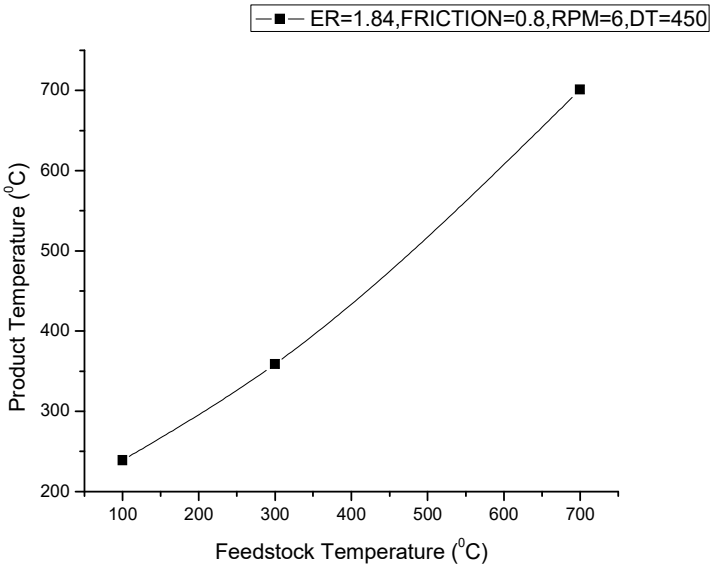

Figure 3.59: Effect of feedstock temperature on product temperature

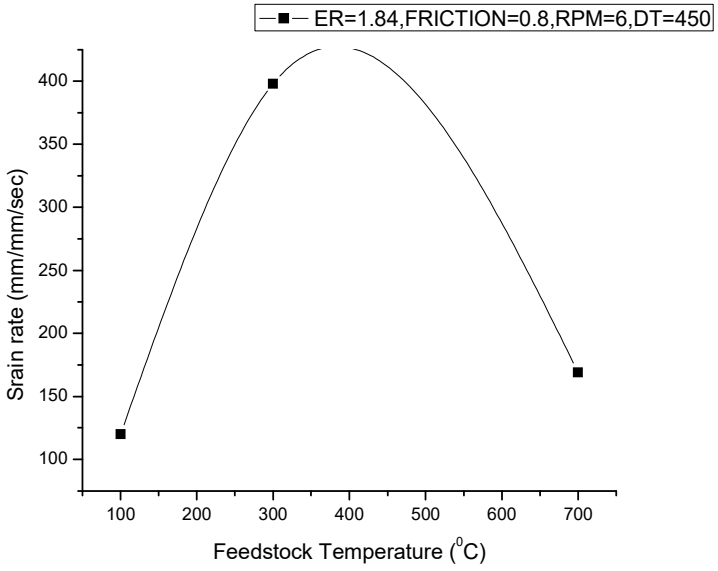

Figure 3.60: Effect of feedstock temperature on strain rate

Figures 3.54-3.60 shows the effect of variation of feedstock temperature versus several output process parameters such as total load required for extrusion, torque required, effective stresses, effective strains, effective strain rate, damage value and product temperature.

The total load as shown in Figure 3.54 required for the deformation or extrusion of feedstock is high if the feedstock temperature lies in the cold range. Load required is much reduced in case of warm temperature range of feedstock. When the feedstock temperature reaches in warm temperature range then shear strength of the feedstock material is reduced thereby reducing work required for the shear deformation in the shear zone near abutment face. Therefore, the total load required for the deformation of feedstock material is considerably reduced if the temperature of feedstock lies in the warm range. The torque required is also reduced if the feedstock temperature lies in the warm range as shown in Figure 3.55. So it is beneficial to use warm temperature range rather than using cold feedstock conditions.

Figure 3.56 depict the distribution of effective stress field under different feedstock temperature. The effective stresses near the die orifice increases considerably with increasing the temperature of feedstock. The concentrations of effective stresses are very high in the adjacent regions of the flash gap. The concentration of effective stresses varies considerably with the variation of feedstock temperatures. Since, the effective stresses are very high near the die orifice, the material of the abutment should have high strength to withstand the effective stresses.

Figure 3.57 and 3.60 clearly illustrate the variation of effective strains and strain rate respectively under different temperature of feedstock. The effective strain gradient is high near the abutment than that near the die orifice. The effective strain of product increases gradually with the increase of feedstock temperature. .

Figure 3.58 shows the effect of feedstock temperature on damage value. The study of damage distribution is generally related to the quality of product obtained through the die orifice and also the quality of feedstock material at the intermediate stages of the process when it passes through the primary and secondary zone through contact spaces of extrusion wheel and shoe. In general, damage value less than 1 is considered to be safe from fracture. It can be seen from the figure that damage values lies in the safer zone under these feedstock temperatures. Damage value generally increases with the increase of feedstock temperature.

Figure 3.59 shows the variation of product temperature under different feedstock temperatures. During the deformation process, the deformation body temperature increases considerably due to friction and shear deformation. The deformation body temperature reaches to 701 ºC if the feedstock temperature is very high. The tooling's in continuous extrusion process cannot work for a long if the temperature exceeds to a limiting value. So, the cooling's become necessary. With increasing the temperature of feedstock, the deformation body temperature increases gradually.
Figures 3.61-3.67 shows the effect of variation of extrusion ratio versus several output process parameters such as total load required for extrusion, torque required, effective stresses, effective strains, effective strain rate, damage value and product temperature.

As the extrusion ratio increases, the total load and torque required to extrude the feedstock material increases continuously due to increase in flow stress of the material as increase of extrusion ratio as shown in Figure 3.61 and 3.62 respectively.

Figure 3.63 shows the effect of extrusion ratio on effective stresses. The effective stresses increases as increase of extrusion ratio due to flow characteristics of the feedstock material which depends on temperature, strain and strain rate.

Figure 3.64 shows the effect of extrusion ratio on effective strains. The value of effective strains increases with the increase in the value of extrusion ratio and is found to be maximum near the bending zone.

Figure 3.65 shows the effect of extrusion ratio on damage value of extruded feedstock material .At very high extrusion ratios the quality of extruded feedstock material deteriorates.

Figure 3.66 shows the effect of extrusion ratio on product temperature. It is observed that as the extrusion ratio increases the temperature of product increases.

Figure 3.67 shows the effect of extrusion ratio on strain rate. As extrusion ratio increases, the strain rate decreases to a particular value and increases thereafter with further increase in the value of extrusion ratio.

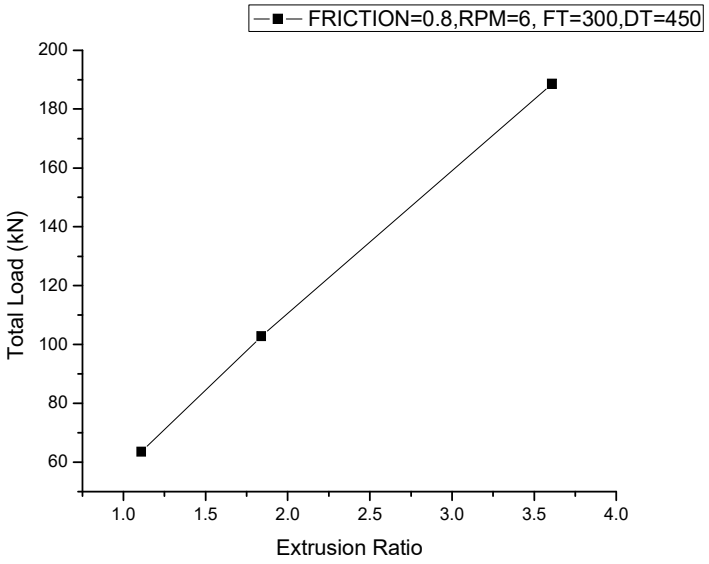

Figure 3.61: Effect of extrusion ratio on total load

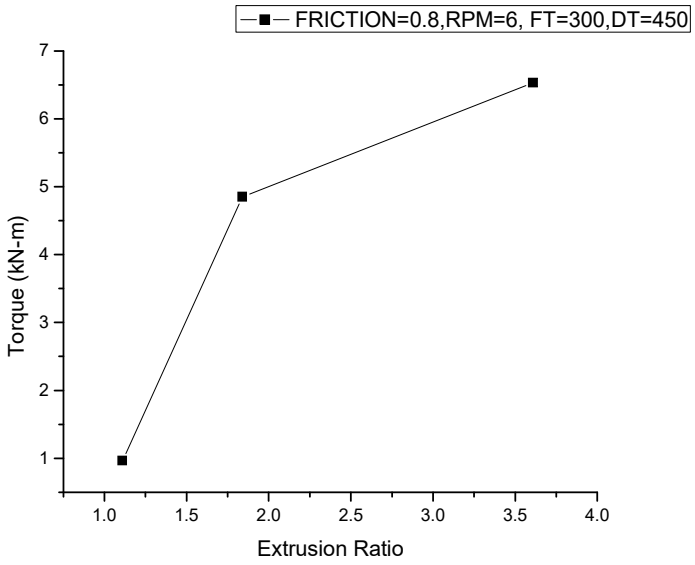

Figure 3.62: Effect of extrusion ratio on torque required

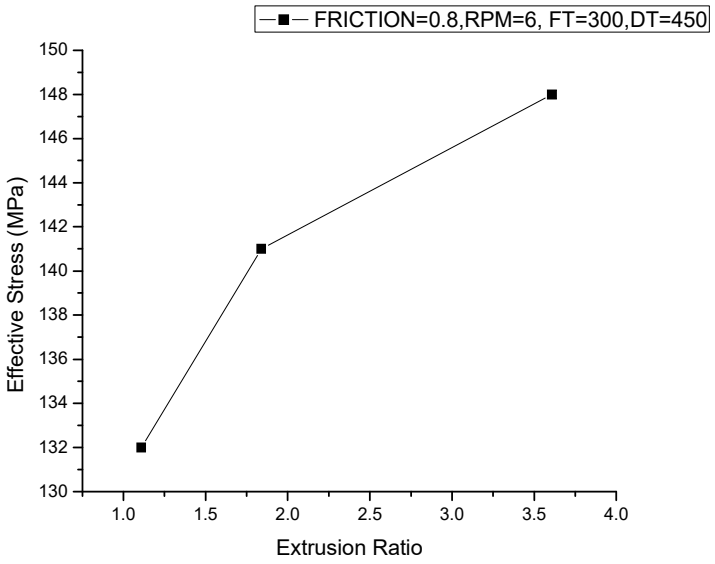

Figure 3.63: Effect of extrusion ratio on effective stresses

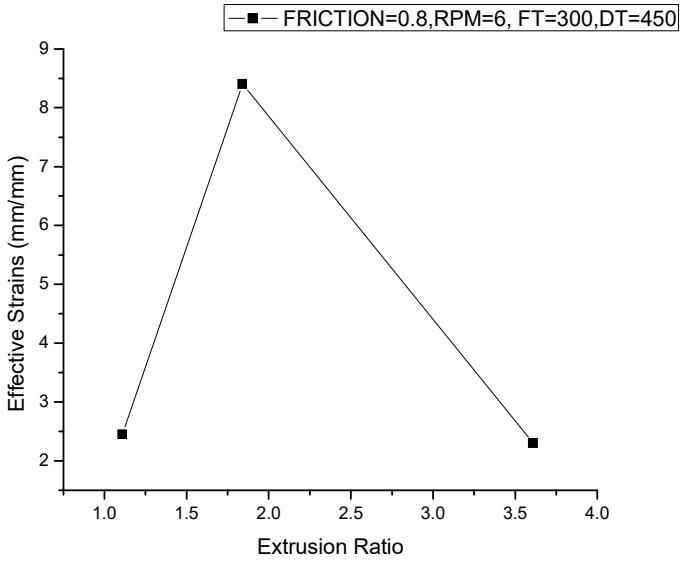

Figure 3.64: Effect of extrusion ratio on effective strains

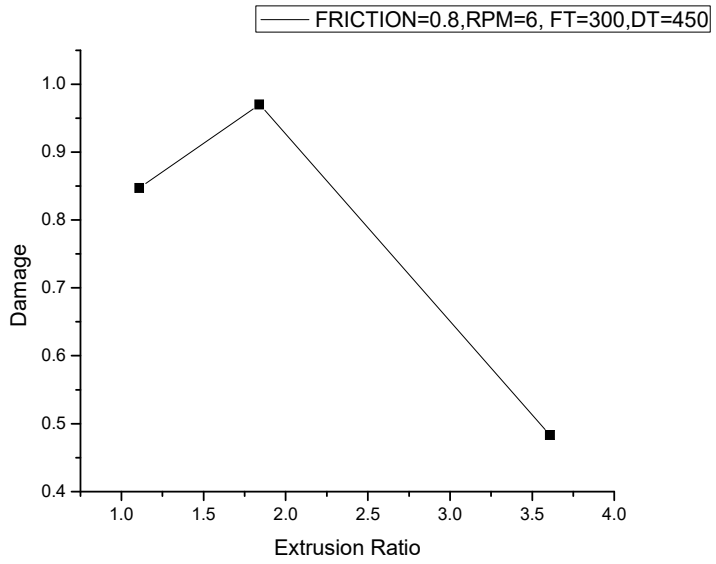

Figure 3.65: Effect of extrusion ratio on damage value

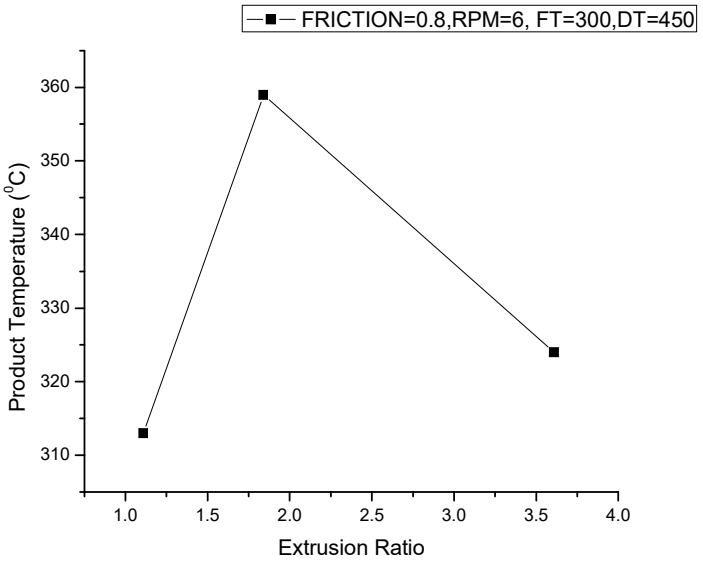

Figure 3.66: Effect of extrusion ratio on product temperature

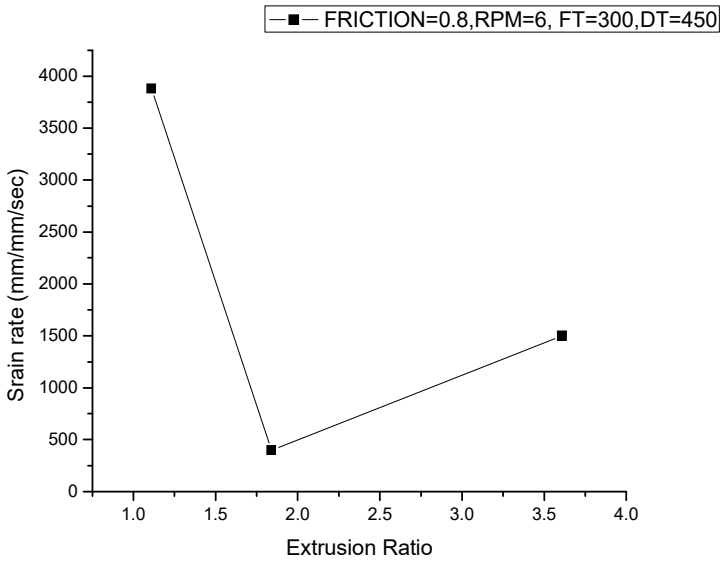

Figure 3.67: Effect of extrusion ratio on strain rate

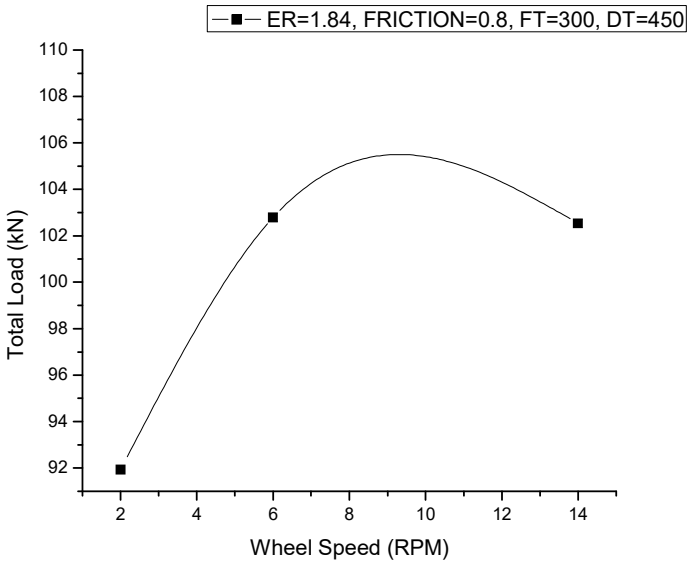

Figure 3.68: Effect of extrusion wheel velocity on total load required

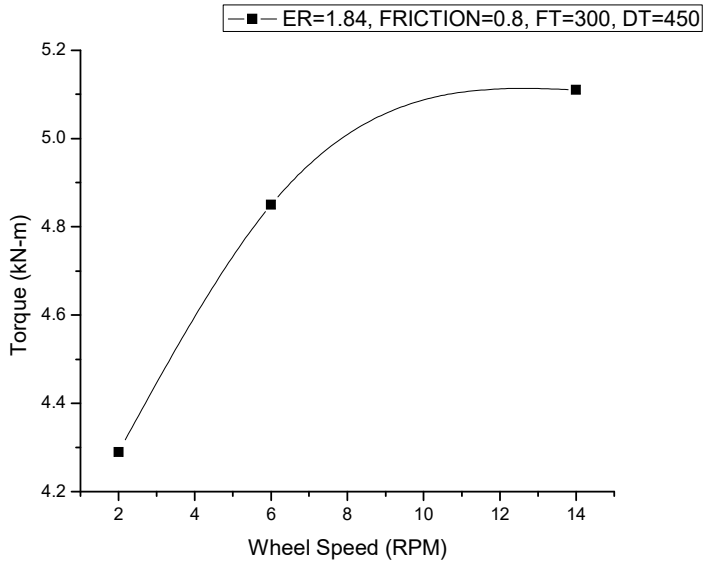

Figure 3.69: Effect of extrusion wheel velocity on torque load required

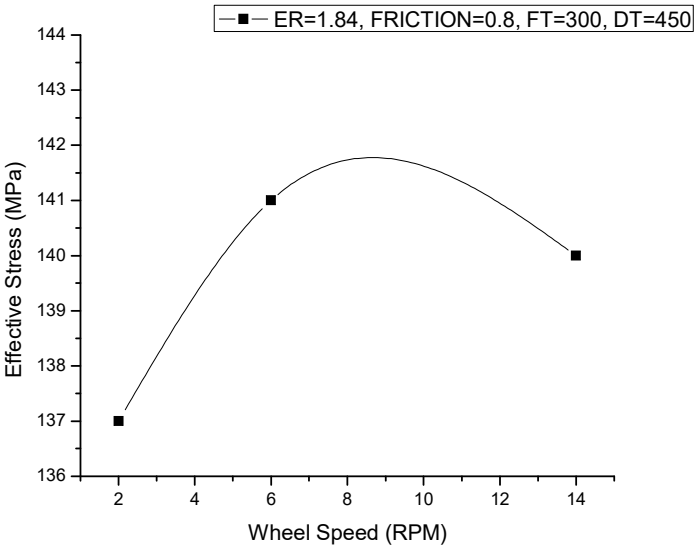

Figure 3.70: Effect of extrusion wheel velocity on effective stresses

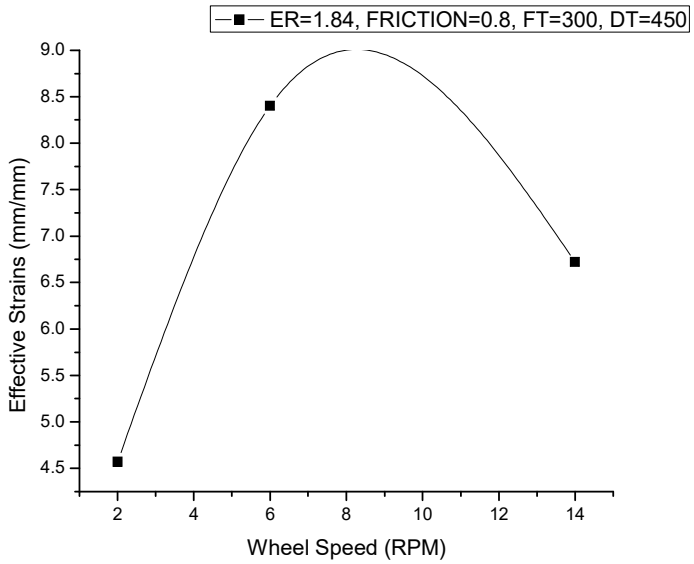

Figure 3.71: Effect of extrusion wheel velocity on effective strains

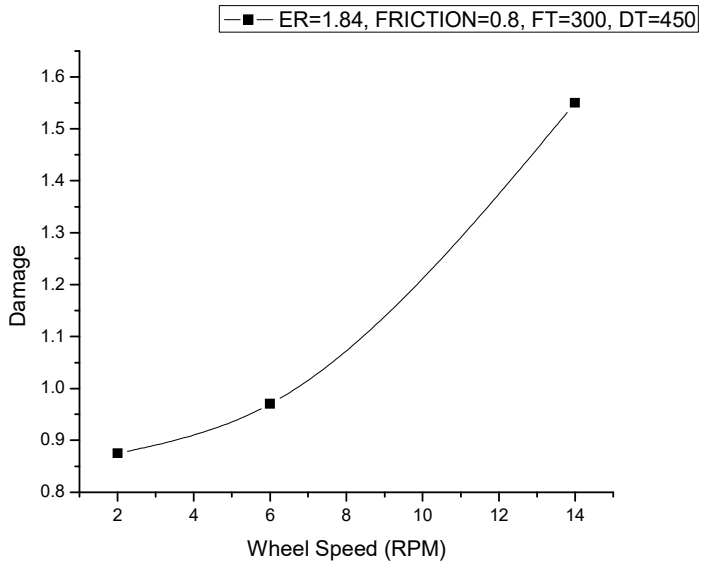

Figure 3.72: Effect of extrusion wheel velocity on damage value

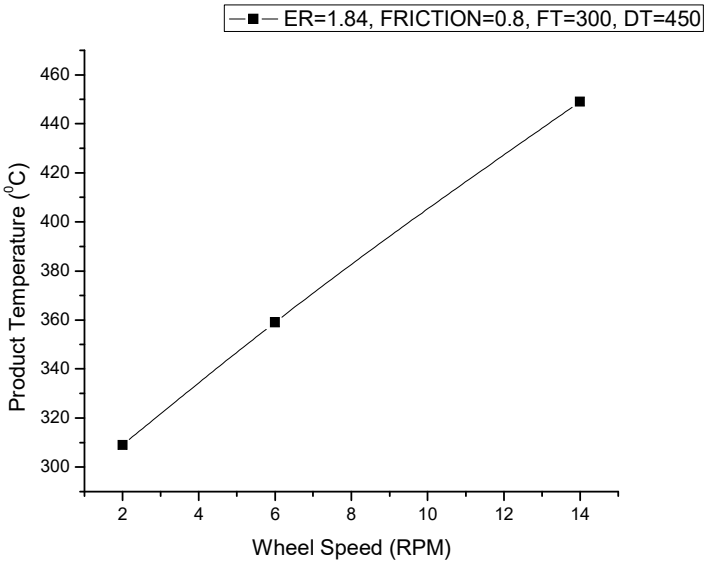

Figure 3.73: Effect of extrusion wheel velocity on product temperature

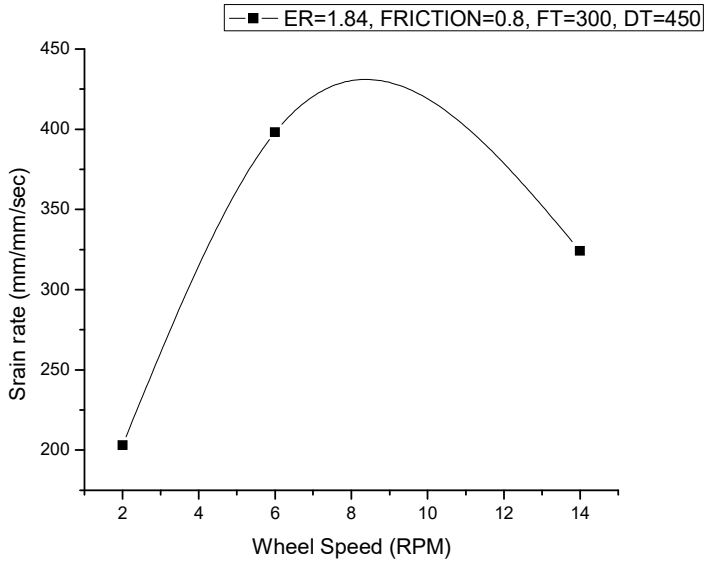

Figure 3.74: Effect of extrusion wheel velocity on strain rate

Figures 3.68-.3.74 shows the effect of variation of extrusion wheel velocity versus several output process parameters such as total load required for extrusion, torque required, effective stresses, effective strains, effective strain rate, damage value and product temperature.

Figure 3.68 shows the effect of wheel velocity on total load required for extrusion of feedstock materials. As the wheel velocity increases, the load required for extrusion increases and becomes maximum at a particular value of wheel velocity and decreases thereafter with further increase in the value of wheel velocity.

Figure 3.69 shows the effect of wheel velocity on torque required for extrusion of feedstock materials. As wheel velocity increases, the torque required for extrusion of feedstock material increases continuously.

Figure 3.70 shows the effect of wheel velocity on effective stresses which increases initially due to flow stress characteristics of the feedstock materials which depend on the temperature, strain and strain rate. The effective stresses increases and becomes maximum when feedstock material hits the abutment and drops thereafter as the extruded material comes out of die exit.

Figure 3.71 shows the effect of wheel velocity on effective strains which increases initially as the wheel speed increases and becomes maximum in the bending zone due to additional shearing and severe plastic deformation.

Figure 3.72 shows the effect of wheel velocity on damage value of product which increases as the wheel speed increases. As the wheel speed increases, due to high strain rate and severe plastic deformation, the damage value of product increases.

Figure 3.73 shows the effect of wheel velocity on extruded feedstock temperature. It can be observed that as the wheel speed increases the product temperature increases as the strain rate increases due to increase of wheel speed which leads to increase of product temperature.

Figure 3.74 shows the effect of wheel velocity on strain rate. The effective strain gradient is high near the abutment than that near the die orifice. The effective strain of product increases gradually with the increase of wheel velocity. It is clear from the figure that distribution of effective strain is almost uniform near the die orifice.

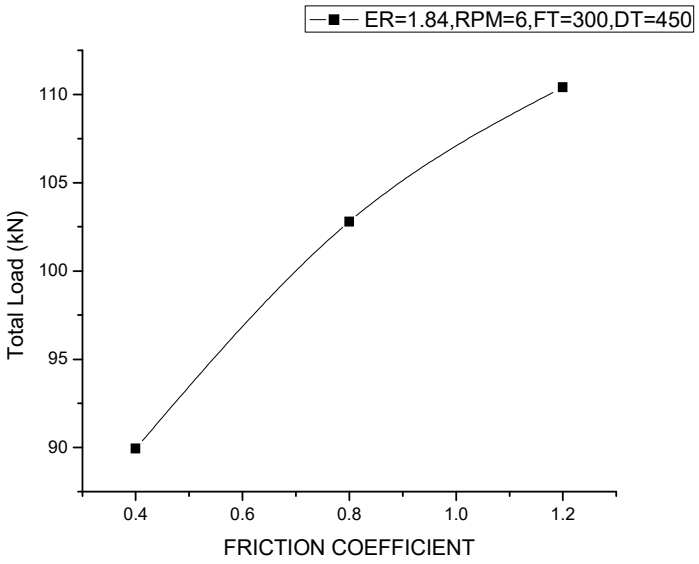

Figure 3.75: Effect of wheel groove friction on total load required

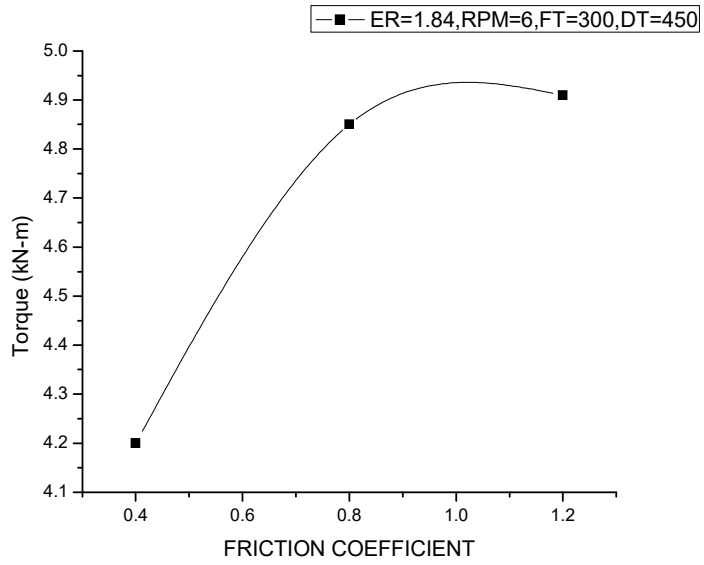

Figure 3.76: Effect of wheel groove friction on torque required

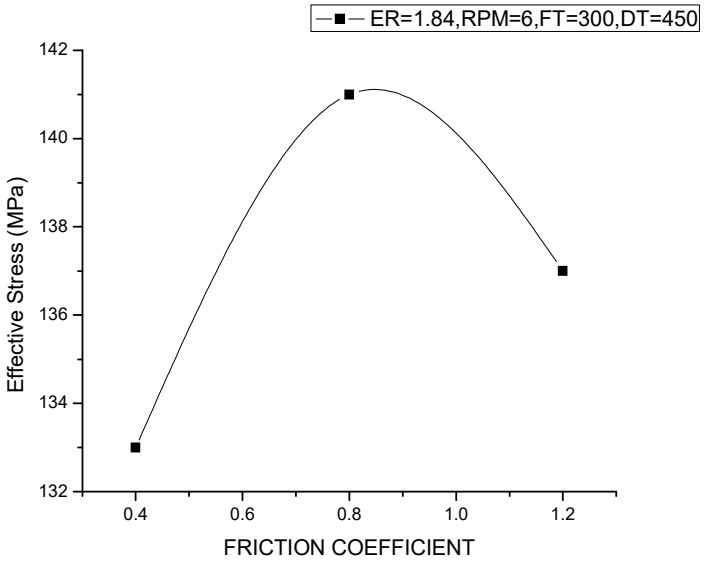

Figure 3.77: Effect of wheel groove friction on effective stress

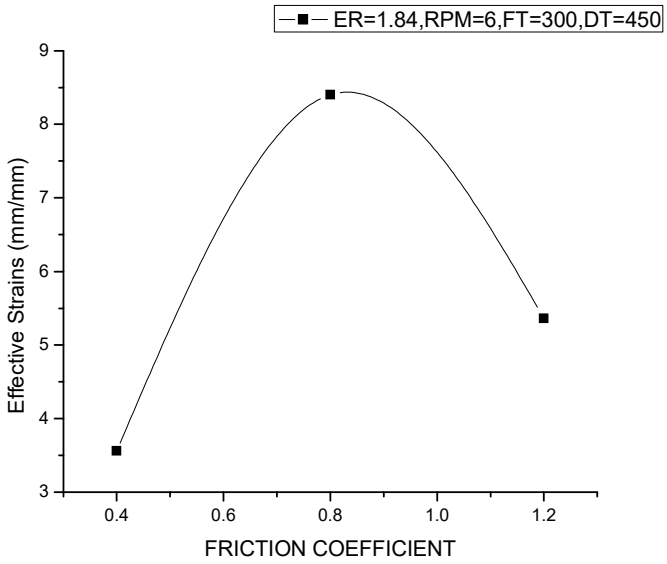

Figure 3.78: Effect of wheel groove friction on effective strains

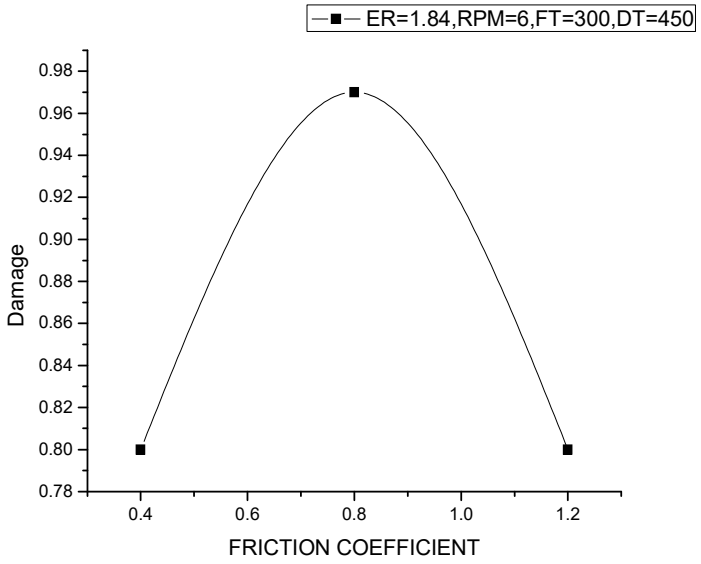

Figure 3.79: Effect of wheel groove friction on damage value

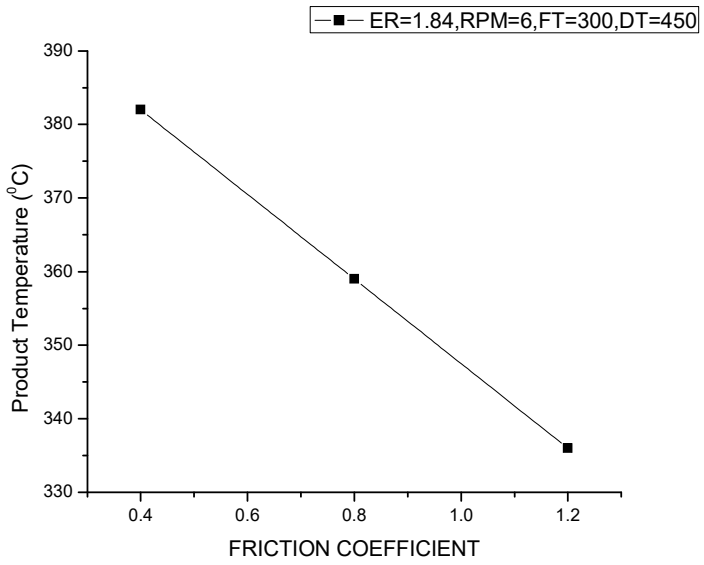

Figure 3.80: Effect of wheel groove friction on product temperature

Figures 3.75-3.3.81 shows the effect of variation of extrusion ratio on several output process parameters such as total load required for extrusion, torque required, effective stresses, effective strains, effective strain rate, damage value and product temperature.

Figure 3.75 and 3.76 shows the effect of wheel groove friction on total load and torque required respectively for extrusion of feedstock material. As the groove friction increases, the total load required for the extrusion increases due to the extra force required to overcome shearing action.

Figure 3.77 shows the effect of wheel groove friction on effective stresses. The effective stresses increases with the increase in the value of wheel groove friction. As the wheel groove friction increases, temperature and strain rate increases which leads to increase in the value of effective stresses.

Figure 3.78 and 3.81 shows the effect of wheel groove friction on effective strains and strain rate respectively. The effective strains and strain rate also increases with increase in the value of wheel groove friction.

Figure 3.79 shows the effect of wheel groove friction on damage value of product. Initially damage value of product increases and becomes maximum at a particular value of wheel groove friction and then decrease thereafter with further increase in the value of wheel groove friction.

Figure 3.80 shows the effect of wheel groove friction on product temperature. It is observed that as the wheel groove friction increases, the product temperature decreases continuously.

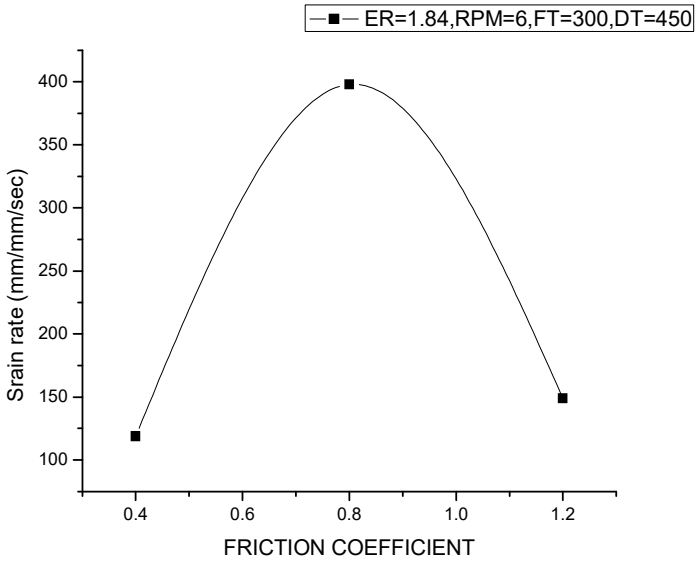

Figure 3.81: Effect of wheel groove friction on strain rate

3.13 Upper bound Analysis of Continuous Extrusion process

An upper bound solution is required to satisfy only the kinematic conditions in terms of strain increments, strain rate and velocities in a plastically deforming medium and does not necessarily satisfy the stress equilibrium equations. An important concept involved is that of a kinematically admissible velocity field. Velocity fields that satisfy the constraint of volume constancy and the velocity boundary conditions are called kinematically admissible velocity fields.

The upper bound theorem [Prager and Hodge, 1951] states that among all possible kinematically admissible velocity fields, the one that minimizes the total power φ_T is the actual velocity field.

$$\varphi_T = \int_{\Omega} \sigma'^{*}_{ij} \dot{\epsilon}^{*}_{ij} d\Omega + \int_{S_i} \tau \left|\Delta v_i\right|^{*}_{S_i} dS_i \qquad (3.8)$$

In the above equation Ω is the plastic deformation zone, τ is the shear stress on velocity discontinuity surfaces S_i. The first term expresses the internal power of deformation over the volume of the deformation zone, while the second term represents the power dissipated in shearing the material over the velocity discontinuity surfaces and at the tool-work interface (i.e. frictional power), Here asterisk (*) indicates that the values

of stress, strain rate and velocity discontinuity are obtained from an assumed kinematically admissible velocity field.

In continuous extrusion process the deformation of the feedstock material to a certain amount begins the moment feedstock enters into the grooved portion of continuous extrusion wheel. Further, the feedstock enters into the primary grip zone and then into the secondary grip zone where the further plastic deformation of the feedstock material takes place to a considerable amount. After its movement in the secondary grip zone, the feedstock is carried forward along with the extrusion wheel up to the abutment. The feedstock strikes the abutment and is converted into soft plastic form which can easily flow in the abutment die chamber. In the abutment die chamber the main plastic deformation and hardening of the feedstock material occurs and the mechanical and metallurgical changes takes place. The plastic deformation of the feedstock material in abutment die chamber can be considered similar to the deformation of billet in container and die land region in conventional extrusion system.

3.14 Introduction to gripping zone and contact pressure in continuous extrusion process

Now consider an extrusion container with a rectangular, instead of a circular hole. This is made in two pieces with a rectangular groove in one, forming three sides of the container, and the flat fourth side as the other as shown in Figure 3.82. If the feedstock, which can be round rod although it does not need to be a precise shape is an interference fit in the groove it will be deformed slightly forming contact areas against each side of the container. If the grooved part is moved and the flat side is kept stationary, there will be a frictional force set up on each of the four contracting sides. Since three of the sides are aiding motion of the billet and only one is resisting, the feedstock will be carried along in the grooved part if a block, called the abutment, is sized to fit the groove and it attached to the stationary side, then as the feedstock is pushed against it an axial compressive stresses will be get up in the feedstock, and if sufficient frictional force is available the billet material will yield and flow to fill the cross section of the groove in front of the abutment. Note that there will also be relative motive between the container and feedstock in this region when the smaller cross section of the billet is made to fill the

larger cross section of groove. The frictional force available to develop this compressive less will depend on the width and length of the contact on the sides of the container (i.e., contact or grip area) together will the coefficient of friction and contact pressure. Continued movement of the grooved part of the container will result in a buildup of pressure from the yield point up to the abutment face at the low pressure end there will be normal frictional forces applying between feedstock and container, dependent on contact pressure area increase eventually the extrusion force will be die orifice introduced into the center of the abutment combination of frictional and shear forces can produce sufficient pressure at the abutment for extrusion to occur though the die. Extrusion will continue till the feedstock is reduced to a critical length where insufficient frictional force length to keep process is going indirect extrusion without a backup punch.

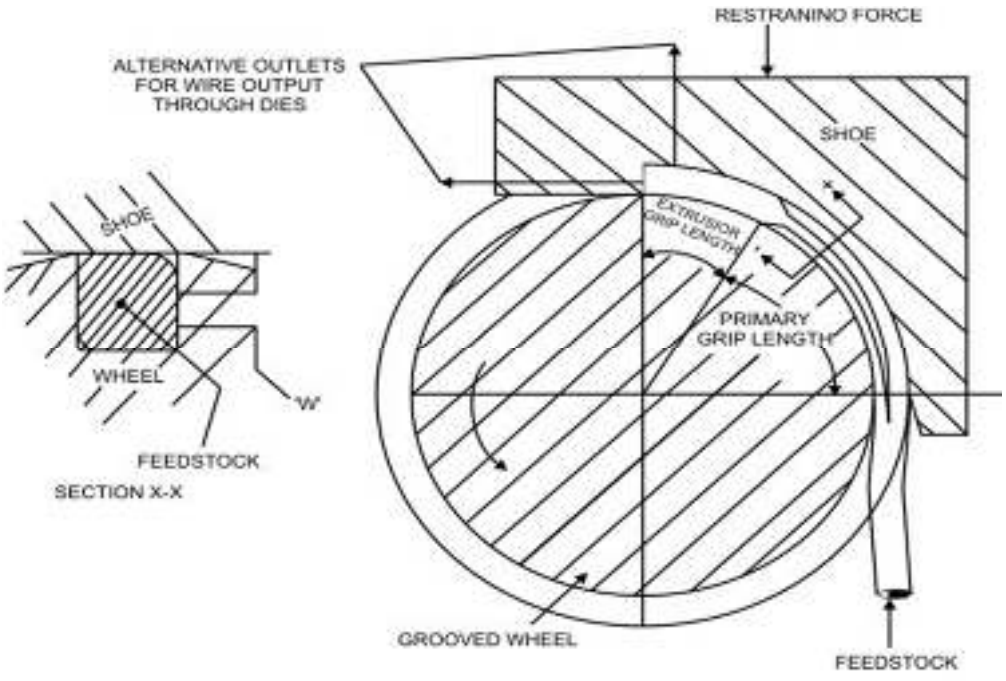

Figure 3.82: Contact area and grip length in continuous extrusion process

To make the process continuous a continuous grooved section pressure container is required and this is most simply provided by having a rotating grooved wheel. The stationary side shoe in the form of a shoe which fits around part of the wheel circumference and is of sufficient length for the process (Figure 3.83). The product may be extruded in either a radial or tangential direction, or indeed in both.

It is possible to predict the grip lengths necessary to ensure that extrusion will occur from knowledge of the geometry, feedstock properties, coefficients of friction, and the extrusion ratio.

Figure 3.83: Detail showing grip lengths

The coining of the feedstock into the groove compresses the material setting up yield stress in the outer fibers contacting the sided of the container. The primary grip length frictional force must set up axial yield in the metal, and only two sides of the groove are effective, the other two sides canceling each other out as already described. Then:

Primary driving force = $2Y\mu \; x \; l_1$ (3.9)

This is force must generate axial yield = YA (3.10)

Where, Y = compressive yield strength of feedstock

x = contact width

μ = coefficient of friction between feedstock and groove,

l_1 = primary grip length

A = cross-sectional area of feedstock = sectional area of groove.

Now if groove depth = groove width = w, then

$A = w^2$

and if,

$x = w/4$

which is typical, then

$l_1 = 2w/\mu$ (3.11)

Extrusion Grip, Length

There is increase in contact stress between the feedstock and container wall form the point at which yielding occurs up to the point at which shearing of the feedstock can occur.

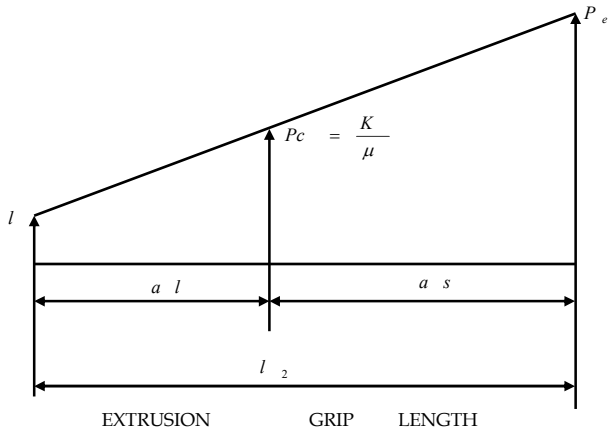

Figure 3.84: Extrusion grip length showing contact pressure

The contact stress for this discontinuity between sliding and shearing is given by:

$Pc = k/\mu$ (Figure 3.84) (3.12)

If,

$L_2 = a_1 + a_s$

Then,

$PeA^1 = 2w\ [a_s + a_l/2]k$

Where l_2 = extrusion grip length

a_1 = length over which sliding can occur

a_s = length over which shearing on occur

w = depth and width of groove

k = shear strength of feedstock

μ = coefficient of friction

P_e= extrusion pressure

P_c = contact pressure

A_l= cross-sectional area of grove (typically w^2)

In the extrusion of metals with low shear strength a_1 is small compared to a_s, then $l_2 = a_s$, the extrusion grip $l_2 = [P_e w / 2K] = [P_e w / Y]$ where Y yield strength of feedstock.

3.15 Analysis of the continuous extrusion process

The following assumptions are made for the analysis of Continuous Extrusion process:

- Material is incompressible and rigid viscoplastic.
- Elastic strain is negligible.
- The friction factor between die and work piece is assumed to be independent of slip.

a) Initial drag

This corresponds to the power consumed when feedstock makes initial entry into the grooved portion of continuous extrusion wheel.

When the feedstock material from the stock roll enters into the grooved potion of extrusion wheel, a minimum amount of power is required by the extrusion wheel to drag it into the grooved portion and further provide the movement into the primary grip zone and secondary grip zone of the extrusion wheel. Since the feedstock makes contact with the three sides as soon as it enters into the groove passage of extrusion and coining wheel, the power consumed in initial frictional drag is given by following expression

$$P_{initial\ drag} = 3\mu_1 Y A V_o \quad (3.13)$$

Where Y= Yield strength of the feedstock material.

μ_1= friction coefficient between feedstock and wall of groove.

A= Contact area of the feedstock in the grooved portion of the wheel.

V_o= Peripheral velocity of the extrusion wheel.

b) Deformation power in the primary gripping zone

After the initial drag of the feedstock material into the grooved portion of the extrusion wheel, the feedstock further moves into the primary grip zone and then into the secondary grip zone contacting the face of the extrusion shoe where the substantial increase in the deformation of the feedstock occurs. In the primary gripping zone, the groove and the extrusion shoe makes a hollow passage for the movement of feedstock

whose three contacting sides are moving and one contacting side of stationary shoe is stationary. Therefore, frictional stress on feedstock due to contacting side of stationary shoe is in opposite direction to the other three frictional contacting stresses. But, there is net forward force because of three contacting sides in the primary gripping zone of the feedstock material in continuous extrusion process.

Therefore, power consumed for the deformation of the feedstock in the primary gripping zone is given by

$$P_{primary\ grip\ zone\ deformation} = (3Y\mu_1 w l_1 - Y\mu_2 w l_2)\ V_o \quad (3.14)$$

Where l_1= length of primary grip zone

l_2= length of secondary grip zone

w = average width of contact between feedstock and groove wall on length l_1

μ_1= friction coefficient between feedstock and wall of groove

μ_2 = friction coefficient between feedstock and stationary shoe wall

Y = Yield strength of the feedstock material

K= Shear strength of feedstock material

V_o= Peripheral velocity of wheel.

c) Power consumed in shear in the secondary grip zone

The feedstock after its movement from the primary grip zone further travels towards the secondary grip zone towards the abutment face along with the extrusion wheel.The deformation of the feedstock material in the secondary gripping zone up to the face of abutment can be considered as shear deformation. In the secondary grip zone also, the forward motion to the feedstock material is provided by the three contacting frictional stresses and the contacting stress due to stationary shoe is in opposing mode restricting the feedstock motion. Therefore power consumed when feedstock shearing deformation occurs in the secondary grip zone is given by:

$$P_{shear\ deformation} = (3\mu_1\ w\ l_2K - \mu_2 w\ l_2K)\ V_o \quad (3.15)$$

l_1= length of primary grip zone

l_2= length of secondary grip zone

w = average width of contact between feedstock and groove wall on length l_1

μ_1= friction coefficient between feedstock and wall of groove

μ_2 = friction coefficient between feedstock and stationary shoe wall

K= Shear strength of feedstock material

V_o= Peripheral velocity of wheel.

d) Power consumed during the turning of feedstock material from abutment face into the die chamber

As soon as feedstock strikes the abutment, its further movement is blocked by the abutment portion thereby causing the conversion of kinetic energy of feedstock into the heat energy. As a result, the feedstock is transformed into soft plastic form causing its easy flow into the die chamber.

When feedstock strikes the abutment, it is transformed into soft plastic form. The feedstock in soft plastic form turns about certain angle and find its way further into the die chamber where the major deformation and mechanical as well as metallurgical changes takes place.

Therefore certain amount of power is consumed when the feedstock turns and makes entry into the die chamber.

Therefore expression for power consumption while turning of feedstock is given by:

$$P_{Turning} = \frac{\bar{\sigma}}{\sqrt{3}} \mu P_1 L_1 V_0 Cos\ \theta \qquad (3.16)$$

$\bar{\sigma}$ = Flow stress of the feedstock material

P_1 : Perimeter of product

V_0: Peripheral velocity of wheel

Θ : Angle between horizontal container surface and feedstock while turning

L_1: Bearing length of feedstock

μ : Coefficient of friction.

e) Deformation power in abutment die chamber

After the turning or entry of feedstock material in the abutment die chamber, further deformation of feedstock material occurs in major form in die chamber. This deformation in abutment die chamber can be considered similar to the deformation of the billet in container, bearing and die land zone of die set in conventional extrusion system. The two die arrangements i.e. square and streamline has been considered for the analysis of extrusion power through abutment die chamber.

The power consumption in abutment die chamber has been calculated from Kumar et al. [1999].

For the details of governing power expression in abutment die chamber refer appendix A.

3.16 Case Studies:

Numerical examples for the extrusion of axisymmetric circular feedstock are taken for study of analysis of continuous extrusion process. The two die arrangements i.e. square and streamline are taken to analyze the power consumption in abutment die chamber. The material and process parameters for several cases are chosen as:

Case 1

Feedstock material: Al 1100 with $\bar{\sigma}$= 21.936 $\bar{\varepsilon}^{0.245}$ as the strain hardening curve.

Feedstock diameter: 9.5 mm

Friction conditions are as follows:

a. Extrusion wheel and feedstock=0.95
b. Coining wheel and feedstock=0.95
c. Extrusion shoe and feedstock=0.95
d. Die-feedstock, abutment-feedstock and bearing-extrudate=0.05

Die profile: 3rd order polynomial

Total reduction in abutment die chamber=60%

Table 3.12: Power consumption from initial entry to abutment chamber

S. No.	Input parameters to the system						Initial drag power (kW)	Power in gripping zone (kW)	Power at abutment face (kW)	Power during turning (kW)
	μ	x	L_1	L_2	w	V_o				
1	0.95	10	140	140	9.5	0.07	0.165	5.9	1.56	5.8

Table 3.13: Power consumption inside the abutment die chamber

Die arrangements a: Square b: Streamlined		Input to the system						Output of the system					Power in abutment die chamber (kW)
	Zones	μ	V_o	V_e	d_i	d_o	L_o	$\bar{\sigma}$	$\bar{\varepsilon}$	P_{opt}	L_{opt}	% red	
a	I	1.0	0.072	0.10	9.5	7.5	42.5	70.3	0.23	0.9	8.5	25.1	0.5+0.9+
	II	0.05	0.10	0.15	7.5	6	-	83.7	0.32	0.5	13.3	35.2	0.006!+0.002*=1.4
b	I	0.05	0.072	0.072	9.5	9.5	42.5	31.5	-	0.35		0	0.35+0.75+0.12*=1.22
	II	0.05	0.072	0.10	9.5	6	-	78.9	0.09	0.75	28.2	60	

Therefore total power consumption for extrusion of 9.5 mm feedstock diameter to 6mm diameter extruded product for square die arrangement for 4 RPM of extrusion wheel is given below:

P = 0.165 + 5.9 + 1.56 + 5.8 + 1.4 = 14.8 kW

Total power consumption for extrusion of 9.5 mm feedstock diameter to 6 mm diameter extruded product for streamline die arrangement for 4 RPM of extrusion wheel is given below:

P=0.165+5.9+1.56+5.8+1.22=14.64 kW

Case 2.

Feedstock material: Al 1100 with $\bar{\sigma}$= 21.936 $\bar{\varepsilon}^{0.245}$ as the strain hardening curve.

Feedstock diameter: 9.5 mm

Diameter of extruded product: 7 mm

Extrusion wheel RPM: 4

Friction conditions are as follows:

a. Extrusion wheel and feedstock = 0.95
b. Coining wheel and feedstock=0.95
c. Extrusion shoe and feedstock=0.95
d. Die-feedstock, abutment-feedstock and bearing-extrudate=0.05
e.

Die profile: 3rd order polynomial

Total reduction in abutment die chamber=45%

Power consumed in initial drag, grip zone, at the abutment face and during turning are tabulated in Table 3.14 whereas power consumption in abutment die chamber is tabulated in Table 3.15.

Table 3.14: Power consumption from initial entry to abutment chamber

S. No.	Input parameters to the system						Initial drag power (kW)	Power in gripping zone (kW)	Power at abutment face (kW)	Power during turning (kW)
	μ	X	L_1	L_2	w	V_o				
1	0.95	10	140	140	9.5	0.07	0.165	5.9	1.56	5.8

Table 3.15: Power consumption inside the abutment die chamber

Die arrangements a: Square b: Streamlined		Input to the system						Output of the system					Power in abutment die chamber (kW)
	Zones	μ	V_o	V_e	d_i	d_o	L_o	$\bar{\sigma}$	$\bar{\varepsilon}$	P_{opt}	L_{opt}	% red	
a	I	1.0	0.05	0.25	9.5	8.0	55	65.8	0.21	0.35	9.3	14.5	0.35+0.7+0.002!+0.0009*
	II	0.05	0.25	0.75	8.0	7.0	-	75.7	0.29	0.7	11.1	33.5	=1.052
b	I	0.05	0.05	0.05	9.5	9.5	55	31.5	-	0.08		0	0.08+0.90+0.0002*=0.98
	II	0.05	0.05	0.4	9.5	7.0	-	76.6	0.08	0.90	24.2	45	

Therefore total power consumption for extrusion of 9.5 mm feedstock diameter to 7mm diameter extruded product for square die arrangement for 4 RPM of extrusion wheel is given below:

$P = 0.165 + 5.9 + 1.56 + 5.8 + 1.052 = 14.47$ kW

Total power consumption for extrusion of 9.5 mm feedstock diameter to 7mm diameter extruded product for streamline die arrangement for 4 RPM of extrusion wheel is given below:

$P = 0.165 + 5.9 + 1.56 + 5.8 + 0.98 = 14.40$ kW

Case 3.

Feedstock material: Al 1100 with $\bar{\sigma} = 21.936\ \bar{\varepsilon}^{0.245}$ as the strain hardening curve.

Feedstock diameter: 9.5 mm

Friction conditions are as follows:

a. Extrusion wheel and feedstock=0.95
b. Coining wheel and feedstock=0.95
c. Extrusion shoe and feedstock=0.95
d. Die-feedstock, abutment-feedstock and bearing-extrudate=0.05

Die profile: 3rd order polynomial

Total reduction in abutment die chamber=29%

Table 3.16: Power consumption from initial entry to abutment chamber

S. No.	Input parameters to the system						Initial drag power (kW)	Power in gripping zone (kW)	Power at abutment face (kW)	Power during turning (kW)
	μ	x	L_1	L_2	w	V_o				
1	0.95	10	140	140	9.5	0.07	0.165	5.9	1.56	5.8

Table 3.17: Power consumption inside the abutment die chamber

Die arrangements a: Square b: Streamlined	Input to the system	Output of the system	Power in abutment die chamber (kW)

	Zones	μ	V_o	V_e	d_i	d_o	L_o	$\bar{\sigma}$	$\bar{\varepsilon}$	P_{opt}	L_{opt}	% red	
a	I	1.0	0.072	0.09	9.5	8.75	32	67.3	0.22	0.09	9.5	11.8	0.09+0.15+0.002!
	II	0.05	0.09	0.12	8.75	8	-	72.7	0.29	0.15	15.3	18.9	+0.0004*=0.24
b	I	0.05	0.072	0.072	9.5	9.5	32	31.5	-	0.02	-	0	0.02+0.115+0.015*=
	II	0.05	0.072	0.17	9.5	8	-	65.6	0.07	0.115	32.2	29	0.15

Therefore total power consumption for extrusion of 9.5 mm feedstock diameter to 8mm diameter extruded product for square die arrangement for 4 RPM of extrusion wheel is given below:

P = 0.165 + 5.9 + 1.56 + 5.8 + 0.24 = 13.66 kW

Total power consumption for extrusion of 9.5 mm feedstock diameter to 8mm diameter extruded product for streamline die arrangement for 4 RPM of extrusion wheel is given below:

P = 0.165 + 5.9 + 1.56 + 5.8 + 0.15 = 13.57 kW

Case 4. If the groove length of the shoe is 320 mm with square and streamline die arrangement.

Feedstock material: Al 1100 with $\bar{\sigma}$= 21.936 $\bar{\varepsilon}^{0.245}$ as the strain hardening curve.

Feedstock diameter: 9.5 mm

Friction conditions are as follows:

a. Extrusion wheel and feedstock=0.95
b. Coining wheel and feedstock=0.95
c. Extrusion shoe and feedstock=0.95
d. Die-feedstock, abutment-feedstock and bearing-extrudate=0.05

Die profile: 3rd order polynomial

Total reduction in abutment die chamber=60%

Power consumed in initial drag, grip zone, at the abutment face and during turning are tabulated in Table 3.18 whereas power consumption in abutment die chamber is tabulated in Table 3.19.

Table 3.18: Power consumption from initial entry to abutment chamber

S. No.	Input parameters to the system						Initial drag power (kW)	Power in primary gripping zone (kW)	Power at abutment face (kW)	Power during turning (kW)
	μ	x	L_1	L_2	w	V_o				
1	0.95	10	160	160	9.5	0.07	0.463	6.72	2.58	6.4

Table 3.19: Power consumption inside the abutment die chamber

Die arrangements a: Square b: Streamlined		Input to the system						Output of the system					Power in abutment die chamber (kW)
	Zones	μ	V_o	V_e	d_i	d_o	L_o	$\bar{\sigma}$	$\bar{\varepsilon}$	P_{opt}	L_{opt}	% red	
a	I	1.0	0.072	0.10	9.5	7.5	42.5	70.3	0.23	0.9	8.5	25.1	0.5+0.9+
	II	0.05	0.10	0.15	7.5	6	-	83.7	0.32	0.5	13.3	35.2	0.006!+0.002*=1.4
b	I	0.05	0.072	0.072	9.5	9.5	42.5	31.5	-	0.35		0	0.35+0.75+0.12*=1.22
	II	0.05	0.072	0.10	9.5	6	-	78.9	0.09	0.75	28.2	60	

Therefore total power consumption for extrusion of 9.5 mm feedstock diameter to 6mm diameter extruded product for square die arrangement for 4 RPM of extrusion wheel is given below:

$P = 0.463 + 6.72 + 2.58 + 6.4 + 1.4 = 17.56$ kW

Total power consumption for extrusion of 9.5 mm feedstock diameter to 6mm diameter extruded product for streamline die arrangement for 4 RPM of extrusion wheel is given below:

$P = 0.463 + 6.72 + 2.58 + 6.4 + 1.22 = 17.38$ kW

3.17 Numerical Examples for Pure Copper feedstock

Numerical examples for the extrusion of axisymmetric pure copper circular feedstock of different diameters are taken for study of analysis of continuous extrusion process. The two die arrangements i.e. square and streamline are taken to analyze the power consumption in abutment die chamber. The material and process parameters for several cases are chosen as:

Case 1

Feedstock material: C 101 with $\bar{\sigma}= 530\ \bar{\varepsilon}^{0.44}$ as the strain hardening curve.

Feedstock diameter: 12.5 mm

Friction conditions are as follows:

a. Extrusion wheel and feedstock=0.95
b. Coining wheel and feedstock=0.95
c. Extrusion shoe and feedstock=0.95
d. Die-feedstock, abutment-feedstock and bearing-extrudate = 0.05

Die profile: 3rd order polynomial

Total reduction in abutment die chamber=76.9%

Table 3.20: Power consumption from initial entry to abutment chamber

S. No.	Input parameters to the system						Initial drag power (kW)	Power in gripping zone (kW)	Power at abutment face (kW)	Power during turning (kW)
	μ	x	L_1	L_2	w	V_o				
1	0.95	12.5	140	140	12.5	0.142	2.6	36	17	6

Table 3.21: Power consumption inside the abutment die chamber

Die arrangements a: Square b: Streamlined		Input to the system						Output of the system					Power in abutment die chamber (kW)
	Zones	μ	V_o	V_e	d_i	d_o	L_o	$\bar{\sigma}$	$\bar{\varepsilon}$	P_{opt}	L_{opt}	% red	
a	I	1.0	0.142	0.16	12.5	9.5	42.5	70.3	0.23	1.9	9.5	35.1	1.9+1.5+

	II	0.05	0.16	0.20	9.5	6	-	83.7	0.32	1.5	14.5	41.8	0.04!+0.02*=3.46
b	I	0.05	0.142	0.142	12.5	12.5	42.5	31.5	-	1.25		0	1.25+1.75+0.15*=3.15
	II	0.05	0.142	0.16	12.5	6	-	78.9	0.09	1.75	30.5	76.9	

Therefore total power consumption for extrusion of 12.5 mm feedstock diameter to 6mm diameter extruded product for square die arrangement for 8 RPM of extrusion wheel is given below:

P = 2.6 + 36 + 17 + 6 + 3.46 = 65.06 kW

Total power consumption for extrusion of 12.5 mm feedstock diameter to 6mm diameter extruded product for streamline die arrangement for 8 RPM of extrusion wheel is given below:

P = 2.6 + 36 + 17 + 6 + 3.15 = 64.75 kW

Case 2

Feedstock material: C 101 with $\bar{\sigma}$= 530 $\bar{\varepsilon}^{0.44}$ as the strain hardening curve.

Feedstock diameter: 12.5 mm

Friction conditions are as follows:

a. Extrusion wheel and feedstock=0.95
b. Coining wheel and feedstock=0.95
c. Extrusion shoe and feedstock=0.95
d. Die-feedstock, abutment-feedstock and bearing-extrudate=0.05

Die profile: 3rd order polynomial

Total reduction in abutment die chamber=68.6%

Power consumed in initial drag, grip zone, at the abutment face and during turning are tabulated in Table 3.22 whereas power consumption in abutment die chamber is tabulated in Table 3.23.

Table 3.22: Power consumption from initial entry to abutment chamber

S. No.	Input parameters to the system						Initial drag power (kW)	Power in gripping zone (kW)	Power at abutment face (kW)	Power during turning (kW)
	μ	x	L_1	L_2	w	V_o				
1	0.95	12.5	140	140	12.5	0.142	2.6	36	17	6

Table 3.23: Power consumption inside the abutment die chamber

Die arrangements a: Square b: Streamlined		Input to the system						Output of the system					Power in abutment die chamber (kW)
	Zones	μ	V_o	V_e	d_i	d_o	L_o	$\bar{\sigma}$	$\bar{\varepsilon}$	P_{opt}	L_{opt}	% red	
a	I	1.0	0.142	0.15	12.5	9.0	32.5	70.3	0.23	1.4	11.0	30.1	1.4+1.1+
	II	0.05	0.15	0.18	9.0	7	-	83.7	0.32	1.1	16.0	38.5	0.04!+0.02*=2.56
b	I	0.05	0.142	0.142	12.5	12.5	32.5	31.5	-	1.05		0	1.05+1.2+0.15*=2.40
	II	0.05	0.142	0.20	12.5	7	-	78.9	0.09	1.2	34.5	68.6	

Therefore total power consumption for extrusion of 12.5 mm feedstock diameter to 7mm diameter extruded product for square die arrangement for 8 RPM of extrusion wheel is given below:

$P = 2.6 + 36 + 17 + 6 + 2.56 = 64.16$ kW

Total power consumption for extrusion of 12.5 mm feedstock diameter to 7mm diameter extruded product for streamline die arrangement for 8 RPM of extrusion wheel is given below:

$P = 2.6 + 36 + 17 + 6 + 2.40 = 64$ kW

Case 3. If groove length of the extrusion shoe is 320 mm with square and streamline die arrangements.

Feedstock material: C 101 with $\bar{\sigma} = 530\ \bar{\varepsilon}^{0.44}$ as the strain hardening curve.

Feedstock diameter: 12.5 mm

Friction conditions are as follows:

a. Extrusion wheel and feedstock=0.95

b. Coining wheel and feedstock=0.95

c. Extrusion shoe and feedstock=0.95

d. Die-feedstock, abutment-feedstock and bearing-extrudate = 0.05

Die profile: 3rd order polynomial

Total reduction in abutment die chamber=76.9%

Table 3.24: Power consumption from initial entry to abutment chamber

S. No.	Input parameters to the system						Initial drag power (kW)	Power in gripping zone (kW)	Power at abutment face (kW)	Power during turning (kW)
	μ	x	L_1	L_2	w	V_o				
1	0.95	12.5	160	160	12.5	0.142	2.6	41	19.38	6.84

Table 3.25: Power consumption inside the abutment die chamber

Die arrangements a: Square b: Streamlined		Input to the system						Output of the system					Power in abutment die chamber (kW)
	Zones	μ	V_o	V_e	d_i	d_o	L_o	$\bar{\sigma}$	$\bar{\varepsilon}$	P_{opt}	L_{opt}	% red	
a	I	1.0	0.142	0.16	12.5	9.5	42.5	70.3	0.23	1.9	9.5	35.1	1.9+1.5+
	II	0.05	0.16	0.20	9.5	6	-	83.7	0.32	1.5	14.5	41.8	0.04!+0.02*=3.46
b	I	0.05	0.142	0.142	12.5	12.5	42.5	31.5	-	1.25		0	1.25+1.75+0.15*=3.15
	II	0.05	0.142	0.16	12.5	6	-	78.9	0.09	1.75	30.5	76.9	

Therefore total power consumption for extrusion of 12.5 mm feedstock diameter to 6mm diameter extruded product for square die arrangement for 8 RPM of extrusion wheel is given below:

$P = 2.6 + 41 + 19.38 + 6.84 + 3.46 = 73.28$ kW

Total power consumption for extrusion of 12.5 mm feedstock diameter to 6mm diameter extruded product for streamline die arrangement for 8 RPM of extrusion wheel is given below:

$P = 2.6 + 41 + 19.38 + 6.84 + 3.15 = 72.97$ kW

Table 3.26: Comparison of Analytical and Simulation Power required for extrusion of Aluminum feedstock

S. No.	Wheel Velocity (RPM)	Extrusion ratio	Analytical Power (kW)	Simulation Power (kW)
1	4	2.5	14.8	16
2		1.84	14.47	15.5
3		1.41	13.66	14.3

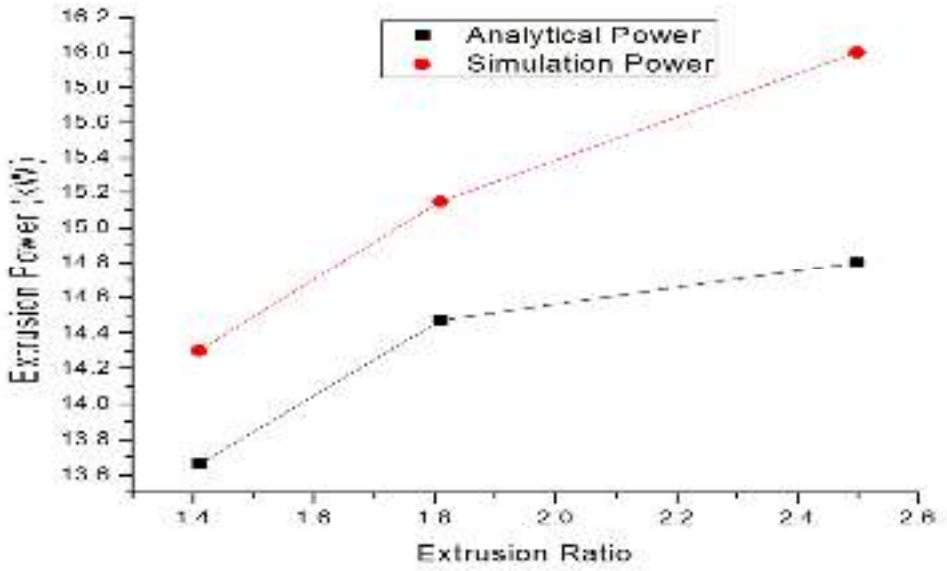

Figure 3.85: Graphical comparison of Analytical and Simulation power for Aluminum feedstock

In this chapter analysis, modeling and simulation of continuous extrusion process for different metals and alloys such as pure Aluminum and Pure Copper has been carried out. Study of several field such as load distribution, torque distribution, effective stress field, effective strain field, damage field, temperature field and velocity field has been done. All the Simulations have been carried out for different feedstock sizes as well as for different extrusion wheel velocities and wheel groove friction conditions. Parametric

study of different simulation parameters such as extrusion wheel speed, extrusion ratio, wheel groove friction etc. and their influence on total forming load have been carried out.

It has been observed that as the extrusion wheel velocity increases, the total load required for the extrusion of feedstock material decreases.

For extrusion of 8 mm Aluminum feedstock material to 6 mm, the total load have been observed as 145 kN, 139 kN and 137 kN at wheel velocities of 4 RPM, 6 RPM and 8 RPM respectively.

For extrusion of 9.5 mm Aluminum feedstock material to 6 mm, the total load have been observed as 222.22 kN, 180 kN, 119.8 kN and 119 kN at wheel velocities of 4 RPM, 6 RPM, 8 RPM and 10 RPM respectively.

For extrusion of 12.5 mm Aluminum feedstock material to 6 mm, the total load have been observed as 794.44 kN, 525.92 kN, 397.91 kN and 322.22 kN at wheel velocities of 4 RPM, 6 RPM, 8 RPM and 10 RPM respectively.

Analysis for total extrusion power has also been made for different extrusion ratio, different die arrangement and for different extrusion shoe groove length. The total extrusion power clearly depends on extrusion ratio, different die arrangement and extrusion shoe groove length. The power consumption is high if the extrusion ratio and extrusion shoe groove length is high with square die arrangement. The power consumption is slightly reduced with the streamlined die arrangement for the same value of extrusion ratio and extrusion shoe groove length

For square die arrangement, analytical powers are 14.8 kW, 14.47 kW and 13.66 kW for extrusion ratio of 2.5, 1.84 and 1.41 respectively at extrusion wheel velocity of 4 RPM whereas simulation powers are 16kW, 15.5 kW and 14.3 kW for extrusion ratio of 2.5, 1.84 and 1.41 respectively at extrusion wheel velocity of 4 RPM. Thus, it can be concluded that power required by the simulation process is greater than analytical process.